UNIVERSITY OF CALIFORNIA
SANTA CRUZ

PROJECTION NEURON FATE SPECIFICATION IN THE MAMMALIAN CEREBRAL CORTEX

A dissertation submitted in partial satisfaction
of the requirements for the degree of

DOCTOR OF PHILOSOPHY

in

MOLECULAR, CELL AND DEVELOPMENTAL BIOLOGY

by

Jeremiah Aaron Tsyporin

March 2023

The dissertation of Jeremiah Aaron Tsyporin
is approved:

Professor Bin Chen, chair

Professor Yi Zuo

Professor Euiseok Kim

Peter Biehl
Dean of Graduate Studies

Table of Contents

List of Figures

List of Tables

Abstract

PROJECTION NEURON FATE SPECIFICATION IN THE MAMMALIAN CEREBRAL CORTEX

Jeremiah Aaron Tsyporin

Projection neurons underly cortical computation and are necessary for proper cortical function. Understanding how these cell types arise is a central question in neuroscience and has wide-ranging implications for treating brain diseases. Genes encoding for transcription factors or chromatin remodeling proteins have been identified that are necessary for generating projection neuron cell types in the cerebral cortex. Exactly how they function is unknown. Using genetically engineered mouse models combined with immunohistochemistry, bulk and single-cell RNA sequencing, chromatin profiling, circuit tracing, and electrophysiology, this work uncovers the molecular mechanisms by which the transcription factors Fezf2, Satb2, and the transcriptional corepressor Tle4, specify cell fate in the developing cerebral cortex. Fezf2 specifies cell fate by functioning as a selective repressor. It regulates subtype-specific identities of corticothalamic and subcerebral neurons by selectively repressing the expression of genes inappropriate for each neuronal subtype. Tle4 works collaboratively with Fezf2 in layer 6 to inhibit layer 5 subcerebral neuronal genes. On the other hand, Satb2 is involved in gene activation and repression; these functions are likely mediated by interactions with ATP-dependent chromatin remodeling

complexes. This work also demonstrates that Satb2 dosage affects cortical development, shedding light on the etiology of patients with a mutant *SATB2* allele.

Fezf2, Tle4, and Satb2 all function to specify subtype identity in postmitotic neurons. These results indicate that a cortical glutamatergic identity is specified by progenitor cells, but subtype-specific identity is achieved through postmitotic fate refinement.

Acknowledgements

Bin, I could not ask for a better mentor. I am grateful that you gave me the freedom to try and fail, for without the failures, there would be no success.

Yi Zuo and Euiseok Kim, for being on my thesis committee and guiding me over the years. Yi, your tough questions during my oral exams helped further my research. Euiseok, I was a new Ph.D. student when you gave your job talk—it was an inspiration, and I'm thankful we've gotten to know each other so well since you started your lab. David Feldheim and Lindsay Hinck for being informal mentors and helping me think about the bigger picture over the years. When I published my first manuscript, Dave, your words of congratulations were, "you know the only thing that matters now is the next one." You keep it real. And Lindsay, you've been a source of honest and sometimes difficult, advice about life and academia.

David Tastad, my co-author and long-time friend. We had an unbelievable amount of fun over the years, and somehow, we produced something meaningful to be proud of in the end. I'm honored we got to work together. Liora Huebner, you reminded me how to love life and laugh when times were tough. I can't thank you enough for that. Tommy Finn, my co-author on the Satb2 project. It's been a wild ride replete with highs and lows. It feels like the end of an era as I write this. Looking forward to staying in touch. Kendy Hoang, for being a great friend and intellectual counterpart over the years. Xiaoyi Guo, I'm glad we suffered through the graduate curriculum

together. Austin Schubert, your enthusiasm for science is contagious and reminded me why I do what I do in the first place. Christian Ortiz, for teaching me all the basics so many years ago.

I'd also like to thank all of the undergraduate students I have had the privilege of mentoring–the following in particular. Ariella Angelini Stewart, you stood out among many and took on every project you could. You came in at 6 am to start experiments, found funding to attend and present at conferences, and pioneered new lab techniques with me that made significant contributions to many ongoing projects in the lab. Angel Garcia, it's been great seeing you flourish in your post-bac at UCSF, you will one day be leader in your field. Cosmo Hahn, your robotically stable hands are a gift, your patients will be glad to have you as a doctor. Daisy Gallardo, my first student to go on and pursue a Ph.D. When I found out that you decided to enroll in one of the top neuroscience programs, I was filled with pride.

To my grandparents Eugenia and Leonid Tsyporin, who survived the siege of Leningrad and later dared to leave the Soviet Union. Alice and Dick Mitani who met and married in the Japanese internment camps after everything was taken from them. You all found love and beauty in the darkest and ugliest of times, facing struggles I could never imagine. To my aunts and uncles, Dick, Karen, Marilyn, Yoav, and cousins Kourtney and Michelle.

To my parents, who always supported me and allowed me to pursue whatever interested me with no expectations or demands, I love you guys.

And thank you to all of my friends.

The text of this dissertation includes a reprint of the following previous published paper:

Tsyporin J, Tastad D, Ma X, Nehme A, Finn T, Huebner L, Liu G, Gallardo D, Makhamreh A, Roberts JM, Katzman S, Sestan N, McConnell SK, Yang Z, Qiu S, Chen B. Transcriptional repression by FEZF2 restricts alternative identities of cortical projection neurons. Cell Rep. 2021 Jun 22;35(12):109269. doi: 10.1016/j.celrep.2021.109269. PMID: 34161768; PMCID: PMC8327856.

Acknowledgement for Tsyporin et al., 2021:

This study was supported by grants to B.C. (NIH R01 MH094589 and R01 NS089777), N.S. (NIH U01 MH116488 and R01 NS095654), S.K.M. (NIH R01 EY08411), and S.Q. (University of Arizona startup funds). We thank Dr. Haihui Xue (Hackensack University Medical Center) for providing the mouse *Tle4* cDNA plasmid. We would like to acknowledge technical support and training from Benjamin Abrams in the UC Santa Cruz Life Sciences Microscopy Center. Use of the Zeiss 880 confocal microscope was made possible by the award of NIH S-10 Instrumentation grant 1S10OD23528-01. We would like to thank Dr. Hannah Maul-Newby and Dr. Melissa Jurica for technical assistance. We also thank our interns and volunteers that helped with the project, Cosmo Hahn, Hansen Lillemark, Emily Brumley, Litzy

Rodriguez, Maanvi Thawani, and Sahiti Annadata. The graphical abstract was created with BioRender.com.

Author contributions for Tsyporin et al., 2021

B.C., J.T., D.T., Z.Y., S.Q., and S.K.M. designed all the experiments; J.T., D.T., X.M., A.N., T.F., L.H., G.L., D.G., A.M., J.M.R., and S.Q. performed all the experiments; N.S. provided resources and contributed to interpretation of the results; J.T., D.T., S.Q., and B.C. analyzed the data and wrote the manuscript; and S.K. analyzed the RNA-seq data. All authors read and edited the manuscript.

The text of this dissertation also includes a draft of the following manuscript in preparation for submission:

Dose dependent regulation of cortical projection neuron development by Satb2

Thomas S. Finn[1,*], Jeremiah Tsyporin[2,*], Sol Katzman[2] Austin Schubert[2], Ariella Angelini Stewart[2], Shenfeng Qiu[3], Bin Chen[2,7,#]

[1] Department of Chemistry and Biochemistry, University of California Santa Cruz, 1156 High Street, Santa Cruz, CA 95064, USA

[2] Department of Molecular, Cell, and Developmental Biology, University of California Santa Cruz, 1156 High Street, Santa Cruz, CA 95064, USA

[3] Department of Basic Medical Sciences, University of Arizona College of Medicine - Phoenix, Phoenix, AZ 85004, USA.

[7]Lead Contact

[#]Correspondence: bchen@ucsc.edu

[*] These authors contributed equally

Chapter 1: Introduction

The human brain is a marvel of complexity. It integrates sensory information from multiple sources to control bodily functions and underpins all cognitive processes. The function of this remarkable structure depends on upwards of 80 billion neurons and a similar number of non-neuronal cells (Azevedo et al., 2009). Santiago Ramon y Cajal's groundbreaking catalogue of neuronal structure, made possible by the visualization techniques pioneered by Camillo Golgi, revealed the enormous complexity and diversity of cell types in the brain. Despite over a century of study, understanding the birth and differentiation of these cell types remains poorly understood.

The structure that underlies the exceptional cognitive abilities of mammals is the neocortex, the most recently evolved brain region (Nieuwenhuys, 1994). It is thought to be primarily responsible for endowing humans with their unique cognitive abilities (Hill and Walsh, 2005; Molnár and Pollen, 2014; Uylings and van Eden, 1991). How this structure develops is poorly understood.

Throughout gestation and into the early adult years, the human neocortex undergoes a complex series of developmental processes building a functional brain; generally, the central nervous system undergoes fundamental developmental patterns typical of all mammals

studied (Silbereis et al., 2016). These processes must be tightly regulated and controlled to ensure proper brain development. Understanding neurodevelopmental processes on a molecular and cellular level is paramount to uncovering the etiology of neurological diseases with a developmental origin. Over the past several decades, the causal genetic and molecular underpinnings of cortical development have begun to be unraveled, providing new insights into fundamental biology and neurological diseases.

Genes identified to be essential for cortical development are implicated in diseases including Autism, Schizophrenia, Bipolar disorder, and many others (Autism Spectrum Disorder Working Group of the Psychiatric Genomics Consortium et al., 2019; Chen et al., 2018; Gandal et al., 2018; Li et al., 2018; Meng et al., 2018). Understanding the molecular and cellular mechanisms underlying the formation of the neocortex is essential for elucidating the etiology of these conditions. Furthermore, this knowledge can inform the development of therapies for brain repair after injury or neurodegeneration and has implications is in understanding the biology of brain tumors and other cancers that activate neurodevelopmental programs (Shue et al., 2022; Yang et al., 2019).

Experimental systems are critical for understanding cortical development. While observational studies of human brain development and disease are fundamental in modern neuroscience, the human brain is

a generally intractable experimental system. Therefore, the field has used model organisms and, more recently, human iPSC-derived brain organoids that faithfully recapitulate some aspects of human brain development.

While brain organoids show incredible promise for uncovering human-specific developmental paradigms, several limitations exist, including composition variations between organoids, limited maturation of later-born neuronal subtypes, and lack of cortical arealization, among others (Andrews and Kriegstein, 2022; Pollen et al., 2019). As protocols and related technology advance, brain organoids will play a crucial role in uncovering the unique aspects of human brain development. Until then, traditional model systems such as flies, worms, and rodents will remain the bedrock of experiments aimed at uncovering fundamental mechanisms of neurodevelopment.

Despite the evolutionary distance between mice and human, and the apparent fact that divergent developmental processes exist endowing humans with more advanced cognitive abilities, many fundamental molecular and developmental mechanisms are conserved (Silbereis et al., 2016). Although all aspects of human cortical development cannot be fully modeled in a mouse, it serves as a tractable experimental system with numerous practical benefits: it has a short gestation time, there is a wealth of genetic toolkits already available for genetic manipulation, inbred

mouse strains provide animals with genetically homogenous backgrounds. Furthermore, we are far from understanding all aspects of nervous system development in any organism—there is still much work to do in uncovering many of the shared fundamental developmental mechanisms underlying the mammalian cerebral cortex. For my thesis research, I have utilized the mouse as a model organism for studying cell fate decisions in the developing cerebral cortex.

Cortical excitatory projection neurons underly cortical computation

The principle neuronal cell types of the neocortex are the cortical projection neurons—excitatory neurons that use glutamate as a neurotransmitter and send axons to nearby and far-off inter and intracortical targets (Figure 1). The second major neuronal type is the gamma-aminobutryric acid (GABA) inhibitory cortical interneurons that make up a bit over 10% of the neurons in the cortex (Keller et al., 2018), and are critical in modulating cortical excitatory neurons; without them there would be no inhibition (Kepecs and Fishell, 2014). The cortical projection neurons are the computational units of the cortex and serve as the primary input system and sole output system.

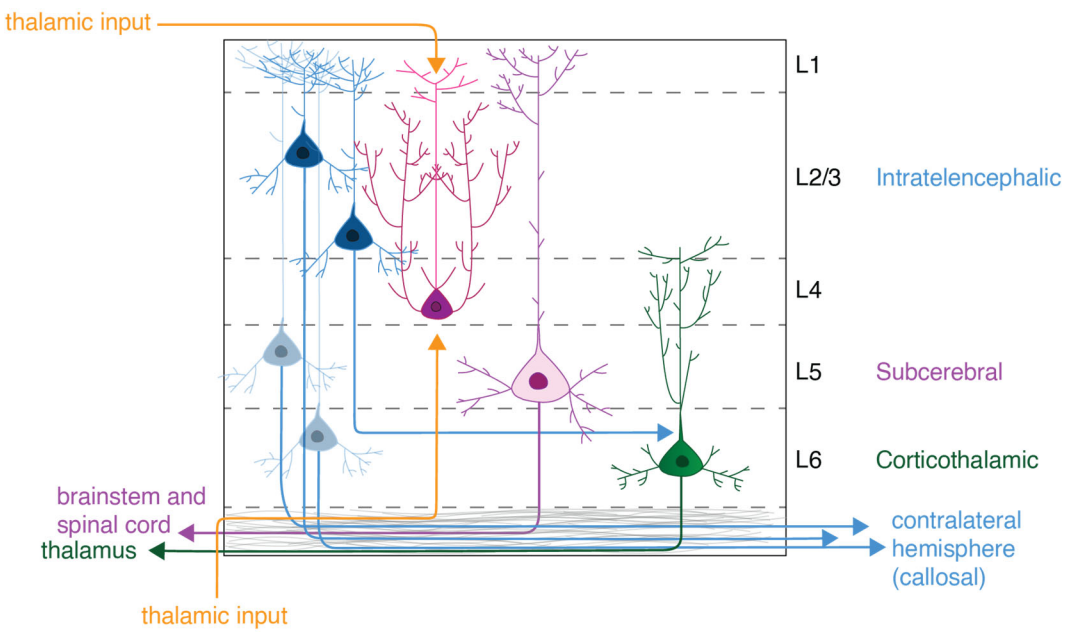

Figure 1: Projection neurons in the cerebral cortex

Schematic of major classes of glutamatergic projection neurons in the mouse cerebral cortex. Intratelencephalic (IT) neurons reside in all cortical layers. The layer 4 neurons that receive thalamic input are IT neurons primarily projecting into the upper-layers. IT neurons in 2/3, 5 and 6, project locally or to the contralateral hemisphere (callosal). Subcerebral (SC) projection neurons reside in layer 5 and project to the brainstem and spinal cord. Corticothalamic (CT) projection neurons primarily reside in layer 6 and project to the thalamus.

Induction of cortical neurogenesis

During development, the neural tube gives rise to the brain and spinal cord. The rostral end of the neural tube morphs into a structure that contains three primary brain vesicles: the forebrain (prosencephalon), midbrain (mesencephalon), and hindbrain (rhombencephalon). The forebrain consists of the telencephalon, which gives rise to the cerebral cortex, hippocampus, basal ganglia, and olfactory bulb, and the diencephalon, which gives rise to the thalamus and hypothalamus. In mammals, the dorsocaudal telencephalon is notably large and gives rise to a greatly expanded cerebral cortex, most of which is the 6-layered neocortex unique to mammals (Rakic, 1988). As the telencephalon develops, a complex interplay of cell-intrinsic and extrinsic factors regionalizes the telencephalon into different progenitor domains that ultimately give rise to different brain regions (Hébert and Fishell, 2008). The progenitor region that gives rise to the cerebral cortex is the dorsal ventricular zone.

After neural tube closure and prior to the onset of neurogenesis, the dorsal ventricular zone consists of neuroepithelial progenitors (NEPs). The NEPs symmetrically divide and greatly expand the progenitor pool. Around E9.5, NEPs begin taking on glial characteristics and typical radial glial cell phenotypes; this marks the onset of neurogenesis (Kriegstein and Alvarez-Buylla, 2009).

Cell-intrinsic and extrinsic factors regulate the switch from symmetric self-renewing divisions to asymmetric neurogenic divisions. Cell intrinsic programs include increased cell cycle length and the expression of neural differentiation genes at the onset of neurogenesis. Extrinsic signaling molecules play central roles in regulating gene expression and timing of neurogenesis. Whether or not there is an intrinsic, ontogenetic timing mechanism within progenitors themselves that regulates the timing of neurogenesis is unknown. However, the effects of extrinsic signaling molecules are critical for properly regulating the pace of neurogenesis.

For instance, during neurogenesis, Wnt signaling occurs in a low to high rostral-caudal, lateral-medial gradient opposite to the gradient of neurogenesis, suggesting that high levels of Wnt inhibit the progression from the self-renewing to neurogenic divisions (Machon et al., 2007). *Pax6*, *Ngn2*, *Tbr2*, and *Meis2*, all genes involved in neurogenesis, are upregulated, following the retreating Wnt gradient (Mutch et al., 2010, 2009). Indeed, prolonged Wnt signaling results in decreased differentiation and expansion of the progenitor pool as cells preferentially re-enter the cell cycle, resulting ultimately in a dramatically expanded cortical surface area (Chenn and Walsh, 2002). Another study found that stabilizing b-catenin delays the generation of Tbr2+ neurogenic progenitors (Wrobel et al., 2007).

As neurogenesis begins, a subpopulation of NEPs express *Tis21*, an antiproliferative gene (Tirone, 2001), that marks neurogenic, but not proliferative, progenitors (Haubensak et al., 2004; Iacopetti et al., 1999) which when overexpressed results in increased consumptive progenitor divisions leading to microcephaly (Iacopetti et al., 1999). Induction of the Tis21 protein is associated with asymmetric neurogenic divisions rather than symmetric self-renewing divisions (Haubensak et al., 2004). *Tis21* mRNA is synthesized during G1 (Iacopetti et al., 1999), the cell-cycle phase in which progenitors are particularly receptive to extrinsic cues (Soufi and Dalton, 2016).

Another critical factor in determining the onset of neurogenesis is cell cycle length, particularly G1, which begins to increase at the onset of neurogenesis (Takahashi et al., 1995). To determine if cell cycle length is a causative mechanism for the promotion of neurogenesis, treatment of whole E9.5 or 10.5 embryos with Olomucine, which lengthens G1, resulted in premature neurogenesis with concomitant expression of *Tis21* (Calegari and Huttner, 2003). Conversely, shortening G1 by overexpressing Cdk4/CyclinD1 delays neurogenesis and increases self-renewal (Lange et al., 2009; Pilaz et al., 2009).

These examples demonstrate the confluence of intrinsic and extrinsic factors regulating the onset of cortical projection neuron generation.

Lineage potential and fate restriction of Radial Glial Cells

RGCs in the dorsal telencephalon are the ultimate source of cortical projection neurons. They are also the source of most cortical oligodendrocytes, astrocytes, and some olfactory bulb interneurons (Kriegstein and Alvarez-Buylla, 2009). Diverse projection neuron subtypes are born in the dorsal ventricular or subventricular zone during cortical histogenesis and integrate into the cortical plate.

RGCs can give rise directly to neurons, but they mainly generate $Tbr2^{+}$ intermediate progenitor cells that function as transit-amplifying cells for excitatory PNs (Hevner et al., 2006; Taverna et al., 2014). The generation of neurons and glia is a distinctly temporally patterned process. The neurons residing deepest (apically) in the cortical plate are born first, and neurons that occupy successively more superficial positions migrate past the older born neurons to their final destinations; in this way, the cortex develops inside-out (Figure 2) (Juric-Sekhar and Hevner, 2019; Kwan et al., 2012; McConnell, 1988, 1995). Once the generation of PNs ceases, RGCs generate multipotent intermediate progenitors, which give rise to astrocytes, oligodendrocytes, and olfactory bulb interneurons (Figure 2) (Guo et al., 2013; Kessaris et al., 2006; Kohwi et al., 2007; Kriegstein and Alvarez-Buylla, 2009; Kwan et al., 2012; Li et al., 2021; Ventura and Goldman, 2007; Young et al., 2007; Zhang et al., 2020b).

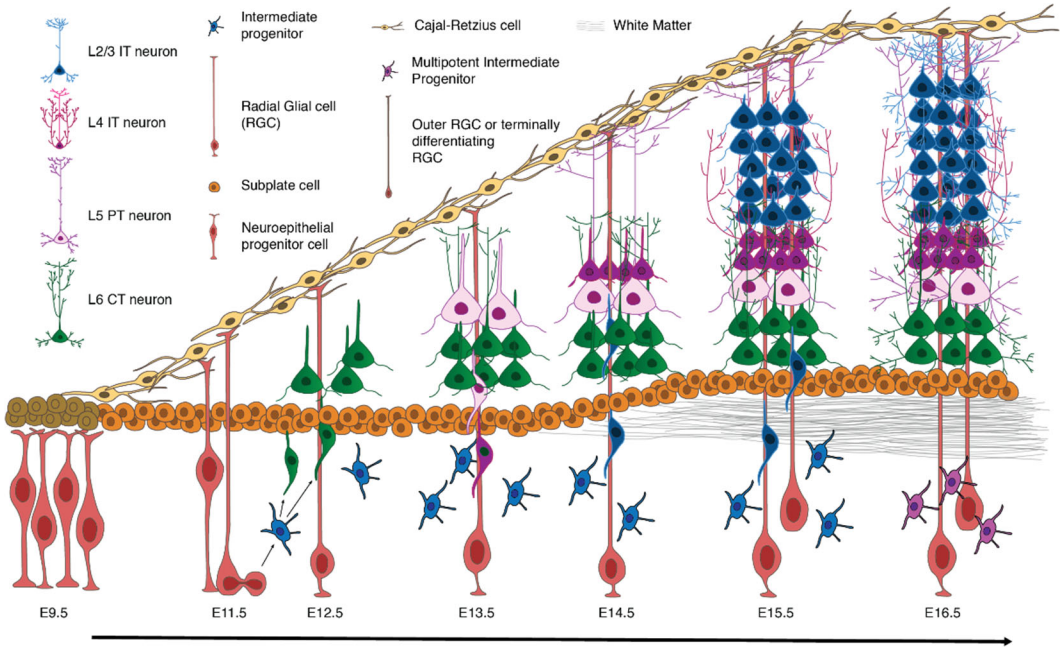

Figure 2: Cortical projection neuron generation in the mouse cerebral cortex

Since the temporal progression of neurogenesis was observed, there has been, and remains, significant debate in the field about many fundamental aspects of the biology of RGCs and their contribution to cortical neuron fate specification. Do different populations of RGCs give rise to distinct neuronal subtypes? Are RGCs multipotent throughout cortical neurogenesis, or does their competency change at different developmental stages?

In 1988, Susan McConnell published seminal work providing a foundation for modern views of RGC progression and competency. At the time, it was known that the cortex is temporally patterned, but the role of environmental and intrinsic mechanisms underlying this pattering was unknown. To determine if proliferative zone progenitors had an intrinsic temporal programming mechanism, McConnell challenged progenitors by implanting them in recipient progenitor zones at different times during development. Using the ferret as a model, at the peak time of upper-layer neurogenesis (P1 or P2), McConnell transplanted tritium-thymidine (3H-T) labeled germinal zone cells into the germinal zones of embryos at the peak time of deep-layer neurogenesis (E32). The 3H-T labeled cells in the adult (>4 weeks) populated upper layers only, instead of adapting to their environment and generating cells of all layers. McConnell then did the reverse experiment and transplanted E32 3H-T labeled progenitors into P1 or P2 host proliferative zones and found that the E32 transplanted cells

generated neurons of all layers instead of adapting to their environment and generating upper-layer neurons only. The findings implied that cells in the ferret progenitor zone are intrinsically multipotent at the onset of cortical projection neuron generation, but upper-layer restricted towards the end of cortical projection neuron generation. This seminal study and many that followed supported the idea that early cortical progenitors are multipotent, but lose the competency to generate early temporal fates as developmental time progresses (Desai and McConnell, 2000; Frantz and McConnell, 1996; McConnell and Kaznowski, 1991).

Decades later, after the advent of genetic mouse models facilitating lineage tracing of genetically identifiable RGC populations, the lineage potential of RGCs was revisited. The observation that the transcription factor Cux2 was specifically expressed in upper-layer neurons and in a subpopulation of RGCs, led to the intriguing possibility that Cux2+ RGCs were intrinsically fate restricted to generate upper-layer neurons (Franco et al., 2012). These upper-layer restricted progenitors would have been missed in McConnell's transplantation experiments due to the heterogenous transplantation of many progenitor types (i.e., multipotent and upper-layer fate-restricted progenitors would have been transplanted together in the E32→P1/2 experiment). To probe the lineage potential of this population of RGCs, a *Cux2-CreER* knock-in line was used to lineage trace cortical progenitors. It was found that Cux2+ RGCs were intrinsically

fate restricted to generate upper-layer projection neurons (Franco et al., 2012). Work that followed contradicted these results and found that clones from *Cux2-CreER+* RGCs consisted of projection neurons of all layers and both types of cortical glia (Eckler et al., 2015). Similarly, Fezf2, a transcription factor expressed in deep-layer neurons, was also expressed in RGCs, suggesting a potential marker for deep-layer restricted RGCs. Lineage tracing the Fezf2+ RGC population with *Fezf2-CreER* revealed that Fezf2+ RGCs are similarly multipotent (Guo et al., 2013). To further corroborate the multipotency of early RGCs and examine the possibility of fate-restricted lineages, exceedingly elegant studies utilizing Mosaic Analysis with Double Markers combined with *Nestin-CreER* or *Emx1-CreER* mouse lines reinforced the notion that single RGCs are multipotent and progressively generate increasingly superficial layer neurons followed by glia (Gao et al., 2014). Additionally, rich single cell RNA sequencing datasets of the dorsal pallium over developmental time infer that projection neuron specification occurs post-mitotically and that cortical RGCs exist as a continuum while separation of cell-type classes occurs in newborn neurons, but not in progenitors, arguing against the existence of fate restricted RGCs (Di Bella et al., 2021).

A recent study using an intersection/subtraction (IS) lineage tracing strategy examined the fates of Lhx2+Fezf2- and Lhx2+Fezf2+ RGCs and concluded that the Fezf2+Lhx2- progenitors give rise to callosal projection

neurons whereas Lhx2+Fezf2+ RGCs generate subcortical projecting axons, indicating two categorically distinct RGC lineages (Matho et al., 2021). The IS reporter expresses RFP upon cre-mediated recombination and GFP upon Cre and FlpO mediated recombination. *Lhx2-CreER/+;Fezf2-FlpO/+;IS* reporter mice were given tamoxifen at E12.5 and examined at P30. The authors observed exclusively GFP+ axons innervating the thalamus (implying that the CT neurons at some point expressed either together or separately *Lhx2* and *Fezf2*), while callosal axons were RFP+ (implying that most of the callosal neurons came from a lineage that expressed *Lhx2* but not *Fezf2*). The authors concluded that at E12.5, Lhx2+Fezf2+ progenitors are fate restricted to generate corticothalamic projection neurons, while the Lhx2+Fezf2- progenitors are fate restricted to generate callosal projection neurons (Matho et al., 2021).

Although an exciting premise, there are alternative interpretations of the data. *Fezf2* is expressed at extremely low levels in RGCs. The following result demonstrates this: *Lhx2-CreER;Ai14* and *Fezf2-CreER;Ai14* embryos were given the same dose of tamoxifen at E10.5 and chased for 24 hours, dense RFP was seen in *Lhx2-CreER;Ai14* embryos while sparse RFP was seen in *Fezf2-CreER;Ai14* embryos. The same experiment performed at E12.5 revealed that about 2-3x fewer RFP+ RGCs in *Fezf2-CreER;Ai14* embryos were labeled, and when given tamoxifen at E13.5, RFP labeling in *Fezf2-CreER;Ai14* embryos was

mostly restricted to postmitotic pyramidal neurons while few RGCs were labeled (Matho et al., 2021). This is likely not due to sparse cells expressing *Fezf2*, as *Fezf2* mRNA is expressed throughout the VZ (Guo et al., 2013), but rather to low levels of Fezf2 and thus the resulting CreER protein. The *Fezf2-CreER* knock in line used in Matho et al. faithfully recapitulated *Fezf2* expression in RGCs and cortical neurons. Among these cells, Fezf2 expression level is highest in layer 5 subcerebral and layer 6 corticothalamic neurons. It is expressed at low levels in RGCs. Because Fezf2 is expressed at exceedingly low levels in the progenitors, and FlpO is generally less efficient than Cre, it is feasible that many Lhx2+Fezf2+ progenitors at E12.5 will give rise to progeny that escape FlpO mediated recombination. Therefore, the presence of GFP+ axons, but not the RFP+ axons in the thalamus of the *Lhx2-CreER/+;Fezf2-FlpO/+;IS* mice is likely due to the Flp-mediated recombination in the corticothalamic neurons, which express Fezf2 at a much higher level than the RGCs. Similarly, the presence of RFP+ axons, but not the GFP+ axons in the corpus callosum is likely due to the low level or absence of Fezf2 expression and lack of Flp-mediated recombination in the callosal neurons. If Lhx2+Fezf2- fate-restricted progenitors are common, then lineage tracing of individual Lhx2-CreER+ cells with low dose tamoxifen will reveal a subset of upper-layer-exclusive clones. A similar analysis with

MADM would be slightly more technically challenging, but serve as a better experiment.

To date, no study has been able to convincingly show evidence for the existence of fate restricted radial glial cells. Novel single cell methods incorporating deep sequencing may uncover a level of unappreciated heterogeneity of RGCs and reveal new subtypes, which may be lineage restricted.

Generating neuronal diversity through transcriptional regulation: terminal selectors, temporal transcription factors, and homeodomain transcription factors

Mechanisms of cell fate specification in *Drosophila* and *C. elegans* have been elucidated in considerable detail. Understanding the mechanisms of cell fate specification in these systems provides an intellectual framework for thinking about cell fate specification in the mammalian cortex.

In *C. elegans*, lineage-dependent regulatory inputs in differentiating neurons activate the expression of terminal selectors, which in turn activate a battery of effector genes to confer cell fate, and remain continuously expressed to maintain cell identity (Hobert and Kratsios, 2019). Terminal selector genes have been proposed in mammals, for

example, *Lhx2* in olfactory receptor neuron specification and maintenance, or *Brn3a* in medial habenular neurons (Hobert and Kratsios, 2019). In the cortex, the transcription factor Fezf2 is necessary for the specification of corticospinal motor neurons and has been proposed to act as a mammalian selector activating cortical spinal motor neuron genes (Lodato et al., 2014), but the findings in Chapter 2 contradict this and instead implicate Fezf2 to be involved exclusively in genetic repression.

In *Drosophila*, temporal pattering of neural progenitors by sequentially expressed temporal transcription factors is a common mechanism in the ventral nerve cord and brain to regulate the generation of neuronal subtypes (Doe, 2017; Konstantinides et al., 2022). In the ventral nerve cord, Hunchback, Kruppel, Pdm, and Castor, are sequentially expressed through gene regulatory cascades. These temporal transcription factors are required for the temporal specification of ventral nerve cord progenitor cells known as neuroblasts and the proper temporal generation of their progeny (Pearson and Doe, 2004).

Cell fate specification in the developing spinal cord is a well understood system of fate specification in the developing mammalian central nervous system. In the developing neural tube, Shh emanating from the floorplate generates a ventral to dorsal gradient complementary to the dorsal to ventral gradient of BMP produced by the roof plate (Martí et al., 1995; Roelink et al., 1995; Ericson et al., 1996; Briscoe et al., 2000).

The graded Shh activity modulates the expression of homeodomain proteins at different threshold concentrations by repressing class I homeodomain proteins Pax7, Dbx1, Dbx2, Irx3, and Pax6. The most ventral expression boarder of each class 1 homeodomain protein specifies the ventral boundary of each progenitor domain, while class 2 homeodomain proteins Nkx6.1 and Nkx6.2 are induced by Shh at different threshold concentrations, and conversely, their most dorsal expression boarder specifies the dorsal boundary of each progenitor domain. The regulation of each homeodomain protein by graded Shh signaling combined with cross-repressive actions between class 1 and class 2 homeodomain proteins creates sharply defined progenitor domains (Jessell, 2000). The homeodomain transcription factors Nkx2.2, Nkx2.9, Nkx6.1, Dbx1, and Pax7 contain an Eh1 domain which interacts with the Tle family of co-repressors to mediate the repressive activities needed to properly pattern the ventral neural tube and ultimately give rise to the correct neuronal subtypes (Muhr et al., 2001). The expression of the class 1 and class 2 homeodomain transcription factors is necessary to give rise to the different neuronal subtypes in the spinal cord. Ectopic expression of homeodomain proteins within the neural tube gives rise to ectopic neural subtypes (Briscoe et al., 2000; Pierani et al., 2001).

These findings highlight the central role of transcriptional regulation in specifying cell identity in the developing nervous system. Understanding

the mechanism of cell fate specification in different systems and model organisms provides an intellectual foundation for designing experiments to understand the generation of cell diversity in the cerebral cortex.

Post-mitotic specification of projection neuron identities in the cerebral cortex

The cortical projection neurons are broadly defined into the following groups: Corticothalamic (CT) projection neurons that primarily reside in layer 6 that project to the thalamus, subcerebral (SC) projection neurons in layer 5 that project to the brainstem and spinal cord, and Intratelencephalic (IT) neurons reside in all cortical layers. The layer 4 neurons that receive thalamic input are IT neurons primarily projecting into the upper-layers. IT neurons in 2/3, 5 and 6, project locally or to the contralateral hemisphere (Greig et al., 2013a; Molyneaux et al., 2007; Zeng, 2022). Recent single cell RNAseq analysis of cortical areas has led to the extensive characterization of a wide variety of cortical projection neurons based on transcriptional identity in the mouse cerebral cortex. Rather than a continuum of similar cell types, differentiated neurons exist as distinct subtypes, and there are as many as 133 subtypes that can be classified based on transcriptional signatures (Tasic et al., 2018). The RGCs, however, exist as a continuum of cells that cannot easily be split into transcriptionally distinct groups (Di Bella et al., 2021). How the

progenitors give rise to transcriptionally distinct classes of projection neurons is a poorly understood and fascinating outstanding question in the field of developmental neuroscience.

Several genes have been identified in mouse that specify the identities of broad classes of projection neurons, and many of the transcription factors encoded by these genes inhibit each other's expression to define classes of projection neurons. For instance, in layer 6 corticothalamic projection neurons, Tbr1, Tle4, and Sox5 inhibit high levels of the layer 5 subcerebral projection neuron determinant, *Fezf2* (Galazo et al., 2022; Han et al., 2011; Kwan et al., 2008; Lai et al., 2008; McKenna et al., 2011; Tsyporin et al., 2021), while high levels of Fezf2 directly repress *Tbr1* (Galazo et al., 2022). *Satb2* is necessary for the development of cortico-cortical projection neurons that mainly reside in the upper layers, and it does so in part by repressing the layer 5 subcerebral neuronal genes (Alcamo et al., 2008; Britanova et al., 2008).

The cell fate-determining genes including *Tbr1*, *Sox5*, *Fezf2*, and *Satb2* function in newborn post-mitotic cells rather than at the level of the progenitor (Alcamo et al., 2008; Britanova et al., 2008; Han et al., 2011; Kwan et al., 2008; Lai et al., 2008; Leone et al., 2008; McKenna et al., 2015, 2011; Molyneaux et al., 2005; Tsyporin et al., 2021), a common pattern in cortical cell-fate specification (Ozkan et al., 2020). These proteins tend to repress each other's expression to define cell identity.

Unlike the homeodomain transcription factors that function by specifying different progenitor domains, the post-mitotic fate determinants Tbr1, Sox5, Fezf2, and Satb2 have no obvious effect on RGC identity, and instead control laminar organization through mutually repressive interactions in the newborn neurons.

The focus of my thesis works aims to elucidate precise molecular mechanisms underlying cell fate specification of glutamatergic projection neurons in the developing cerebral cortex, primarily through interrogating the functions of Fezf2, Tle4, and Satb2.

Chapter 2: Transcriptional repression by FEZF2 restricts alternative identities of cortical projection neurons

Summary:

Projection neuron subtype identities in the cerebral cortex are established by expressing pan-cortical and subtype-specific effector genes that execute terminal differentiation programs bestowing neurons with a glutamatergic neuron phenotype and subtype-specific morphology, physiology, and axonal projections. Whether pan-cortical glutamatergic and subtype-specific characteristics are regulated by the same genes or controlled by distinct programs remains largely unknown. Here, we show that FEZF2 functions as a transcriptional repressor, and it regulates subtype-specific identities of both corticothalamic and subcerebral neurons by selectively repressing expression of genes inappropriate for each neuronal subtype. We report that TLE4, specifically expressed in layer 6 corticothalamic neurons, is recruited by FEZF2 to inhibit layer 5 subcerebral neuronal genes. Together with previous studies, our results indicate that a cortical glutamatergic identity is specified by multiple parallel pathways active in progenitor cells, whereas projection neuron subtype-specific identity is achieved through selectively repressing genes associated with alternate identities in differentiating neurons.

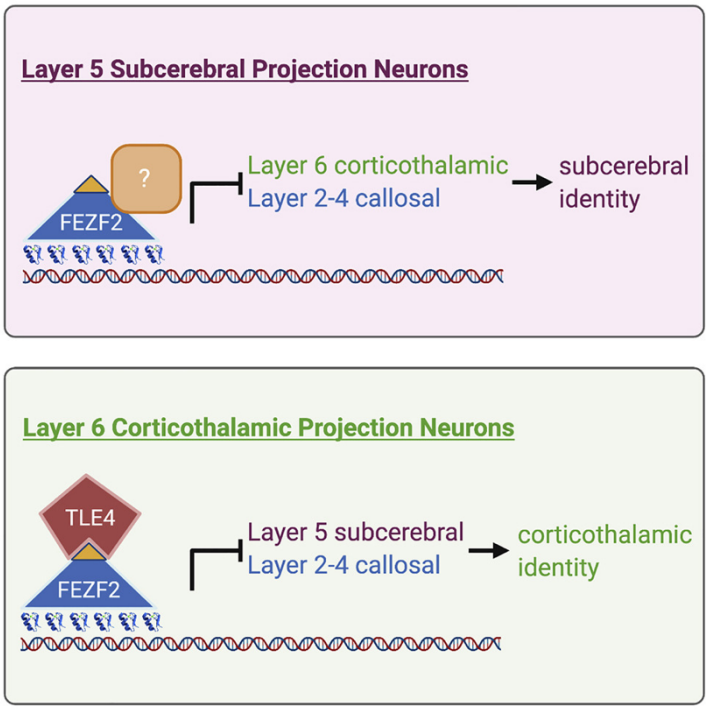

Figure 3: Graphical abstract

Introduction

Projection neuron subtype identities in the developing cerebral cortex are established by expressing pan-cortical and subtype-specific genes, which execute terminal differentiation programs and bestow neurons with a glutamatergic phenotype and subtype-specific morphology, physiology, and axonal projections. Whether the pan-cortical glutamatergic phenotype and subtype-specific characteristics are regulated by the same genetic program or controlled by distinct genes remains largely unknown. In *C. elegans*, expression of terminal effector genes is activated by terminal selector genes, which are transcription factors that act in differentiating neurons by binding to common *cis*-

regulatory elements in effector genes and activating their expression (Hobert and Kratsios, 2019). Whether similar mechanisms are utilized in developing mammalian brains is unknown, except the corticospinal motor neurons (CSMNs), a subset of subcerebral projection neurons specified by the transcriptional regulator FEZF2 (Lodato et al., 2014).

Although recent advances in single-cell RNA sequencing (scRNA-seq) technologies have allowed classification of neurons into different clusters based on gene expression in individual cells (Tasic et al., 2018), neocortical excitatory neurons can be broadly classified into 3 major subtypes based on where they project axons (Leone et al., 2008). Corticocortical neurons, located in layers 2–6, project axons to the ipsilateral (intracortical) or contralateral (callosal) cortex. The subcerebral neurons projecting to the thalamus (corticothalamic neurons) mostly reside in layer 6, whereas the subcerebral neurons projecting to the midbrain, hindbrain, and spinal cord are confined to layer 5B (O'Leary and Koester, 1993). Determining the molecular mechanisms underlying the differentiation of these neuronal subtypes is essential for understanding the regulatory logic of cell fate specification in the neocortex.

Prior studies have identified several genes that broadly specify the identities of cortical projection neuron subtypes and revealed that the development of these subtypes depends on a network of transcription factors that cross-inhibit one another's expression. The zinc-finger

transcription factor *Fezf2* is expressed in deep-layer neurons. It promotes a subcerebral neuronal identity and suppresses expression of subtype-determining genes for corticothalamic (*Tbr1*) and callosal (*Satb2*) neurons (B. Chen et al., 2005a; Chen et al., 2008a; J.-G. Chen et al., 2005; Molyneaux et al., 2005). *Bcl11b*, also known as *Ctip2*, encodes a zinc-finger transcription factor expressed at high levels in layer 5 subcerebral neurons and at low levels in layer 6 corticothalamic neurons (McKenna et al., 2011). It regulates extension and fasciculation of subcerebral axons (Arlotta et al., 2005). *Tbr1* and *Sox5* are both expressed at high levels in corticothalamic projection neurons. They promote a corticothalamic neuronal fate and directly repress *Fezf2* expression and subcerebral identity in layer 6 neurons (Han et al., 2011; Kwan et al., 2008; Lai et al., 2008; McKenna et al., 2011). *Satb2* was initially reported to be specifically expressed in callosal neurons, where it promotes a callosal neuron identity by repressing genes, including *Bcl11b*, that are essential for subcerebral axon development (Alcamo et al., 2008; Britanova et al., 2008). Recent studies have shown that *Satb2* is also dynamically expressed in subcerebral neurons and is required for their fate specification (Leone et al., 2015; McKenna et al., 2015).

Despite the identification of these critical transcription factors, the molecular logic for cortical neuron subtype specification remains elusive. *Fezf2* has been the prototypic transcription factor for studying this

process in subcerebral neurons. A recent study reported that *Fezf2* directly activates the expression of genes conferring glutamatergic and subcerebral neuronal identity and represses genes associated with GABAergic and callosal neuron phenotypes, suggesting that, similar to *C. elegans* neurons (Hobert and Kratsios, 2019), the subtype identities of cortical excitatory neurons are specified by terminal selector genes (Lodato et al., 2014). However, the ability of *Fezf2* to directly activate the expression of terminal effector genes has not been rigorously tested. *Fezf2* is expressed in both radial glial cells (RGCs) and in postmitotic neurons (B. Chen et al., 2005a; Chen et al., 2008a; J.-G. Chen et al., 2005; Guo et al., 2013; Molyneaux et al., 2005), and it is unclear whether *Fezf2* is required in RGCs or in newly generated neurons to specify a subcerebral neuronal fate. The N-terminal of the FEZF2 protein contains an engrailed homology domain (EH1 domain), which is known to recruit the transducin-like enhancer of split (TLE) family transcriptional co-repressors (Hashimoto et al., 2000). It remains to be determined whether FEZF2 functions as a transcriptional repressor, an activator, or both during cortical development. Finally, previous studies and recent scRNA-seq analyses revealed that, in addition to subcerebral neurons, *Fezf2* is expressed in corticothalamic and deep-layer callosal neurons (Clare et al., 2017; Molyneaux et al., 2007; Tantirigama et al., 2016; Tasic et al., 2018). If *Fezf2* is the terminal selector gene for

subcerebral neurons, what is the function of *Fezf2* in these other neuronal subtypes?

Members of the TLE family are co-repressors that are not capable of binding DNA, but instead interact with diverse sequence-specific DNA-binding transcription factors and repress transcription of downstream genes (Jennings and Ish-Horowicz, 2008; Turki-Judeh and Courey, 2012). TLE proteins critically regulate a wide range of organogenesis, including neurogenesis, osteogenesis, and hematopoiesis (Agarwal et al., 2015; Xing et al., 2018). One class of proteins that recruit TLEs are the homeodomain family of transcription factors, through the specific interaction between the EH1 motif of the homeodomain proteins and the WD40 repeats of the TLEs. This interaction is essential for NKX2.2, NKX2.9, NKX6.1, DBX2, and PAX7 to pattern the developing neural tube in mammals (Muhr et al., 2001). The presence of an EH1 domain in the N-terminal of FEZF2 suggests that it may recruit TLE4 as a transcriptional co-repressor. Indeed, a previous study demonstrated that FEZF2 and TLE4 proteins in *Xenopus* physically interact with each other (Zhang et al., 2014).

Here, we investigate how FEZF2 regulates cell fate specification of cortical projection neurons. We demonstrate that, instead of being a terminal selector gene, *Fezf2* functions as a selective repressor in multiple neuronal subtypes to repress the expression of genes associated with

alternate subtypes. We show that, in corticothalamic neurons, FEZF2 and TLE4 co-regulate the molecular differentiation, dendritic morphology, and function of these neurons. Together with previous studies, our results suggest that distinct genetic programs act sequentially to regulate the differentiation of cortical projection neurons, with genes expressed in progenitor cells specifying the pan-cortical glutamatergic phenotype, and subtype-specifying transcription factors functioning in postmitotic cells to selectively repress the expression of genes associated with alternate subtype identities.

Results

Fezf2 is required in postmitotic neurons to regulate the development of both subcerebral and corticothalamic identities

To determine whether *Fezf2* acts in cortical RGCs or in postmitotic neurons to specify projection neuron subtype identities, we generated *Fezf2* conditional knockout mice (*Fezf2 cko*) using a *Fezf2*^{Flox} allele (Shim et al., 2012) and the *Nex*^{Cre} allele (Goebbels et al., 2006) to delete *Fezf2* in postmitotic neurons. Western blot analysis using a C-terminal FEZF2 antibody revealed that, although FEZF2 protein was absent in the *Fezf2*$^{-/-}$ null mutant cortices, a faint band of full-length FEZF2 was detected in the *Nex*^{Cre} *Fezf2*$^{Flox/-}$ (*Fezf2 cko*) cortices, indicating that the recombination was incomplete (Figure 4A). In addition,

a smaller 20-kDa band was detected in *Fezf2 cko* cortices, corresponding to the truncated C-terminal half and DNA-binding domain of FEZF2 (Figure 4A, Figure ***5***A, and Figure ***5***B).

We compared cortices from *Fezf2 cko* mice to *Fezf2*$^{+/-}$ and *Fezf2*$^{-/-}$ cortices at postnatal day 0 (P0) and P7 (Figure 4Figure ***4***E, and Figure ***5***). The *Fezf2*$^{-}$ null mutant allele contained a *PLAP* (human placenta alkaline phosphatase) knockin gene under the control of the endogenous *Fezf2* promoter and enabled us to directly observe the axons from *Fezf2*-expressing neurons (B. Chen et al., 2005a). The phenotypes of *Fezf2 cko* and *Fezf2*$^{-/-}$ cortices were similar: (1) the expression of subcerebral neuronal genes, including BCL11B and BHLHB5, were significantly reduced in layer 5 neurons (Figure 4B and Figure ***4***D); (2) expression of corticothalamic neuron genes, such as TBR1, and genes expressed at high levels in the callosal neurons, such as SATB2, were increased in layer 5 (Figure 5C and**Figure *5***D), suggesting that subcerebral neurons adopted corticothalamic and callosal identities; (3) expression of corticothalamic neuronal genes, such as TLE4, ZFPM2 (FOG2), and FOXP2 were decreased in layer 6 neurons (Figure 4Figure 5EFigure 5F); (4) expression of BCL11B was increased in layer 6, demonstrating that the molecular distinction between subcerebral and corticothalamic neurons failed to be refined in these cells (Figure 4BFigure ***4***D,Figure ***5***B, Figure ***5***E, and Figure ***5***F); (5) PLAP^{+} subcerebral

axons were significantly reduced in the pyramidal decussation (Figure 4E); and (6) consistent with a previous report (Diao et al., 2018), PLAP^{+} corticothalamic axons to the dorsal lateral geniculate nucleus (dLGN) and other thalamic nuclei were severely reduced in both *Fezf2 cko* and *Fezf2*$^{-/-}$ mice (Figure 4E).

Despite these similarities, the phenotypes of *Fezf2 cko* and *Fezf2*$^{-/-}$ cortices were not identical, likely due to incomplete recombination in *Fezf2 cko* mice (Figure 4A). Specifically, *Fezf2 cko* cortices contained a few BCL11B^{+}BHLHB5^{+} subcerebral neurons (Figure 4BFigure ***4***D), and some PLAP^{+} corticospinal axons were able to project to the pyramidal decussation (Figure 4E). However, the similarity between the phenotypes of *Fezf2 cko* and *Fezf2*$^{-/-}$ mice indicates that *Fezf2* is required in postmitotic neurons to regulate the molecular identities and axonal projections of both subcerebral and corticothalamic neurons.

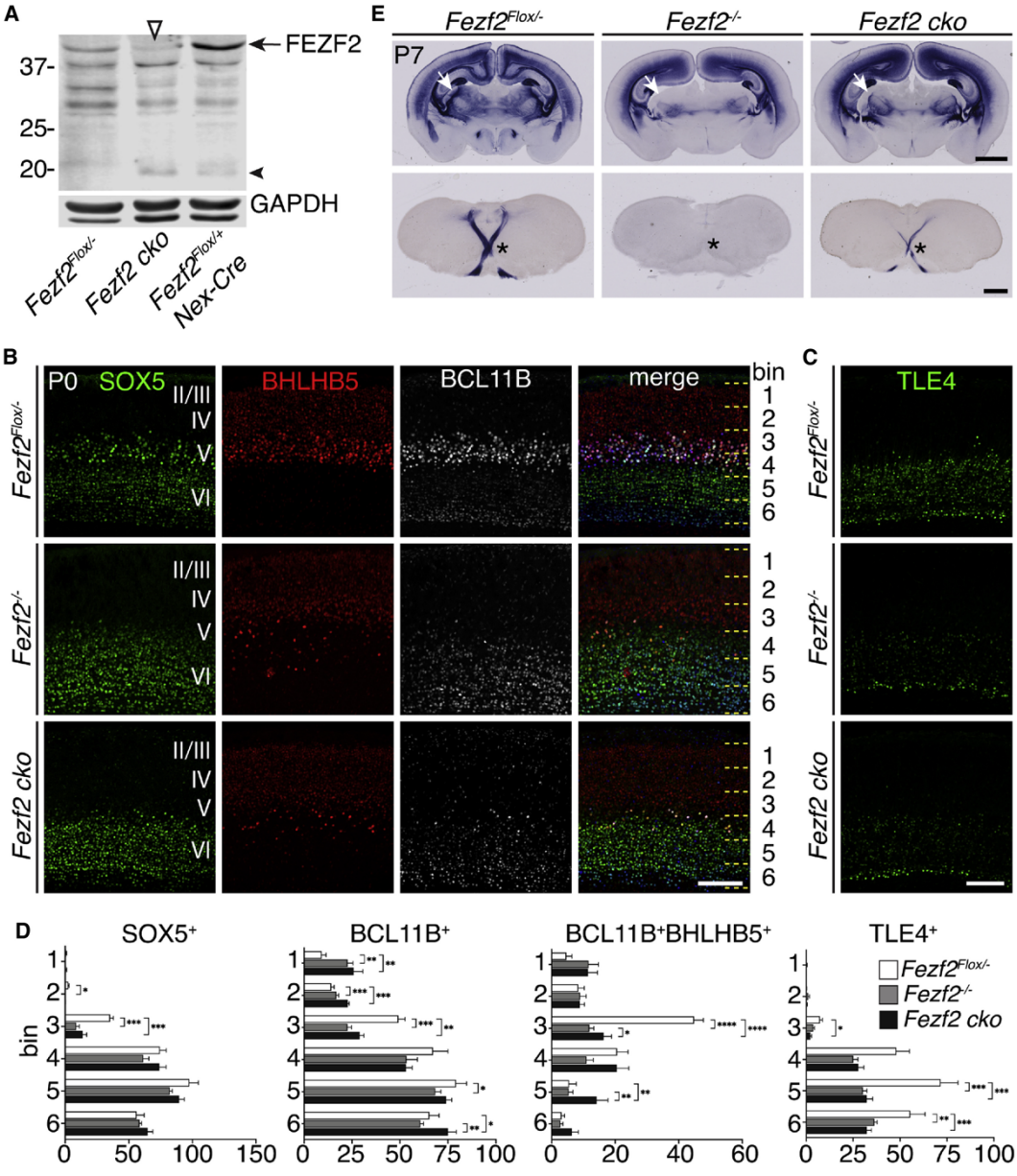
A
FEZF2
37-
25-
20-
GAPDH
Fezf2Flox/-
Fezf2 cko
Fezf2Flox/+ Nex-Cre
E
Fezf2Flox/-
Fezf2-/-
Fezf2 cko
P7
B
P0 SOX5
BHLHB5
BCL11B
merge
bin
II/III
IV
V
VI
C
TLE4
D
SOX5+
BCL11B+
BCL11B+BHLHB5+
TLE4+
bin
Fezf2Flox/-
Fezf2-/-
Fezf2 cko

Figure 4: Fezf2 functions in postmitotic neurons to specify cell identity

(A) Strategy for generating the *Fezf2-EnR* BAC transgenic mouse line.
(B) Western blot analysis of dissected cortices at P7. FEZF2 signal was normalized to GAPDH signal in each lane. n = 3 brains per genotype. Arrow, FEZF2 protein; empty triangles, non-specific bands. Signal intensities were measured using ImageStudioLite and normalized to a Gapdh internal loading control. Statistical significance was determined using one-way ANOVA followed by post hoc Tukey's t test ($*p < 0.05$, $**p < 0.01$, $***p < 0.0001$). Error bars represent SEM.
(C) Immunostaining for FEZF2 on brain sections from P7 *Fezf2*$^{+/-}$, *Fezf2*$^{-/-}$, and *Fezf2*$^{-/-}$; *Fezf2-EnR* (*EnR*) mice. Scale bar: 100 μm.
(D) Immunostaining for BCL11B, SATB2, and BHLHB5 on P7 brain sections. Scale bar for low magnification: 500 μm. Scale bar for high magnification: 100 μm.
(E–H) Quantifications of marker^{+} cells per 10,000 μm^2 in each bin. Heatmaps show the mean numbers of cells per 10,000 μm^2 for each bin. n = 3 mice per genotype, 3 sections per brain. In all graphs, error bars represent ± SEM. Statistical significance was determined using one-way ANOVA followed by post hoc Tukey's t test ($*p < 0.05$; $**p < 0.01$; $***p < 0.001$; $****p < 0.0001$). Binning was shown in (D).
(I) PLAP staining of brain sections of P7 *Fezf2*$^{+/-}$, *Fezf2*$^{-/-}$, and *Fezf2*$^{-/-}$*; EnR mice*. The top row shows coronal cortical sections; the bottom row shows coronal sections at the level of pyramidal decussation. Scale bars: 1 mm for top row; 500 μm for bottom row. White arrows, LGN; *pyramidal decussation.

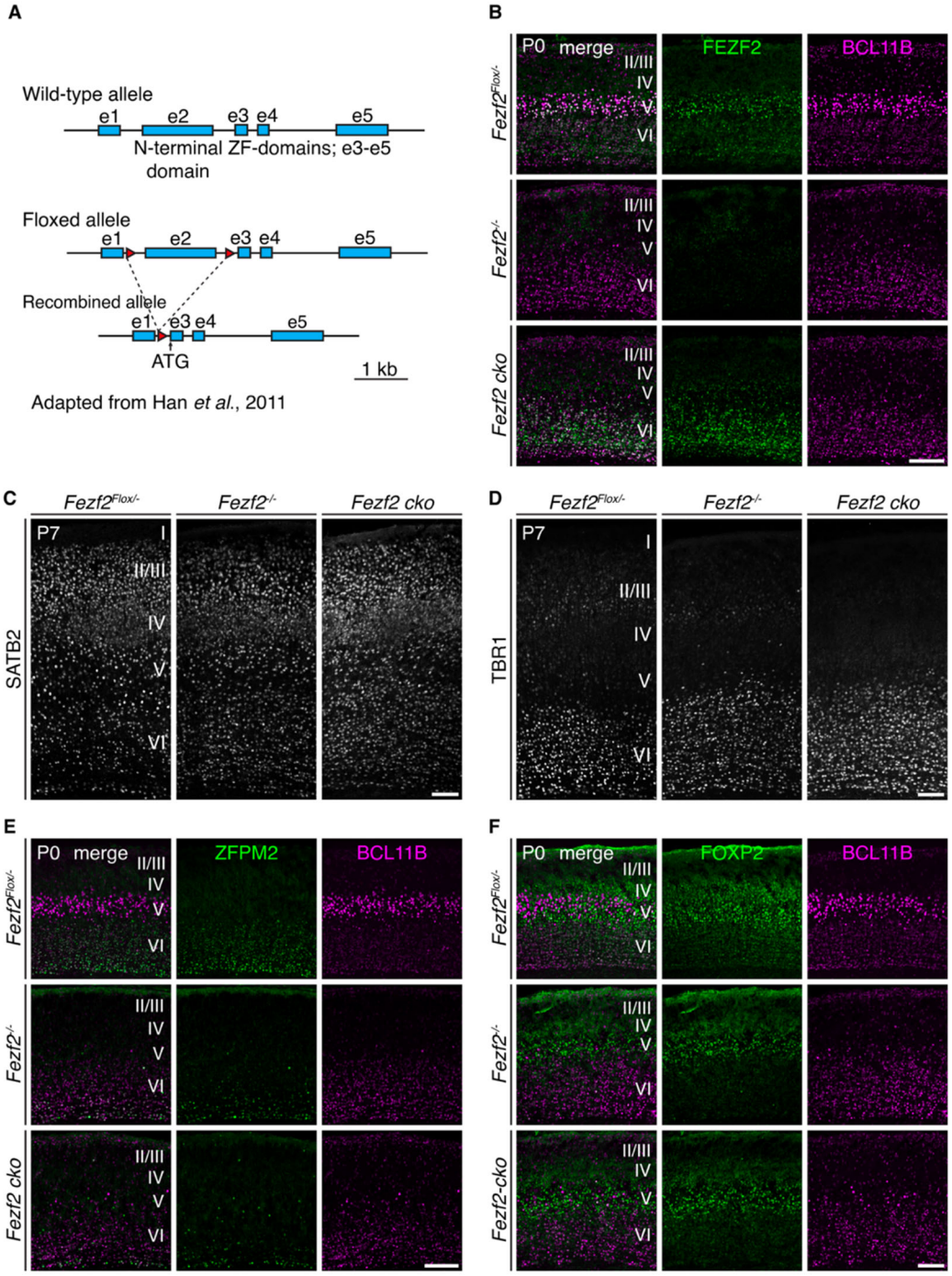
A
Wild-type allele
e1
e2
e3 e4
e5
N-terminal ZF-domains; e3-e5 domain
Floxed allele
Recombined allele
ATG
1 kb
Adapted from Han et al., 2011
B
P0 merge
FEZF2
BCL11B
Fezf2Flox/-
Fezf2-/-
Fezf2 cko
II/III
IV
V
VI
C
Fezf2Flox/-
Fezf2-/-
Fezf2 cko
P7
I
SATB2
D
TBR1
E
ZFPM2
F
FOXP2
Fezf2-cko

Figure 5: The *Fezf2-/-* and *Fezf2 cko* mice show similar molecular defects in the cortical projection neurons

(A) The recombined *Fezf2^{Flox}* allele encodes a truncated FEZF2 protein consisting of the zinc finger DNA binding domain alone.
(B) Immunostaining using a C-terminal FEZF2 antibody shows the complete absence of FEZF2 protein in the *Fezf2$^{-/-}$* mice, and increased expression of the truncated FEZF2 protein in layer 6 in the *Fezf2 cko* mice.
(C) SATB2 protein expression is increased in the deep layers of *Fezf2$^{-/-}$* and *Fezf2 cko* cortices.
(D) TBR1 protein expression is increased in the layer 5 of *Fezf2$^{-/-}$* and *Fezf2 cko* cortices.
(E-F) ZFPM2 (E) and FOXP2 (F) expression is reduced in layer 6 of *Fezf2$^{-/-}$* and *Fezf2 cko* cortices. Scale bars: 100 μm.

FEZF2 functions as a transcriptional repressor to specify cortical projection neuron subtypes

FEZF2 consists of an N-terminal half containing an EH1 domain and other sequences and a C-terminal half consisting of six C2H2-type zinc-finger motifs (Hashimoto et al., 2000). Zinc-finger motifs are involved in DNA binding, and the EH1 domain recruits TLE family transcriptional co-repressors. To test whether FEFZ2 functions as a transcriptional repressor, an activator, or both, we generated expression plasmids encoding a full-length FEZF2 protein, a chimeric protein consisting of the transcriptional repressor domain of the engrailed protein (EnR) fused with the DNA-binding domain of FEZF2 (*pCAG-Fezf2-EnR*), or a chimeric protein consisting of the VP16 transcription activator domain (VP16) fused with the DNA-binding domain of FEZF2 (*pCAG-Fezf2-VP16*; Figure 7A). We co-electroporated each plasmid with a *pCAG-EGFP* plasmid into the cortical ventricular zone of embryonic day 15.5 (E15.5) wild-type embryos and examined the brains at P5 (Figure 7B). In all the electroporated brains, GFP^+ neurons were located in layers 2 and 3 and GFP^+ callosal axons were observed. GFP^+ axons were not detectable in the thalamus or pons of brains electroporated with the *pCAG-EGFP* plasmid alone or in brains electroporated with *pFezf2-VP16* plasmids. However, both full-length FEZF2 and FEZF2-EnR directed layer 2 and 3 neurons to project GFP^+ axons into the thalamus and cerebral peduncle (Figure 7B).

To determine whether FEZF2 functions primarily as a transcriptional repressor during deep-layer neuronal differentiation, we generated a transgenic line expressing the FEZF2-EnR chimeric protein using a bacterial artificial chromosome (BAC) (Figure 6A). This BAC consisted of a 200-kb region flanking the *Fezf2* gene. We inserted the FEZF2-EnR open reading frame at the endogenous *Fezf2* translation start site, immediately followed by a transcription termination signal. Western blot analysis confirmed that endogenous FEZF2 protein was not expressed from the *Fezf2-EnR* transgenic allele (Figure 6B). Immunostaining showed that expression of the FEZF2-EnR protein recapitulates that of endogenous *Fezf2* (Figure 6C).

We then determined whether FEZF2-EnR can rescue the defects resulting from a loss of *Fezf2* by comparing the brains of *Fezf2*$^{+/-}$, *Fezf2*$^{-/-}$, and *Fezf2*$^{-/-}$*; Fezf2-EnR* mice (Figure 6D-I, andFigure ***7***C-E). The expression patterns of subcerebral neuronal markers, such as BCL11B and BHLHB5 (Figure 6D, Figure ***6***E, and Figure ***6***G), were restored in layer 5 neurons in *Fezf2*$^{-/-}$*; Fezf2-EnR* mice. Similarly, the expression patterns of corticothalamic neuronal genes, such as TLE4, FOXP2, and ZFPM2 (Figure 7C-7E) were restored. The ectopic expression of TBR1 (data not shown), FOSL2 (Figure 7C), and SATB2 (Figure 6DFigure 6F) in layer 5 was no longer detected. Furthermore, PLAP^{+} axons projected into the pyramidal decussation, the dLGN, and other thalamic nuclei in

the *Fezf2*$^{-/-}$*; Fezf2-EnR* mice (Figure 6I). Thus, the *Fezf2-EnR* allele rescued the defects observed in layer 5 and layer 6 neurons in *Fezf2*$^{-/-}$ mice, indicating that FEZF2 functions as a transcriptional repressor.

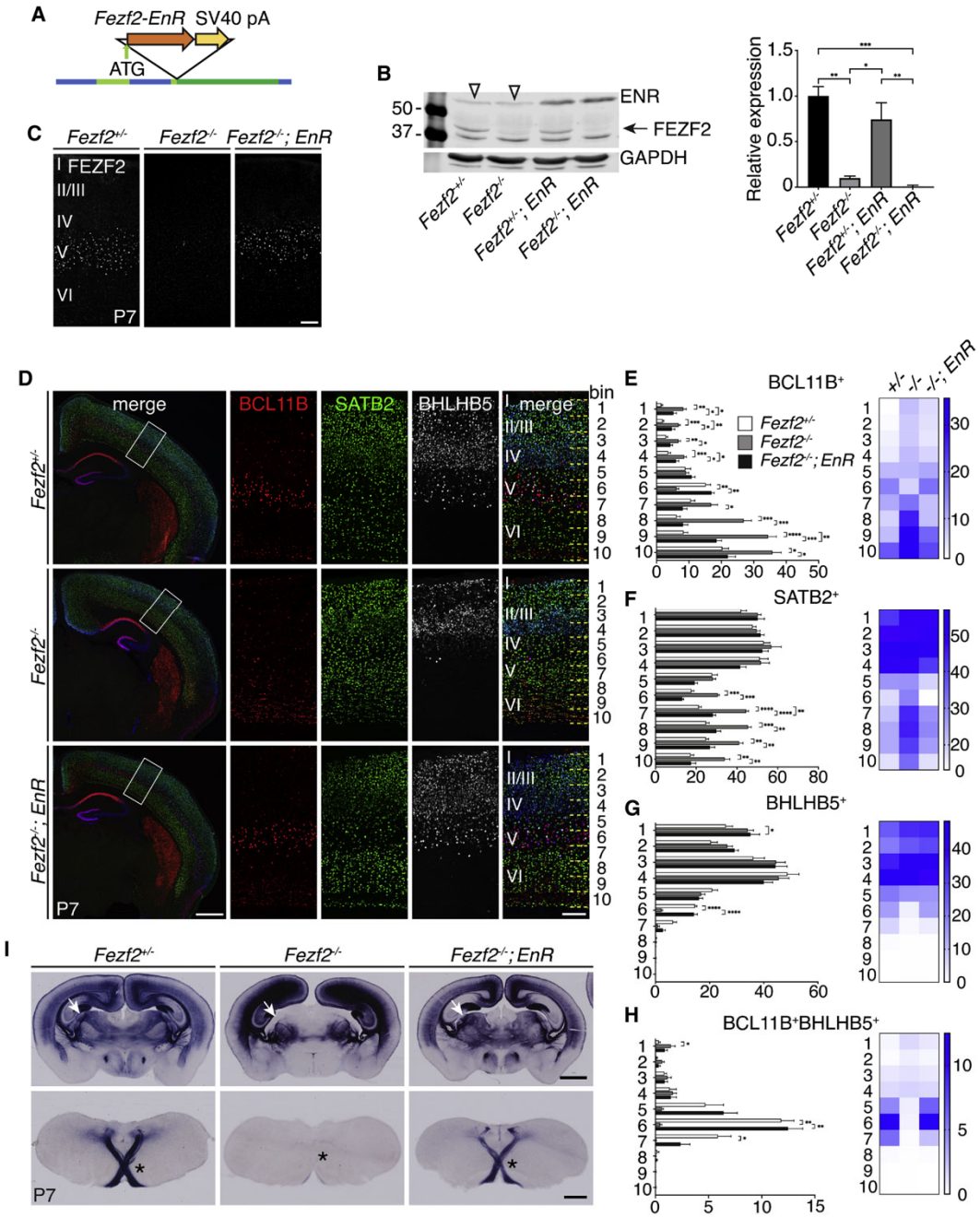

Figure 6: FEZF2 functions as a transcriptional repressor in cortical development

(A) Strategy for generating the *Fezf2-EnR* BAC transgenic mouse line.
(B) Western blot analysis of dissected cortices at P7. FEZF2 signal was normalized to GAPDH signal in each lane. n = 3 brains per genotype. Arrow, FEZF2 protein; empty triangles, non-specific bands. Signal intensities were measured using ImageStudioLite and normalized to a Gapdh internal loading control. Statistical significance was determined using one-way ANOVA followed by post hoc Tukey's t test ($*p < 0.05$, $**p < 0.01$, $***p < 0.0001$). Error bars represent SEM.
(C) Immunostaining for FEZF2 on brain sections from P7 *Fezf2*$^{+/-}$, *Fezf2*$^{-/-}$, and *Fezf2*$^{-/-}$; *Fezf2-EnR* (*EnR*) mice. Scale bar: 100 μm.
(D) Immunostaining for BCL11B, SATB2, and BHLHB5 on P7 brain sections. Scale bar for low magnification: 500 μm. Scale bar for high magnification: 100 μm.
(E–H) Quantifications of marker^{+} cells per 10,000 μm^2 in each bin. Heatmaps show the mean numbers of cells per 10,000 μm^2 for each bin. n = 3 mice per genotype, 3 sections per brain. In all graphs, error bars represent ± SEM. Statistical significance was determined using one-way ANOVA followed by post hoc Tukey's t test ($*p < 0.05$; $**p < 0.01$; $***p < 0.001$; $****p < 0.0001$). Binning was shown in (D).
(I) PLAP staining of brain sections of P7 *Fezf2*$^{+/-}$, *Fezf2*$^{-/-}$, and *Fezf2*$^{-/-}$*; EnR mice*. The top row shows coronal cortical sections; the bottom row shows coronal sections at the level of pyramidal decussation. Scale bars: 1 mm for top row; 500 μm for bottom row. White arrows, LGN; *pyramidal decussation.

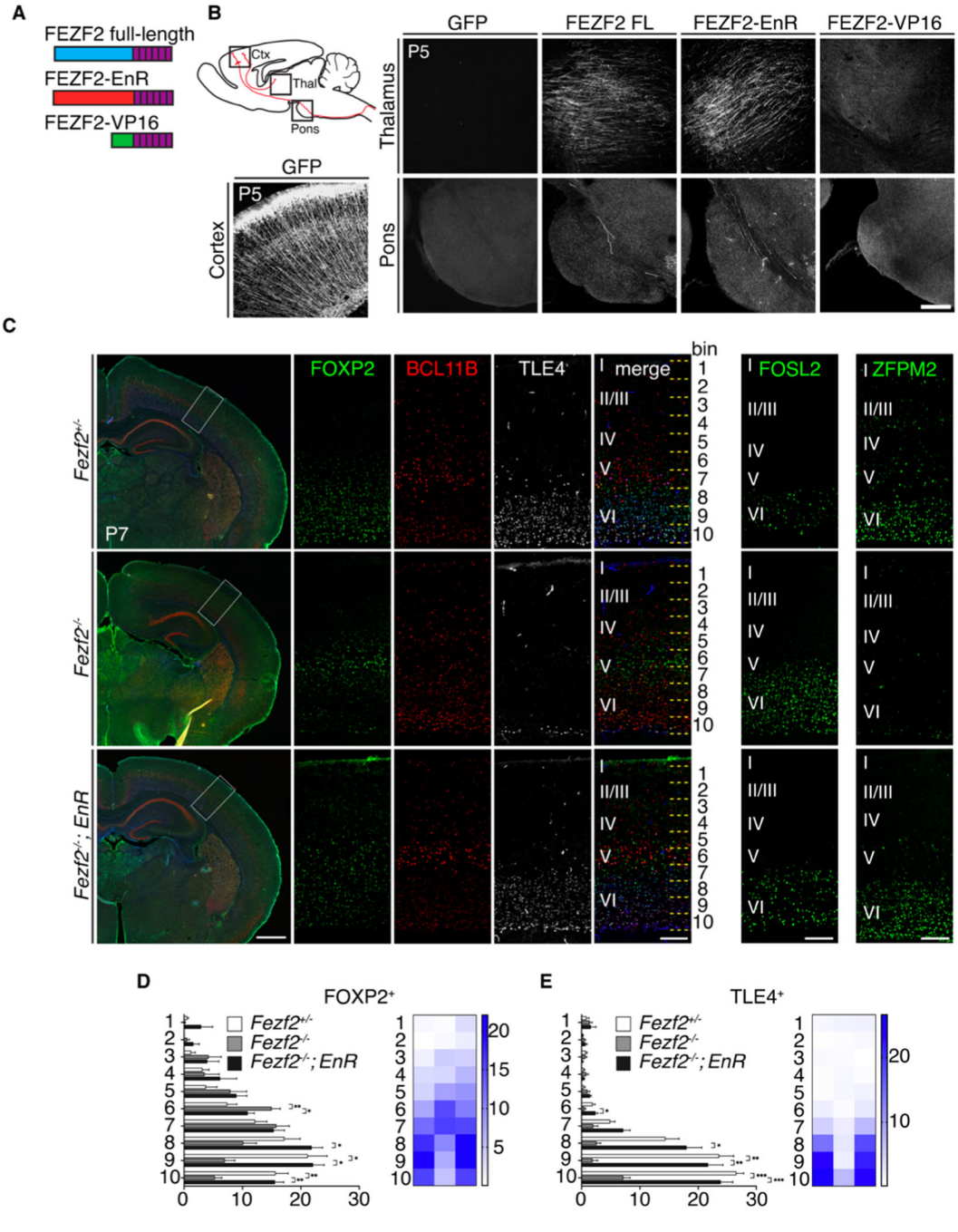
A
FEZF2 full-length
FEZF2-EnR
FEZF2-VP16
B
Ctx
Thal
Pons
GFP
FEZF2 FL
FEZF2-EnR
FEZF2-VP16
P5
Thalamus
Pons
Cortex
C
bin
FOXP2
BCL11B
TLE4
merge
FOSL2
ZFPM2
Fezf2+/-
Fezf2-/-
Fezf2-/-; EnR
P7
I
II/III
IV
V
VI
D
FOXP2+
E
TLE4+

Figure 7: FEZF2 functions as a transcriptional repressor during cortical development

(A) Schematic representations of full-length FEZF2 protein, the FEZF2-EnR chimeric protein, and the FEZF2-VP16 chimeric protein. blue: the N-terminal half of FEZF2; purple: the 6 C2H2-type zinc finger motifs of FEZF2; red: the EnR transcriptional repressor domain; green: the VP16 transcriptional activator domain.

(B) Over-expression of full-length FEZF2, FEZF2-EnR, and FEZF2-VP16 into layer 2/3 neurons by *in utero* electroporation at E15.5, and the effect on axonal projection was assessed at P5 using GFP immunostaining. GFP labeled cells and axons in three boxed areas (cortex, thalamus and pontine nuclei) were shown. Scale bar, 200 μm.

(C) Immunostaining of FOXP2, BCL11B, TLE4 and FOSL2 in brains of P7 *Fezf2*$^{+/-}$, *Fezf2*$^{-/-}$, and *Fezf2*$^{-/-}$*; Fezf2-EnR* mice. Scale bars: low mag, 500 μm, high mag 100 μm.

(D-E) Quantifications of marker^{+} cells per 10,000 μm^2 per bin. n=3 brains per genotype, 3 sections per brain. In all graphs, error bars represent ± SEM. Statistical significance was determined using one-was ANOVA followed by post hoc Tukey's t-test (*p<0.05, **p<0.01, ***p<0.001). Heatmaps show mean numbers of cells per 10,000μm^2 for each bin.

Fezf2-EnR broadly rescues gene expression defects in the *Fezf2*$^{-/-}$ cortices

To further investigate how FEZF2 regulates projection subtype identities, we performed bulk RNA-seq analysis of cortices from P0 *Fezf2*$^{-/-}$, *Fezf2*$^{-/-}$*; Fezf2-EnR*, and control *Fezf2*$^{+/+}$ mice (Figure 8 and Figure ***11***). Compared to the *Fezf2*$^{+/+}$ mice, the expression levels of 408 genes were mis-regulated in the *Fezf2*$^{-/-}$ cortices ($p < 0.05$). 140 genes showed reduced expression, and 268 showed increased expression. DAVID analysis (https://david.ncifcrf.gov) revealed that the top Gene Ontology (GO) terms associated with mis-regulated genes in *Fezf2*$^{-/-}$ cortices were extracellular region, multicellular organism development, collagen fibril organization, synapse, and cell junction. We examined the expression of these mis-regulated genes in specific subtypes of cortical neurons using the DeCoN dataset (Molyneaux et al., 2015) and found that 88 of the 140 genes showing reduced expression in *Fezf2*$^{-/-}$ cortices were subtype specific: 34 genes were enriched in subcerebral neurons; 43 in corticothalamic neurons; and 11 in corticocortical neurons. Among the 268 genes showing increased expression in *Fezf2*$^{-/-}$ cortices, 125 were subtype specific: 54 were enriched in corticocortical neurons; 43 in corticothalamic neurons; and 28 in subcerebral neurons (Figure 8A). Consistent with the immunohistochemistry results (Figure 6 and Figure ***7***), RNA-seq analysis

of the *Fezf2*$^{-/-}$*; Fezf2-EnR* cortices revealed that *Fezf2-EnR* broadly rescues these gene expression defects in the *Fezf2*$^{-/-}$ cortices (Figure 8A).

We performed *in situ* hybridization to validate the RNA-seq analysis. Expressions of layer 5 subcerebral neuronal genes *Ephb1*, *Tcerg1*, and *Ldb2* were reduced in the *Fezf2*$^{-/-}$ cortices, and their expressions were restored in layer 5 neurons in *Fezf2*$^{-/-}$*; Fezf2-EnR* mice (Figure 8B). Corticothalamic neuronal gene *Wnt7b* and the subplate neuronal gene *Ctgf* showed reduced expressions in the *Fezf2*$^{-/-}$ cortices; their expressions were rescued in the *Fezf2-EnR* mice (Figure 8C). *Kif26a*, a gene expressed in multiple neuronal subtypes, showed reduced expression in *Fezf2*$^{-/-}$ cortices; its expression was restored in *Fezf2*$^{-/-}$*; Fezf2-EnR* mice (Figure 8C). Expression of the corticothalamic neuronal gene, *Cryab*, was increased in the *Fezf2*$^{-/-}$ cortices; its expression was restored in *Fezf2*$^{-/-}$*; Fezf2-EnR* mice (Figure 8C). The broad rescue of gene expression defects in the *Fezf2*$^{-/-}$ cortices by the *Fezf2-EnR* allele demonstrates that FEZF2 functions as a transcriptional repressor in specifying cortical projection neuron identities.

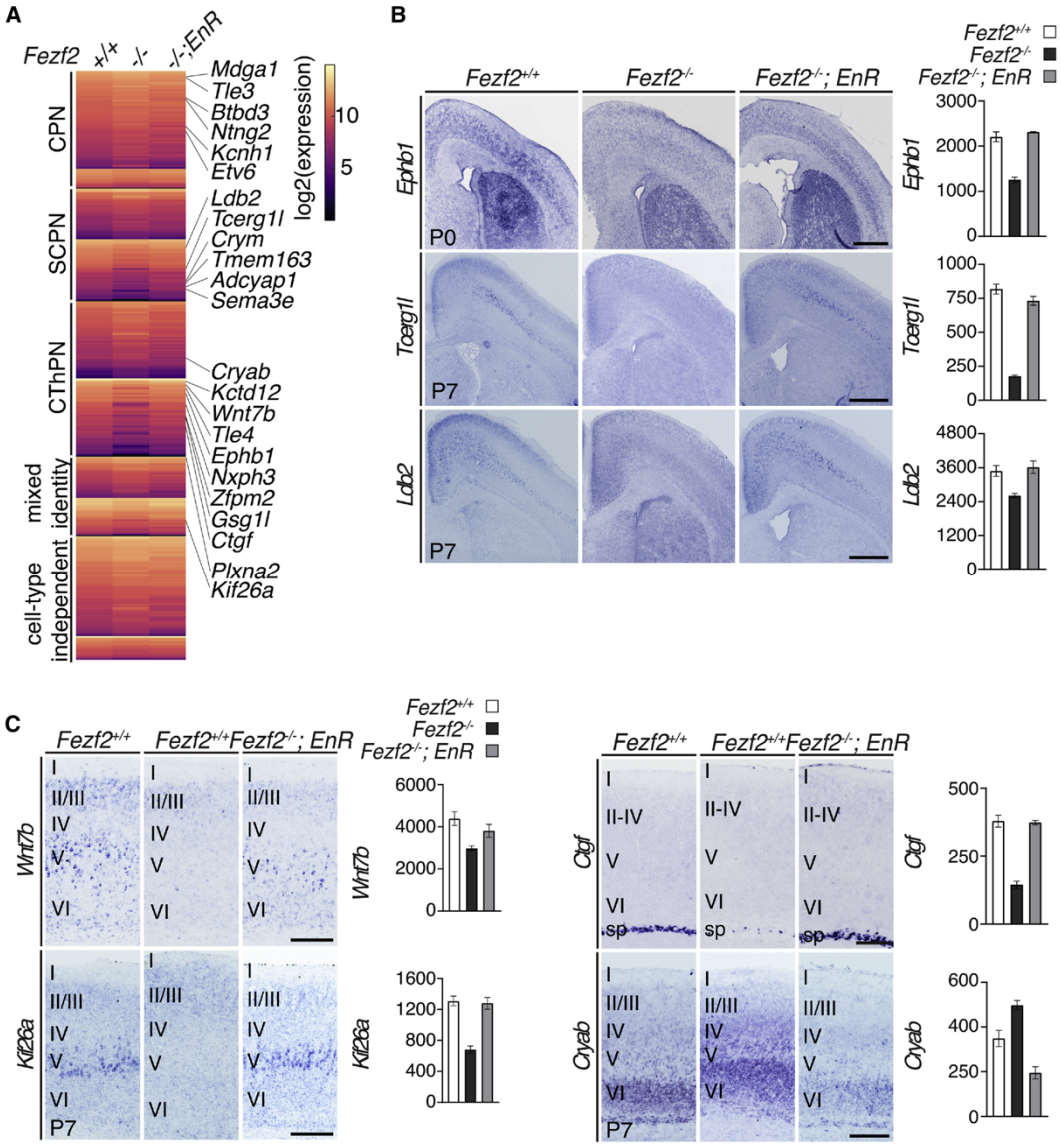
A
Fezf2 +/+ -/- -/-;EnR
log2(expression)
10
5
CPN
SCPN
CThPN
mixed identity
cell-type independent
Mdga1
Tle3
Btbd3
Ntng2
Kcnh1
Etv6
Ldb2
Tcerg1l
Crym
Tmem163
Adcyap1
Sema3e
Cryab
Kctd12
Wnt7b
Tle4
Ephb1
Nxph3
Zfpm2
Gsg1l
Ctgf
Plxna2
Kif26a
B
Fezf2+/+
Fezf2-/-
Fezf2-/-; EnR
Ephb1
Tcerg1l
Ldb2
P0
P7
P7
C
Wnt7b
Kif26a
Ctgf
Cyab
I
II/III
II-IV
IV
V
VI
sp
P7

Figure 8: Genes mis-regulated in *Fezf2*$^{-/-}$ cortices were enriched in projection neuron subtype-specific genes

(A) Left heatmap shows normalized gene expression levels in P0 *Fezf2*$^{-/-}$ (n = 4), *Fezf2*$^{-/-}$*; Fezf2-EnR* (n = 2), and control *Fezf2*$^{+/+}$ (n = 3) cortices. The subtype specificities for the mis-regulated genes were determined based on the DeCoN dataset. CPN, callosal projection neuronal genes; CThPN, corticothalamic neuronal genes; SCPN, layer 5 subcerebral projection neuronal genes; mixed identity, genes expressed in more than one neuronal subtype; cell-type independent, genes expressed in all subtypes.
(B and C) *In situ* hybridization and RNA-seq analyses showed reduced expressions for *Ephb1*, *Tcerg1l*, *Ldb2*, *Wnt7b*, *Kif26a*, and *Ctgf* and increased expression of *Cryab* in *Fezf2*$^{-/-}$ cortices, which were restored in the *Fezf2*$^{-/-}$*; Fezf2-EnR* mice. Bar graphs showed normalized mRNA expression levels detected by RNA-seq in the cortices for the P0 *Fezf2*$^{+/+}$ (n = 3 mice), *Fezf2*$^{-/-}$ (n = 4 mice), and *Fezf2*$^{-/-}$*; Fezf2-EnR* (n = 2 mice) mice. Error bars represent SEM. Scale bars: 500 μm in (B) and 200 μm in (C).

TLE4 and FEZF2 are co-expressed in differentiating corticothalamic neurons and interact with each other

The N-terminal region of the FEZF2 protein contains an EH1 motif, which can recruit the TLE family co-repressors (Muhr et al., 2001). A previous study reported that *Xenopus* FEZF2 and TLE4 proteins directly interact with each other (Zhang et al., 2014). Indeed, co-immunoprecipitation experiments revealed that the mouse FEZF2 and TLE4 also can bind to each other (Figure 9A). To determine whether FEZF2 recruits TLE4 to regulate the development of deep-layer neurons, we performed immunostaining using antibodies against FEZF2 and TLE4, which showed that the two proteins were co-expressed in layer 6 neurons (Figure 9B).

To identify the neuronal subtype that expresses TLE4, we performed retrograde tracing by injecting fluorescence-conjugated cholera toxin beta subunit (CTB) into the thalamus, pyramidal decussation, or contralateral cortex (Figure 9C). More than 99% of retrogradely labeled corticothalamic neurons expressed TLE4, whereas labeled subcerebral neurons and callosal neurons did not (<1%). Thus, TLE4 is specifically expressed in corticothalamic neurons.

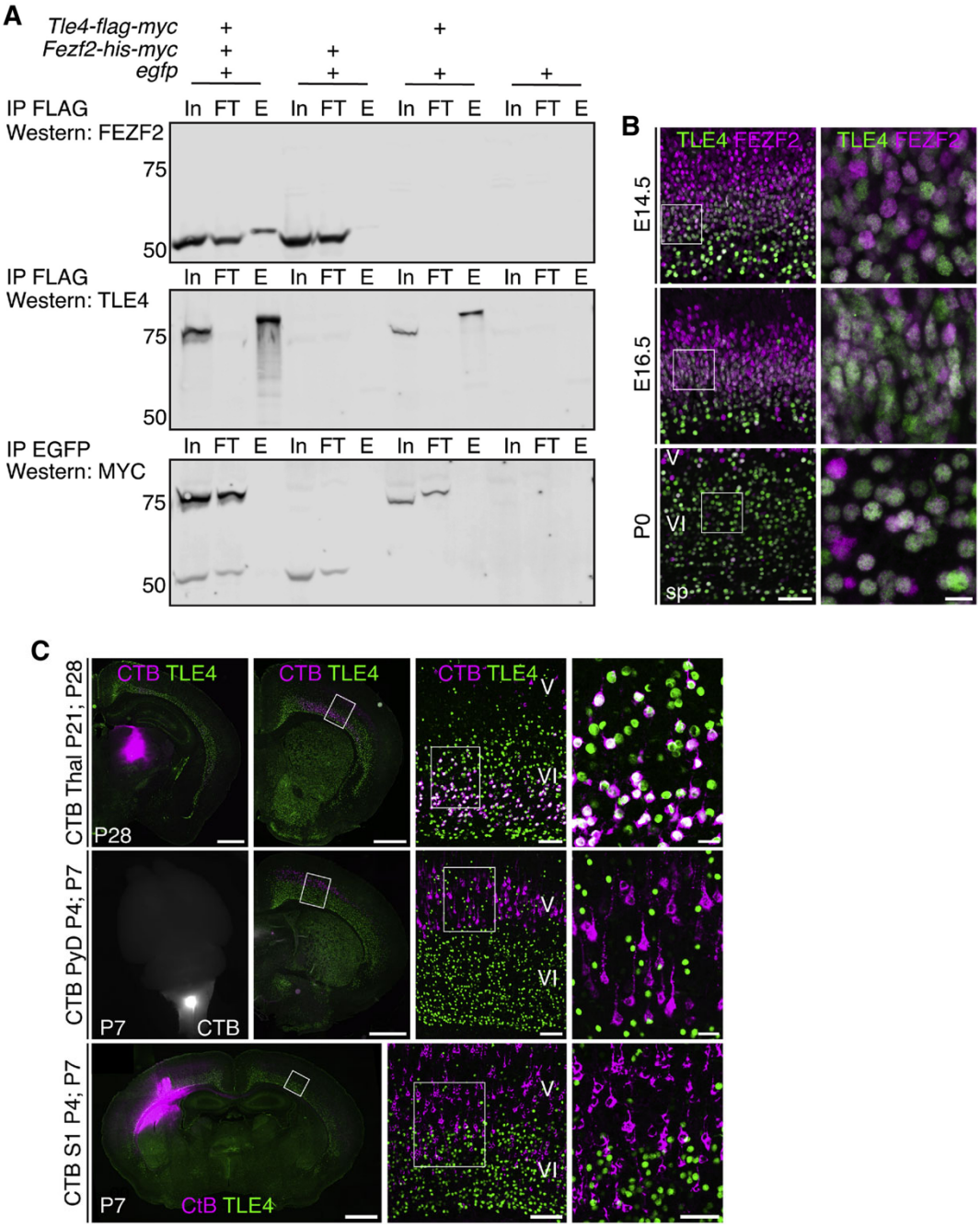
A
Tle4-flag-myc
Fezf2-his-myc
egfp
IP FLAG
Western: FEZF2
IP FLAG
Western: TLE4
IP EGFP
Western: MYC
In FT E
75
50
B
TLE4 FEZF2
E14.5
E16.5
P0
V
VI
sp
C
CTB TLE4
CTB Thal P21; P28
P28
CTB PyD P4; P7
P7
CTB
CTB S1 P4; P7
CtB TLE4

Figure 9: TLE4 and FEZF2 can bind to each other and are co-expressed in the corticothalamic neurons

(A) Co-immunoprecipitation experiment showed that mouse FEZF2 and TLE4 proteins can bind each other. E, elution; FT, flow through; In, input. The bands around 50 KD are FEZF2-HIS-MYC; the bands around 75 KD are TLE4-FLAG-MYC.
(B) Immunostaining for TLE4 and FEZF2 on brain sections from E14.5, E16.5, and P0 in wild-type mice. Low-mag single z-plane image scale bar: 50 μm; high-mag maximum z-projection image scale bar: 10 μm.
(C) Combined retrograde tracing and immunostaining show that TLE4 is expressed in >99% of retrogradely labeled corticothalamic neurons in M1 (1,034 $TLE4^+CTB^+$ among 1,050 CTB^+ cells), 0% of the traced subcerebral projection neurons (930 cells), and 0.1% of the callosal projection neurons (2 $TLE4^+CTB^+$ among 1,783 CTB^+ cells). n = 3 mice for each injection location and 3 sections per brain were quantified. Low-mag scale bars: 1,000 μm. Scale bars in the second column from the right: 100 μm. Scale bars in the rightmost column: 20 μm.

Corticothalamic axons developed normally in the *Tle4*$^{LacZ/LacZ}$ mice

To test the function of *Tle4* in the specification and differentiation of corticothalamic neurons, we generated a *Tle4* mutant allele (*Tle4*^{LacZ}) by inserting a *BGal-ires-Plap* cassette into the 4th intron of the *Tle4* gene (Figure 11A). The BGAL and PLAP reporters enabled us to label the cell bodies and axons of *Tle4* heterozygous and mutant neurons (Figure 11B Figure 11D). In *Tle4*$^{+/LacZ}$ brains, BGAL expression recapitulated the endogenous pattern of TLE4 expression (Figure 11B). Immunostaining revealed that TLE4 protein was not present in *Tle4*$^{LacZ/LacZ}$ mice (Figure 11C). In both *Tle4*$^{+/LacZ}$ and *Tle4*$^{LacZ/LacZ}$ mice, PLAP^{+} axons extended from cortex to the thalamus, with no obvious difference between control and mutant brains (Figure 11D). We performed anterograde tracing by injecting adeno-associated virus (AAV)-mcherry virus into the primary motor cortex (M1), primary somatosensory cortex (S1), and primary visual cortex (V1) cortical areas, which confirmed that corticothalamic axons developed normally in *Tle4*$^{LacZ/LacZ}$ mice (Figure 11E; data not shown).

Molecular differentiation of corticothalamic neurons is defective in *Tle4*$^{LacZ/LacZ}$ mice

We performed RNA-seq analysis of control and *Tle4*$^{LacZ/LacZ}$ P0 cortices (n = 3 mice for each genotype). 428 genes were mis-regulated in the *Tle4*$^{LacZ/LacZ}$ cortices ($p < 0.05$; Student's t test). Using the DeCoN

dataset (Molyneaux et al., 2015), we examined the neuronal subtype-specific expression of all mis-regulated genes. Among the 228 genes with reduced expression, 11 were associated with corticocortical neurons, 56 were specifically expressed in corticothalamic neurons, and 24 in subcerebral neurons. Among the 200 upregulated genes, 14 were associated with corticocortical neurons, 45 were enriched in subcerebral neurons, and 14 in corticothalamic neurons (Figure 10A).

We performed immunohistochemistry and *in situ* hybridization to validate the RNA-seq results. Consistent with the normal corticothalamic axons observed in *Tle4*$^{LacZ/LacZ}$ brains, the expression of TBR1 and SOX5, two genes essential for specifying a corticothalamic neuron identity, were not significantly affected (Figure 12A andFigure ***12***B). However, the number of BGAL^{+} neurons was significantly reduced in layer 5 and layer 6a in *Tle4*$^{LacZ/LacZ}$ mice (Figure 10B). Expression of other layer 6 neuron markers, such as ZFPM2 (Figure 10B) and FOXP2 (Figure 12C), was also significantly reduced. High expression levels of FEZF2, BCL11B, BHLHB5, *Ldb2*, and *Tcerg1l* are normally associated with layer 5 subcerebral neurons, but in *Tle4*$^{LacZ/LacZ}$ mice, their expression was significantly increased in layer 6 (Figure 10C,Figure ***10***D, Figure ***16***A,Figure 16B).

The reduced numbers of BGAL^{+}, ZFPM2^{+}, and FOXP2^{+} cells in *Tle4*$^{LacZ/LacZ}$ mice could be due to reduced neuronal production,

increased cell death, or defective molecular differentiation, while the increased numbers of cells expressing BCL11B, FEZF2, and other subcerebral neuron markers in layer 6 could be due to a migration defect of layer 5 neurons or the mis-regulation of these genes in layer 6 neurons. To ascertain whether the production or migration of layer 5 and 6 neurons was affected in *Tle4*$^{LacZ/LacZ}$ mice, we performed birthdating experiments by injecting EdU into pregnant mice on E12.5 or E13.5 and analyzing the brains of *Tle4*$^{LacZ/LacZ}$ and littermate control mice at P7. For both labeling dates, we saw no significant change in the number or distribution of EdU^{+} cells in the deep layers of *Tle4*$^{LacZ/LacZ}$ cortices (Figure 13A andFigure ***13***B). We then stained sections from control and *Tle4*$^{LacZ/LacZ}$ cortices at E14, P0, and P7 with an antibody against activated caspase 3 (AC3) and observed no significant difference in the numbers of AC3^{+} cells between genotypes at any age (Figure 13).

Together, these results indicate that, in *Tle4*$^{LacZ/LacZ}$ mice, corticothalamic neurons were generated in appropriate numbers, migrated to their normal laminar destinations, and projected axons to the thalamus. However, the molecular differentiation of these neurons was impaired, resulting in the expression of genes normally associated with layer 5 subcerebral neurons.

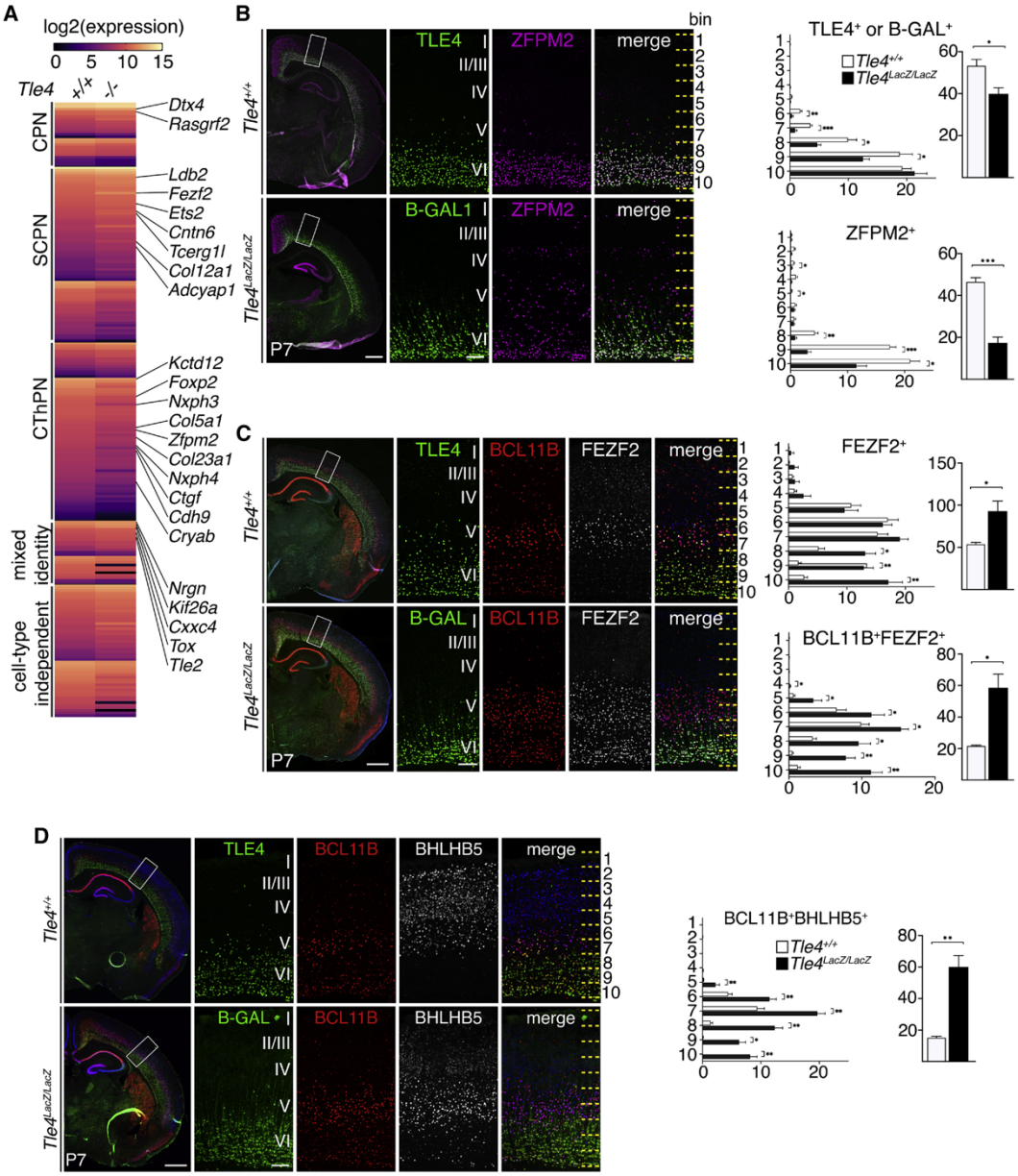
A
log2(expression)
0 5 10 15
Tle4 +/+ -/-
CPN
SCPN
CThPN
mixed identity
cell-type independent
Dtx4
Rasgrf2
Ldb2
Fezf2
Ets2
Cntn6
Tcerg1l
Col12a1
Adcyap1
Kctd12
Foxp2
Nxph3
Col5a1
Zfpm2
Col23a1
Nxph4
Ctgf
Cdh9
Cryab
Nrgn
Kif26a
Cxxc4
Tox
Tle2
B
bin
Tle4+/+
Tle4LacZ/LacZ
TLE4
B-GAL1
ZFPM2
merge
I
II/III
IV
V
VI
P7
TLE4+ or B-GAL+
Tle4+/+
Tle4LacZ/LacZ
ZFPM2+
C
BCL11B
FEZF2
FEZF2+
BCL11B+FEZF2+
D
BHLHB5
BCL11B+BHLHB5+

Figure 10: Molecular differentiation of corticothalamic neurons was defective in *Tle4*$^{LacZ/LacZ}$ brains

(A) Heatmap showing normalized gene expression levels in the *Tle4*$^{+/+}$ and *Tle4*$^{LacZ/LacZ}$ cortices. The subtype specificities for the mis-regulated genes were determined based on the DeCoN dataset.
(B) Immunostaining of TLE4 or B-GAL and ZFPM2 in the P7 brains and quantifications of the numbers of TLE4^{+} or B-GAL^{+} and ZFPM2^{+} cells by bin and total cell counts.
(C) Immunostaining of TLE4 or B-GAL, BCL11B, and FEZF2 in the P7 brains and quantifications of the FEZF2^{+} and BCL11B^{+}FEZF2^{+} cells by bin and total cell counts.
(D) Immunostaining of TLE4 or B-GAL, BCL11B, and BHLHB5 in the P7 brains and quantifications of the BCL11B^{+}BHLHB5^{+} cells n = 3 brains per genotype, 3 sections per brain. Quantifications of marker^{+} cells per 10,000 μm^2 in each bin are shown. In all graphs, error bars represent ± SEM. Statistical significance was determined using the unpaired Student's t test ($^{*}p < 0.05$; $^{**}p < 0.01$; $^{***}p < 0.001$). Scale bars: low-mag, 500 μm; high-mag, 100 μm.

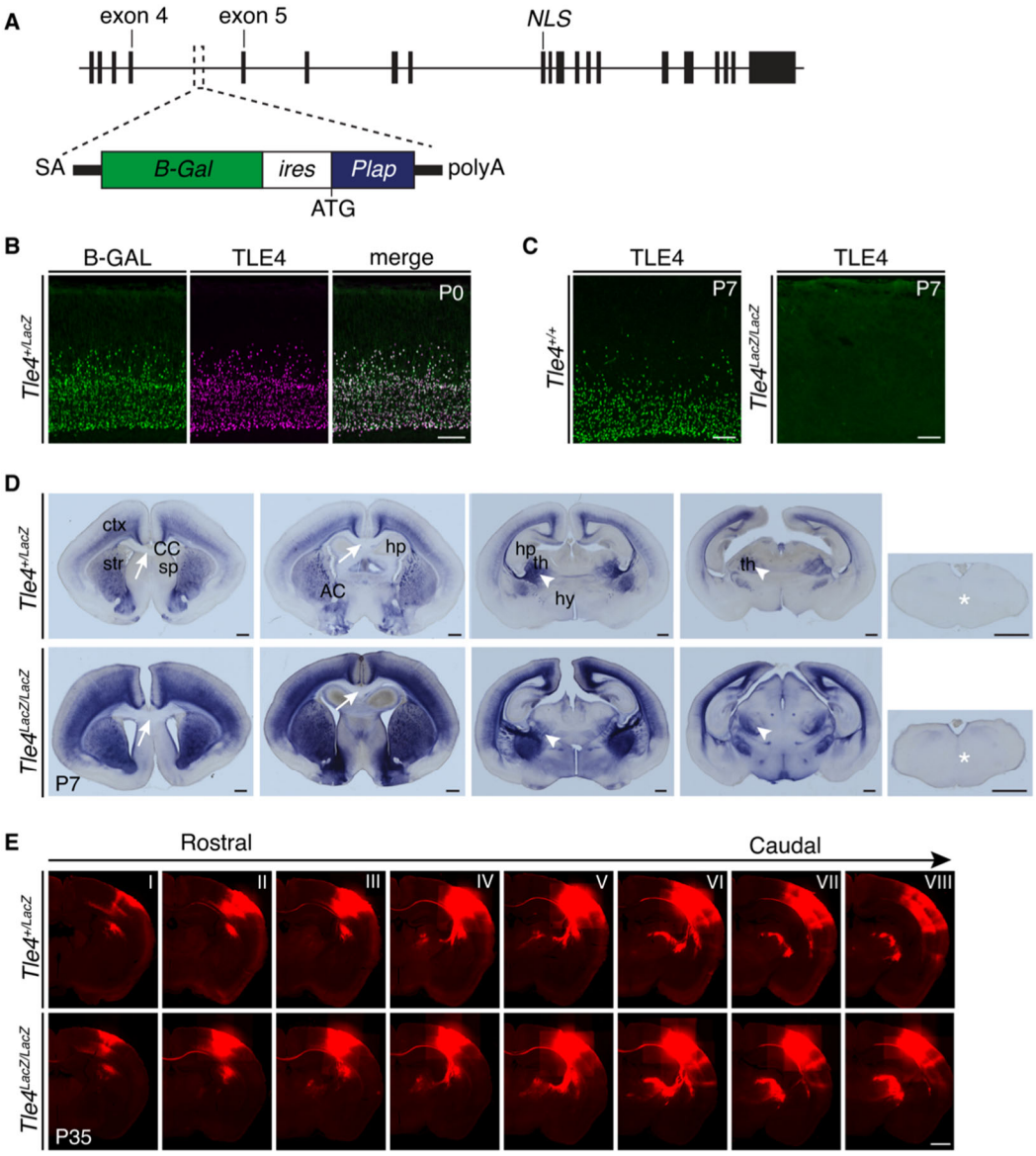
A
exon 4
exon 5
NLS
SA
B-Gal
ires
Plap
polyA
ATG
B
B-GAL
TLE4
merge
P0
Tle4+/LacZ
C
TLE4
TLE4
P7
P7
Tle4+/+
Tle4LacZ/LacZ
D
ctx
str
CC
sp
hp
AC
hp
th
hy
th
*
Tle4+/LacZ
Tle4LacZ/LacZ
P7
*
E
Rostral
Caudal
I
II
III
IV
V
VI
VII
VIII
Tle4+/LacZ
Tle4LacZ/LacZ
P35

Figure 11: Corticothalamic neurons project axons properly into the thalamus of *Tle4LacZ/LacZ* mice

(A) Knockout strategy for *Tle4*. The SA-B-Gal-ires-Plap cassette was inserted into the intron after exon 4. *SA*: splicing acceptor; *B-Gal*: β-galactosidase; *ires*: internal ribosome entry site; *Plap*: human placental alkaline phosphatase; *NLS: nuclear localization signal.*
(B) Immunostaining showed that B-GAL recapitulates TLE4 expression pattern in the *Tle4*$^{+/LacZ}$ mice. Scale bar: 100 µm.
(C) TLE4 protein is not detected by immunostaining in the *Tle4*$^{LacZ/LacZ}$ mice Scale bar: 100µm.
(D) PLAP staining of P7 *Tle4*$^{+/LacZ}$ and *Tle4*$^{LacZ/LacZ}$ mice. arrows: corpus callosum; arrowheads: thalamus; *: pyramidal decussation. Scale bars for all images in (D): 500 µm. AC: anterior commissure; ctx: cerebral cortex, CC: corpus callosum, str: striatum, sp: septum, hp: hippocampus; hy: hypothalamus; th: thalamus.
(E) AAV-mCherry was injected into the primary somatosensory cortex in the *Tle4*$^{+/LacZ}$ and *Tle4*$^{LacZ/LacZ}$ mice at P21, and brains were collected at P35. Eight consecutive 50-µm sections (I-VIII) are shown. Scale bar: 1mm.

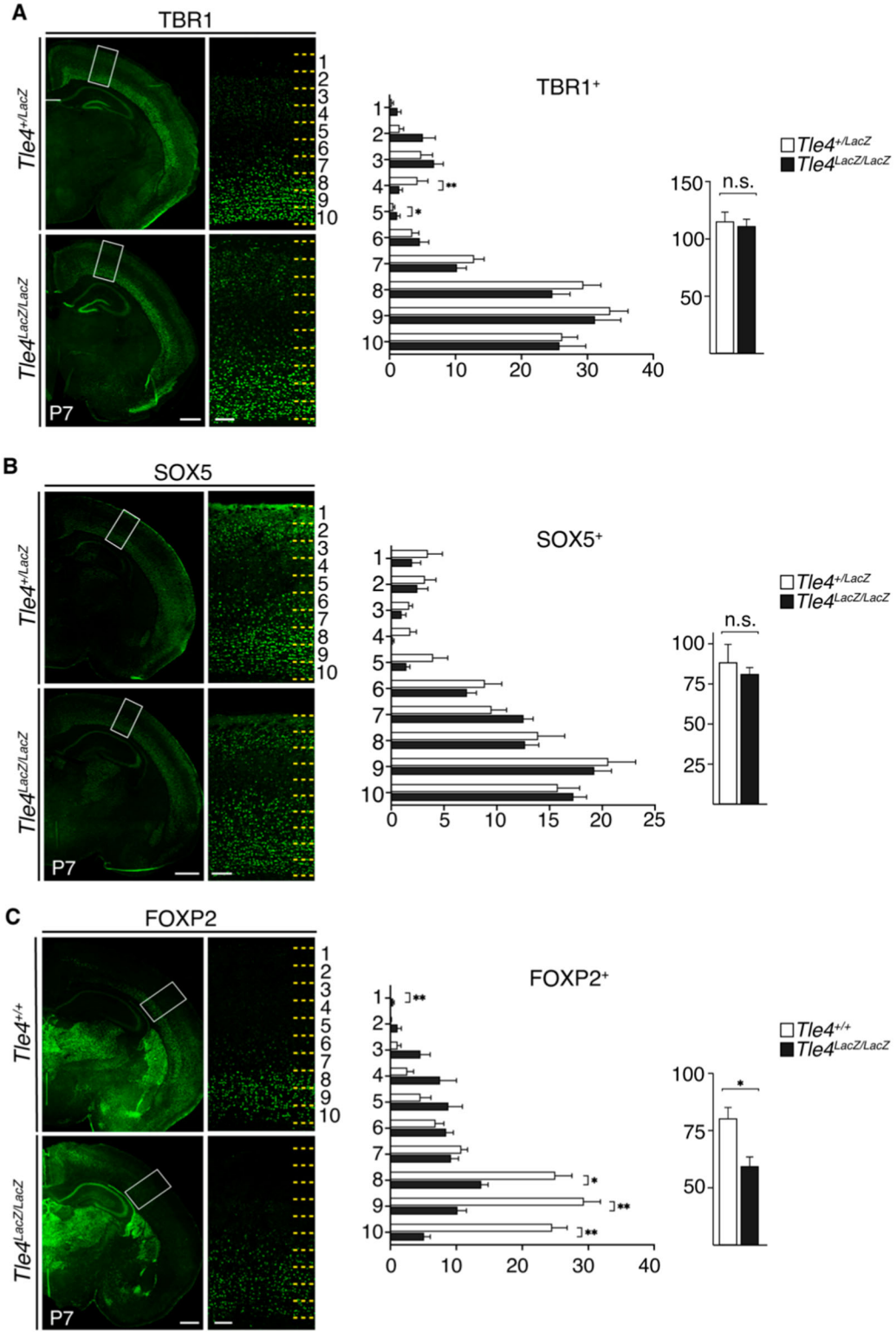
A
TBR1
Tle4+/LacZ
Tle4LacZ/LacZ
P7
1
2
3
4
5
6
7
8
9
10
TBR1+
**
*
0
10
20
30
40
Tle4+/LacZ
Tle4LacZ/LacZ
150
100
50
n.s.
B
SOX5
Tle4+/LacZ
Tle4LacZ/LacZ
P7
SOX5+
0
5
10
15
20
25
Tle4+/LacZ
Tle4LacZ/LacZ
100
75
50
25
n.s.
C
FOXP2
Tle4+/+
Tle4LacZ/LacZ
P7
FOXP2+
**
*
**
**
0
10
20
30
40
Tle4+/+
Tle4LacZ/LacZ
100
75
50
*

Figure 12: The numbers of TBR1^{+} and SOX5^{+} layer 6 neurons were not affected in *Tle4*$^{LacZ/LacZ}$ cortices, while the number of FOXP2^{+} cells was reduced

(A) TBR1 staining, quantification by bin and the total numbers of TBR1^{+} cells in *Tle4*$^{+/LacZ}$ and *Tle4*$^{LacZ/LacZ}$ cortices.
(B) SOX5 staining, quantification by bin and the total numbers of SOX5^{+} cells in *Tle4*$^{+/LacZ}$ and *Tle4*$^{LacZ/LacZ}$ cortices.
(C) FOXP2 staining, quantification by bin and the total numbers of FOXP2^{+} cells in *Tle4*$^{+/LacZ}$ and *Tle4*$^{LacZ/LacZ}$ cortices. n=3 brains per genotype, 3 sections per brain. In all graphs, error bars represent ± SEM. Scale bars: low mag, 500 μm, high mag 100 μm.

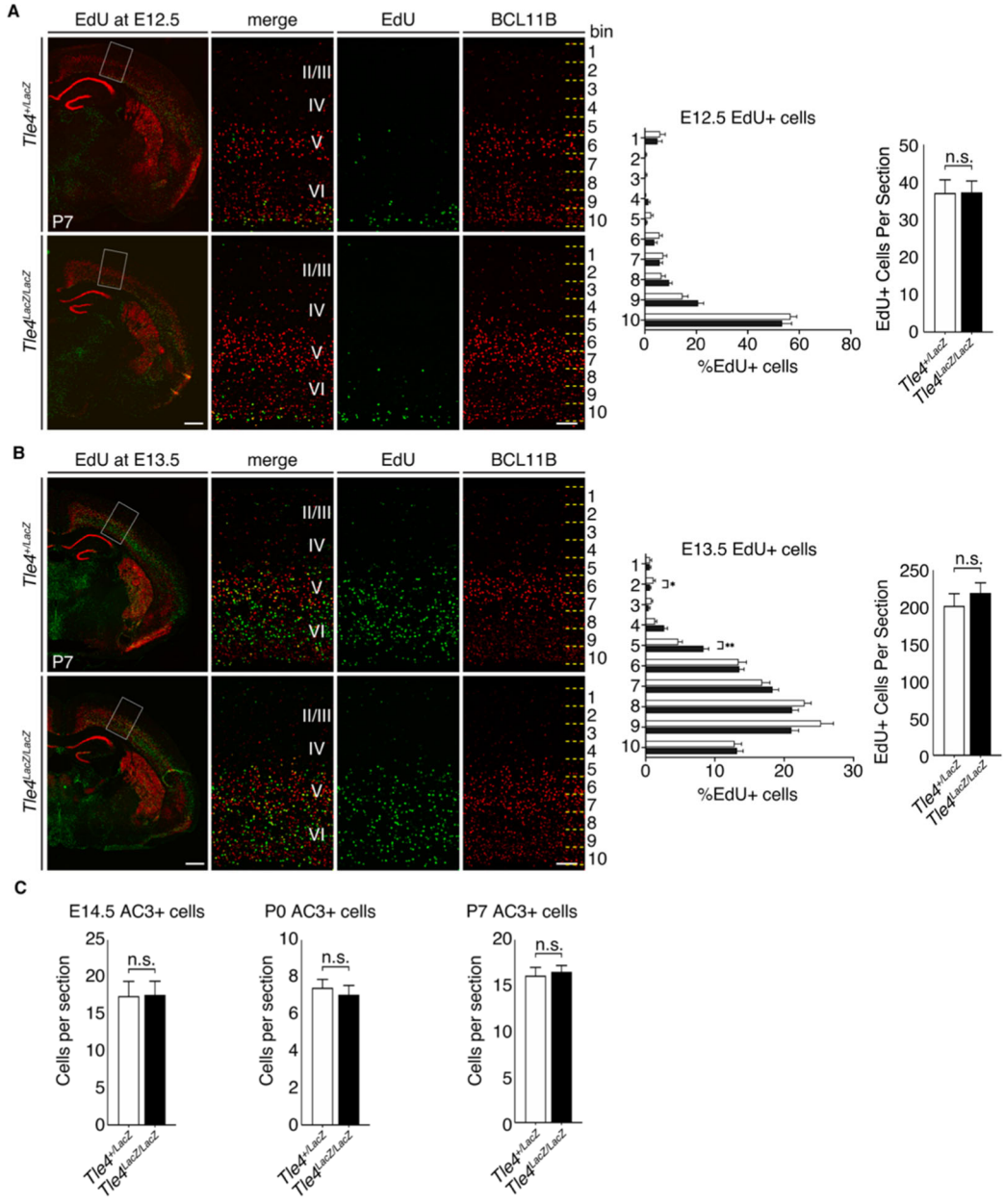
A
EdU at E12.5
merge
EdU
BCL11B
bin
Tle4+/LacZ
Tle4LacZ/LacZ
P7
II/III
IV
V
VI
E12.5 EdU+ cells
%EdU+ cells
EdU+ Cells Per Section
n.s.
B
EdU at E13.5
E13.5 EdU+ cells
C
E14.5 AC3+ cells
P0 AC3+ cells
P7 AC3+ cells
Cells per section

Figure 13: EdU birthdating and apoptosis analysis of the *Tle4*$^{+/LacZ}$ and *Tle4*$^{LacZ/LacZ}$ cortices

(A) EdU was given at E12.5, and brains were analyzed at P7. Quantifications show the %EdU^{+} cells per bin, and EdU^{+} cells per 750 µm wide section.
(B) EdU was given at E13.5, brains were analyzed at P7. Quantifications show the %EdU+ cells per bin, and total numbers of EdU+ cells per 500 µm wide section.
(C) Quantifications of AC3+ cells per section at E14.5, P0 and P7. n=3 mice per genotype and 3 sections per brain. Statistical significance for quantifications in (A-C) were determined using the unpaired student's t-test (*$p<0.05$, **$p<0.01$). Scale bars: low mag, 500 µm, high mag 100 µm.

Morphological and electrophysiological defects of corticothalamic neurons in *Tle4*$^{LacZ/LacZ}$ mice

We next investigated whether *Tle4* is required for the morphological and functional differentiation of corticothalamic neurons. We injected retrobeads into the ventral posteromedial nucleus (VPM) of the thalamus (Landisman and Connors, 2007) of *Tle4*$^{+/+}$ and *Tle4*$^{LacZ/LacZ}$ mice (P27–P35) and performed whole-cell patch-clamp recordings and morphological analyses on labeled corticothalamic neurons in S1 (Figure 14A and Figure ***14***B). Sholl analysis on reconstructed dendritic arbors revealed a significant reduction in the branching ($F_{(2,286)} = 3.4$; $p = 0.034$) and length ($F_{(2,253)} = 7.3$; $p = 0.0009$) of dendrites in mutant mice (Figure 14C). Mutant corticothalamic neurons also show significantly increased spine density, decreased spine head diameter, and increased spine length (Figure 14D).

Patch-clamp recordings revealed that corticothalamic neurons in *Tle4*$^{LacZ/LacZ}$ mice exhibited increased excitability, as demonstrated by an increased number of action potentials (APs) firing in response to current steps (Figure 14E; $F_{(1,110)} = 38.9$; $p < 0.001$); however, the AP threshold was unaffected (Figure 14F). Mutant corticothalamic neurons showed an increased membrane resistance and decreased membrane capacitance (Figure 14G; $p < 0.05$ for both). The amplitude ($p = 0.02$; Kolmogorov-Smirnov test) and frequency ($t_{31} = 2.7$; $p = 0.011$) of miniature

excitatory postsynaptic currents (mEPSC) were reduced in *Tle4*$^{LacZ/LacZ}$ mice compared to wild-type mice (Figure 14H), but no significant change in the amplitude or frequency of miniature inhibitory postsynaptic currents (mIPSC) was observed (Figure 14I). These results collectively indicate that *Tle4* is critical for the morphological development and function of corticothalamic neurons in somatosensory cortex.

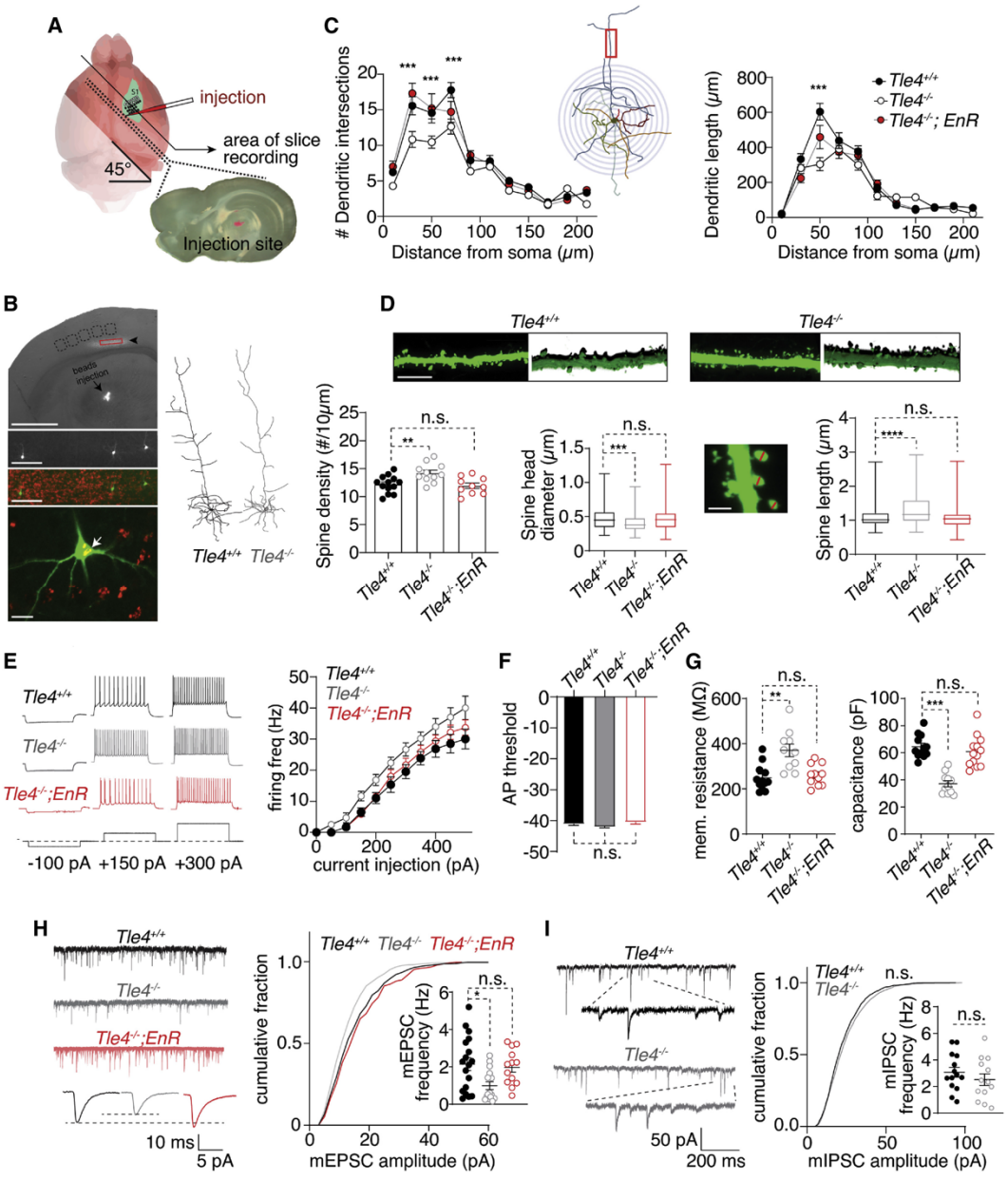
A
injection
area of slice recording
45°
Injection site
C
Dendritic intersections
Distance from soma (μm)
Dendritic length (μm)
Tle4+/+
Tle4-/-
Tle4-/-; EnR
B
beads injection
Tle4+/+ Tle4-/-
D
Tle4+/+
Tle4-/-
Spine density (#/10μm)
Spine head diameter (μm)
Spine length (μm)
n.s.
Tle4+/+
Tle4-/-
Tle4-/-;EnR
E
Tle4+/+
Tle4-/-
Tle4-/-;EnR
-100 pA +150 pA +300 pA
firing freq (Hz)
current injection (pA)
F
AP threshold
G
mem. resistance (MΩ)
capacitance (pF)
H
10 ms
5 pA
cumulative fraction
mEPSC amplitude (pA)
mEPSC frequency (Hz)
I
50 pA
200 ms
mIPSC amplitude (pA)
mIPSC frequency (Hz)

Figure 14: *Tle4*$^{LacZ/LacZ}$ mice show disrupted morphological and electrophysiological properties in corticothalamic neurons in S1, which were rescued by the *Fezf2-EnR* allele

(A) Schematic illustration of retrobeads injection into VPM of thalamus and preparation of S1 slices for patch-clamp recording.
(B) A brightfield image overlaid with bead$^+$ layer 6 corticothalamic neurons (arrowhead). Scale bars: 1 mm top image; 100 µm middle images. An enlarged view shows a beads$^+$ corticothalamic neuron and its morphology (white arrow) revealed by biocytin-avidin-Alexa 488. Scale bar: 20 µm. Right: two examples of representative dendritic arbors reconstructed from the beads$^+$ corticothalamic neurons in a *Tle4*$^{+/+}$ and a *Tle4*$^{LacZ/LacZ}$ mouse.
(C) Sholl analysis on the dendritic intersection numbers and dendritic length. Left panel shows a significant difference among the genotypes ($F_{(2, 297)} = 21.7$; $p < 0.0001$. Tukey's multiple comparison tests:
between *Tle4*$^{+/+}$ [n = 4 mice, 9 cells] and *Tle4*$^{LacZ/LacZ}$ mice [n = 5 mice, 11 cells], $p < 0.0001$; between *Tle4*$^{+/+}$ and *Tle4*$^{LacZ/LacZ}$; *Fezf2-EnR* [n = 4 mice, 10 cells] mice, $p = 0.96$. $^{***}p < 0.001$,
between *Tle4*$^{+/+}$ and *Tle4*$^{LacZ/LacZ}$ mice, Sidak's multiple comparison test).
Right panel shows dendritic length distribution. Genotype has a significant effect ($F_{(2, 253)} = 7.54$; $p = 0.0007$. Tukey's multiple comparisons test:
between *Tle4*$^{+/+}$ and *Tle4*$^{LacZ/LacZ}$, $p = 0.0006$;
between *Tle4*$^{+/+}$ and *Tle4*$^{LacZ/LacZ}$*; Fezf2-EnR*, $p = 0.42$. $^{****}p < 0.0001$,
between *Tle4*$^{+/+}$ and *Tle4*$^{LacZ/LacZ}$, Sidak's multiple comparison test).
(D) Representative images of dendritic spines and their 3D projection images. Compared to the *Tle4*$^{+/+}$ neurons (n = 4 mice, 12 cells, 20 spine lengths, 184 spine diameters), there was a significant increase in spine density ($^{**}p = 0.007$; one way ANOVA with Dunnett's multiple comparison) and spine length ($^{****}p < 0.0001$; Kruskal-Wallis test followed by Dunn's multiple comparison test) and a significant decrease in spine head diameter ($^{**}p < 0.0013$) for the *Tle4*$^{LacZ/LacZ}$ corticothalamic neurons (n = 4 mice, 11 cells, 209 spine lengths, 194 spine diameters). No significant difference in spine density, spine length, or spine head diameter was detected between the corticothalamic neurons
in *Tle4*$^{+/+}$ and *Tle4*$^{LacZ/LacZ}$; *Fezf2-EnR* mice (n = 4 mice, 10 cells, 177 spine lengths, 192 spine diameters). Scale bars: 10 µm top image; 2 µm lower image.
between *Tle4*$^{+/+}$ (n = 5 mice, 15 cells; $^{*}p = 0.015$; Dunn's multiple comparison following Kruskal-Wallis test) was restored by the *Fezf2-EnR* allele (n = 4 mice, 13 cells; between *Tle4*$^{+/+}$ and *Tle4*$^{LacZ/LacZ}$*; Fezf2-EnR*: $p = 0.99$; Dunn's multiple comparison test).

(E) Representative action potential firing responses from a *Tle4*$^{+/+}$, *Tle4*$^{LacZ/LacZ}$, and a *Tle4*$^{LacZ/LacZ}$; *Fezf2-EnR* corticothalamic neuron. Genotype has a significant effect on the current-AP responses ($F_{(2, 165)}$ = 24.1; p < 0.0001). Compared to *Tle4*$^{+/+}$ neurons (n = 5 mice, 18 cells), *Tle4*$^{LacZ/LacZ}$ neurons (n = 6 mice, 12 cells) show increased firing in response to depolarizing current steps (p < 0.0001; Dunnett's multiple comparison), which was reversed in *Tle4*$^{LacZ/LacZ}$; *Fezf2-EnR* mice (n = 5 mice, 13 cells; p = 0.14).
(F) AP threshold did not differ between *Tle4*$^{+/+}$ (n = 5 mice, 18 cells), *Tle4*$^{LacZ/LacZ}$ (n = 6 mice, 12 cells), or *Tle4*$^{LacZ/LacZ}$; *Fezf2-EnR* neurons (n = 5 mice, 13 cells; $F_{(2,32)}$ = 2.5; p = 0.09; one-way ANOVA with Dunnett's multiple comparison).
(G) Genotype has a significant effect on membrane input resistance ($F_{(2,30)}$ = 10.8; p = 0.0003; one-way ANOVA). *Tle4*$^{LacZ/LacZ}$ neurons (n = 5 mice, 11 cells) show increased input resistance compared to *Tle4*$^{+/+}$ neurons (n = 5 mice, 12 cells; p = 0.0003; Dunnett's multiple comparison test), which was rescued in *Tle4*$^{LacZ/LacZ}$; *Fezf2-EnR* (n = 4 mice, 11 cells) mice (p = 0.87). Genotype has a significant effect on membrane capacitance ($F_{(2,33)}$ = 28.0; p < 0.0001). Compared to *Tle4*$^{+/+}$ neurons (n = 5 mice, 12 cells), *Tle4*$^{LacZ/LacZ}$ neurons (n = 5 mice, 11 cells) show decreased membrane capacitance (p = 0.0003; Dunnett's multiple comparison test), which was rescued in *Tle4*$^{LacZ/LacZ}$; *Fezf2-EnR* mice (n = 4 mice, 13 cells; between *Tle4*$^{+/+}$ and *Tle4*$^{LacZ/LacZ}$; *Fezf2-EnR*: p = 0.52).
(H) Left: representative mEPSC traces from *Tle4*$^{+/+}$, *Tle4*$^{LacZ/LacZ}$, and *Tle4*$^{LacZ/LacZ}$; *Fezf2-EnR* neurons. Right: cumulative plot on mEPSC amplitude is shown. Between *Tle4*$^{+/+}$ (n = 5 mice, 8 cells, 1,135 measurements) and *Tle4*$^{LacZ/LacZ}$ (n = 5 mice, 6 cells, 1,069 measurements), *p < 0.02, Kolmogorov-Smirnov test; between *Tle4*$^{LacZ/LacZ}$ and *Tle4*$^{LacZ/LacZ}$; *Fezf2*-EnR (n = 4 mice, 9 cells, 1,158 measurements), p = 0.57. Inset: a significant decrease in mEPSC frequency in *Tle4*$^{LacZ/LacZ}$ neurons (n = 5 mice, 18 cells) between *Tle4*$^{+/+}$ (n = 5 mice, 15 cells; *p = 0.015; Dunn's multiple comparison following Kruskal-Wallis test) was restored by the *Fezf2-EnR* allele (n = 4 mice, 13 cells; between *Tle4*$^{+/+}$ and *Tle4*$^{LacZ/LacZ}$; *Fezf2-EnR*: p = 0.99; Dunn's multiple comparison test).
(I) No significant change in mIPSC amplitude and frequency was observed between *Tle4*$^{+/+}$ (n = 5 mice, 14 cells) and *Tle4*$^{LacZ/LacZ}$ neurons (n = 5 mice, 13 cells; cumulative amplitude: p = 0.43; frequency: p = 0.17. Kolmogorov-Smirnov test). Note that the *Tle4*^{LacZ} allele was labeled as *Tle4*$^{-}$ in the figure to prevent crowding.
All error bars represent ± SEM.

Expression of FEZF2-EnR rescued the molecular, morphological, and functional defects of layer 6 neurons in *Tle4*$^{LacZ/LacZ}$ cortices

The co-expression of FEZF2 and TLE4 in corticothalamic neurons suggests that they function together in regulating the development of these neurons. To test this, we generated *Tle4*$^{LacZ/LacZ}$*; Fezf2-EnR* mice and compared them to *Tle4*$^{+/+}$ and *Tle4*$^{LacZ/LacZ}$ mice. The number of B-GAL^{+} cells in *Tle4*$^{LacZ/LacZ}$*; Fezf2-EnR* mice was restored to the number of TLE4^{+} cells seen in *Tle4*$^{+/+}$ mice (Figure 15A andFigure ***15***B). The expression of genes normally enriched in subcerebral neurons, such as BCL11B, BHLHB5, *Tcerg1l*, and *Ldb2*, was no longer increased in layer 6 neurons in *Tle4*$^{LacZ/LacZ}$*; Fezf2-EnR* mice (Figure 15AFigure 15C-F,Figure ***16***AFigure 16B). However, expression of corticothalamic neuron genes, including ZFPM2 and FOXP2, and the subplate gene *Ctgf*, was not restored (Figure 16CFigure ***16***F; data not shown). These results show that FEZF2 and TLE4 function together to prevent the high-level expression of subcerebral neuronal genes in corticothalamic neurons. They also suggest that, besides serving as a transcriptional co-repressor for FEZF2, TLE4 has additional functions in regulating the molecular differentiation of corticothalamic neurons.

We next compared the dendritic morphology and function of corticothalamic neurons in *Tle4*$^{LacZ/LacZ}$*; Fezf2-EnR* mice to *Tle4*$^{+/+}$ mice (Figure 14). Sholl analysis revealed that *Fezf2-EnR* rescued the

decreased dendritic branching (p = 0.96) and length (p = 0.42) observed in *Tle4*$^{LacZ/LacZ}$ corticothalamic neurons (Figure 14C). The changes in spine density (p = 0.88), spine head diameter (p = 0.98), and spine length (p = 0.99) were also reversed (Figure 14D). Patch-clamp experiments showed that the *Fezf2-EnR* allele normalized the increased neuronal excitability associated with *Tle4*$^{LacZ/LacZ}$ neurons (Figure 14E). Corticothalamic neurons in *Tle4*$^{LacZ/LacZ}$*; Fezf2-EnR* and wild-type mice showed similar membrane resistance (p = 0.53), capacitance (p = 0.87; Figure 14G), and mEPSC amplitude cumulative distribution and frequency (Figure 14H). These data suggest that FEZF2 and TLE4 together regulate the morphological and functional differentiation of corticothalamic projection neurons.

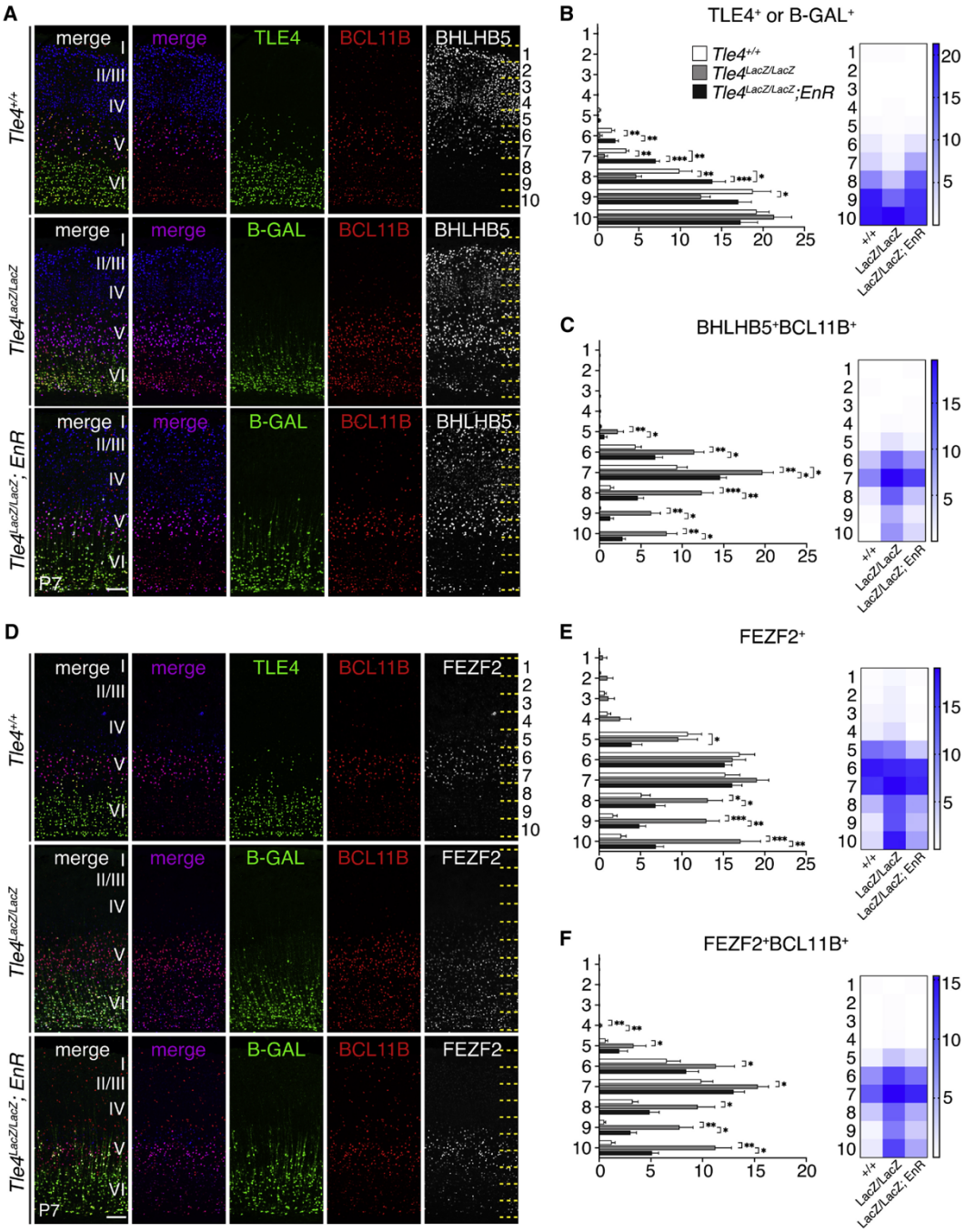
A
merge
merge
TLE4
BCL11B
BHLHB5
B-GAL
FEZF2
Tle4+/+
Tle4LacZ/LacZ
Tle4LacZ/LacZ; EnR
I
II/III
IV
V
VI
P7
B
TLE4+ or B-GAL+
Tle4+/+
Tle4LacZ/LacZ
Tle4LacZ/LacZ;EnR
+/+
LacZ/LacZ
LacZ/LacZ; EnR
C
BHLHB5+BCL11B+
D
E
FEZF2+
F
FEZF2+BCL11B+

Figure 15: FEZF2-EnR represses the increased expression of subcerebral neuronal genes in the corticothalamic neurons in the *Tle4*$^{LacZ/LacZ}$ mice

(A) Immunostaining of TLE4 or B-GAL, BCL11B, and BHLHB5 in the cortices of P7 *Tle4*$^{+/+}$, *Tle4*$^{LacZ/LacZ}$, and *Tle4*$^{LacZ/LacZ}$; *Fezf2-EnR* mice. Scale bar: 100 μm.
(B) Quantifications of TLE4^{+} cells in the *Tle4*$^{+/+}$ cortices and the B-GAL^{+} cells in *Tle4*$^{LacZ/LacZ}$ and *Tle4*$^{LacZ/LacZ}$; *Fezf2-EnR* cortices.
(C) Quantifications of the numbers of BCL11B^{+}BHLHB5^{+} cells.
(D) Immunostaining of TLE4, B-GAL, BCL11B, and FEZF2 in the cortices of P7 *Tle4*$^{+/+}$, *Tle4*$^{LacZ/LacZ}$, and *Tle4*$^{LacZ/LacZ}$; *Fezf2-EnR* mice. Scale bar: 100 μm.
(E) Quantifications of the FEZF2^{+} cells by bin.
(F) Quantifications of the numbers of FEZF2^{+}BCL11B^{+} cells. n = 3 brains per genotype, 3 sections per brain.
In all graphs, error bars represent ± SEM. Statistical significance was determined using one-way ANOVA followed by post hoc Tukey's t test ($^{*}p < 0.05$; $^{**}p < 0.01$; $^{***}p < 0.001$).

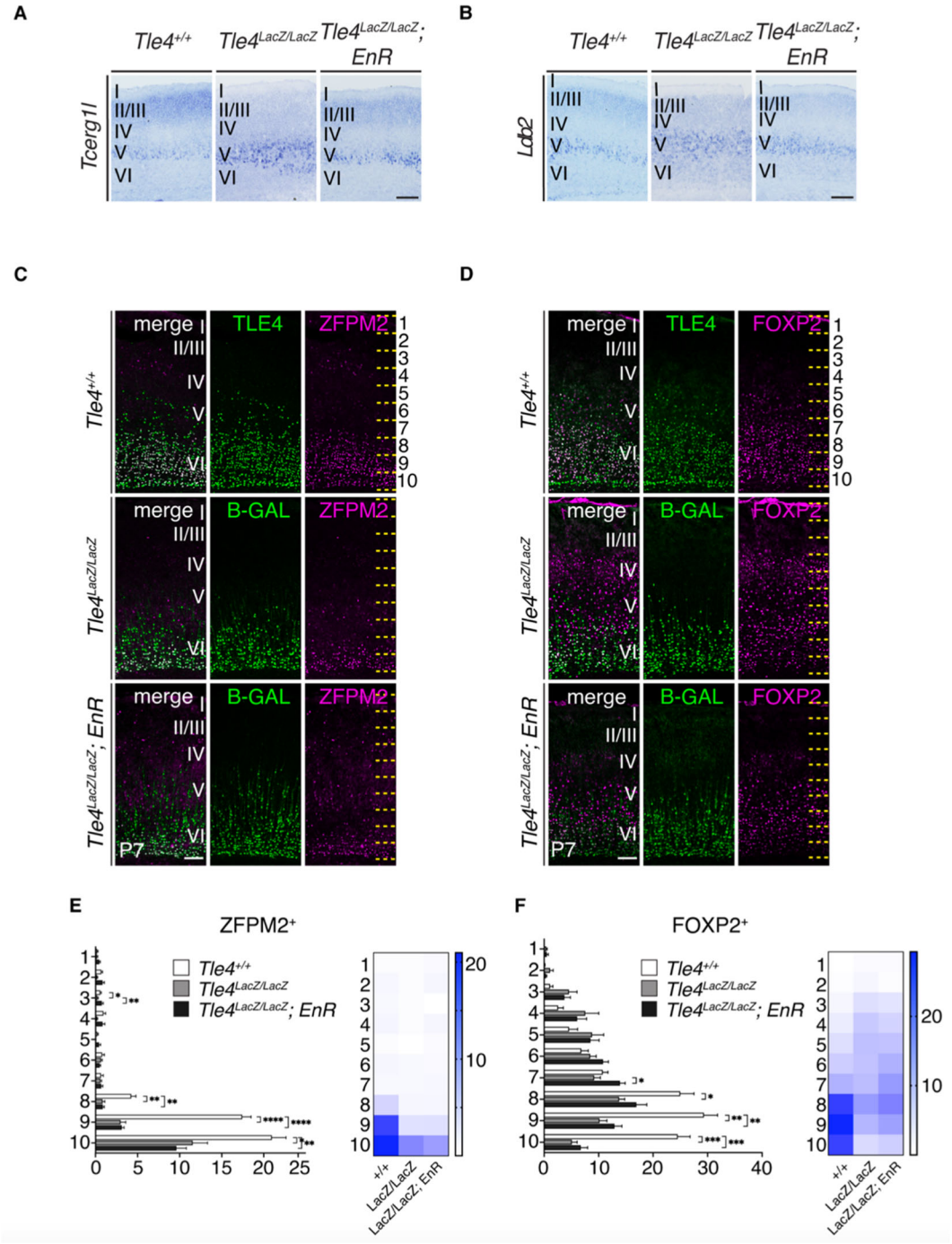
A
Tle4+/+
Tle4LacZ/LacZ
Tle4LacZ/LacZ; EnR
Tcerg1l
B
Ldb2
C
D
merge
TLE4
FOXP2
ZFPM2
B-GAL
P7
E
ZFPM2+
F
FOXP2+

Figure 16: Increased expression of layer 5 subcerebral neuronal markers *Tcerb1l* and *Ldb2* were rescued, but reduced expression of layer 6 neuronal markers ZFPM2 and FOXP2 were not rescued in the *Tle4*$^{LacZ/LacZ}$ mice by the *Fezf2-EnR* allele

(A-B) In situ hybridization showed increased expressions for *Tcerg1l* and *Ldb2* in the *Tle4LacZ/LacZ* cortices, which were rescued in the *Tle4*$^{LacZ/LacZ}$; *Fezf2-EnR* mice. Scale bars: 100μm.
(C) Immunostaining for TLE4, B-GAL, and ZFPM2 in the cortices of P7 *Tle4*$^{+/+}$, *Tle4*$^{LacZ/LacZ}$ and *Tle4*$^{LacZ/LacZ}$; *Fezf2-EnR* mice. Scale bars: 100μm.
(D) Immunostaining for TLE4, B-GAL and FOXP2. Scale bars: 100 μm.
(E) Quantifications of the ZFPM2^{+} cells by bin.
(F) Quantifications of the FOXP2^{+} cells by bin. n=3 brains per genotype, 3 sections per brain. Quantifications of marker+ cells per 10,000 μm^2 in each bin. In all graphs, error bars represent ± SEM. Statistical significance was determined using the unpaired student's t-test (*p<0.05, **p<0.01, ***p<0.001).

Discussion

Deciphering the molecular logic for establishing neuronal subtype identities in the developing cerebral cortex is fundamental for understanding how neuronal diversity is established in the mammalian brain. In this study, we examined the molecular control of two broad classes of cortical projection neurons—the corticothalamic and the layer 5 subcerebral projection neurons—by focusing on the function of FEFZ2.

Prior studies demonstrated that FEFZ2 is a master regulator for CSMNs, a subpopulation of layer 5 subcerebral neurons. In *Fezf2*$^{-/-}$ mice, layer 5 subcerebral neurons were absent, and instead, the mutant layer 5b neurons demonstrated the molecular features and axonal projection patterns of corticothalamic or corticocortical neuron subtypes (B. Chen et al., 2005a; Chen et al., 2008a; Molyneaux et al., 2005). Complementing these studies, ectopic expression of *Fezf2* in late cortical progenitors or upper-layer neurons or in the progenitors of the lateral ganglionic eminence led to the differentiation of neurons with gene expression and axon projections associated with corticothalamic or subcerebral neurons (J.-G. Chen et al., 2005; Chen et al., 2008a; De la Rossa et al., 2013; Lodato et al., 2014; Molyneaux et al., 2005; Rouaux and Arlotta, 2010, 2013), suggesting that FEZF2 functions as a selector gene for subcerebral neurons. To test this, Lodato et al., 2014 performed gene expression analyses of cortical progenitors and neurons that overexpressed FEZF2

and chromatin immunoprecipitation sequencing (ChIP-seq) analysis of neurospheres that overexpressed FEZF2-FLAG. Results from these experiments led the authors to conclude that FEZF2 functions as both a transcriptional activator and a repressor. They suggested that FEZF2 directly induces CSMN glutamatergic identity by activating expression of genes including *Vglut1* (*Slc17a7*) and that it inhibits a GABAergic fate by repressing the transcription of genes such as *Gad1* (Lodato et al., 2014). They further reported that FEZF2 directly activates CSMN-specific genes by binding to their proximal promoters and represses genes expressed in corticocortical projection neurons (Lodato et al., 2014).

Here, we directly tested whether FEZF2 functions as a transcriptional activator, a repressor, or both by comparing the activities of full-length FEZF2, FEZF2-EnR, and FEZF2-VP16 chimeric proteins using two different assays. Results from both overexpression and rescue experiments showed that FEZF2-EnR recapitulated the activity of full-length FEZF2 protein, while the FEZF2-VP16 was less relevant in our assays. Thus, in contrast to prior work, our studies demonstrate that FEZF2 functions primarily as a transcriptional repressor, in context of the formation of the corticospinal tract and neuronal identity. It is not clear why our results differ so markedly from those of Lodato et al., 2014, although it seems possible that ChIP-seq experiments may have overestimated the

binding sites for FEZF2 in normal cortical neurons (Jain et al., 2015; Teytelman et al., 2013).

FEZF2 is required for establishing the molecular identity and axonal projections of both subcerebral and corticothalamic neurons. In the absence of *Fezf2*, subcerebral neurons exhibit molecular features and axonal projection patterns associated with corticothalamic or corticocortical neuron subtypes (B. Chen et al., 2005a; Chen et al., 2008a; McKenna et al., 2011). Previous reports (Diao et al., 2018; Komuta et al., 2007) and our current study show that, in *Fezf2*$^{-/-}$ mice, corticothalamic neurons also exhibit defects in gene expression and axonal projections. We found that *Fezf2 cko* corticothalamic neurons showed increased expression of certain subcerebral neuronal genes, such as BCL11B and the truncated FEZF2, indicating that corticothalamic neurons partially assume the molecular identity of subcerebral neurons in the absence of *Fezf2* function. Together, these results suggest that FEZF2 inhibits the expression of distinct and specific target genes in subcerebral neurons and in corticothalamic neurons, and by doing so, FEZF2 prevents each class of neurons from adopting an alternate neuronal subtype identity. Consistent with this, the *Fezf2-EnR* allele rescued the molecular identities and axonal projections of both the subcerebral and corticothalamic subtypes in *Fezf2*$^{-/-}$ mice.

How does FEZF2 function as a transcriptional repressor? One possibility is that FEZF2 binds to an enhancer or promoter sequence and physically prevents the binding of a transcriptional activator. Another possibility is that the binding of FEZF2 to an enhancer or promoter recruits additional transcriptional co-repressor(s), and together they actively repress gene expression. In *Nex-Cre; Fezf2*$^{Flox/-}$ mice, a truncated FEZF2 protein consisting of just the DNA binding domain was expressed, yet in these mice, subcerebral and corticothalamic neurons and their axons showed similar defects as in *Fezf2*$^{-/-}$ null mutant mice (Figure 4Figure 5). This result indicates that the N-terminal half of the FEZF2 protein is essential for its transcriptional repressor function, likely by recruiting transcriptional co-repressors, and that FEZF2 is unlikely to repress gene expression simply by blocking the binding of a transcriptional activator.

Indeed, FEZF2 contains an EH1 motif, which can recruit TLE family transcription co-repressors (Hashimoto et al., 2000). The co-expression of FEZF2 and TLE4 in corticothalamic neurons suggests that TLE4 may be one of its co-repressors. Similar to *Fezf2*$^{-/-}$ mice, corticothalamic neurons in *Tle4*$^{LacZ/LacZ}$ mice showed increased expression of genes associated with subcerebral neurons, indicating that TLE4 is involved in refining the molecular identity of corticothalamic neurons by preventing high-level expression of some subcerebral neuronal genes. We found that the *FEZF2-EnR* allele, which does not depend on TLE family transcription

co-repressors for its function, prevented the high expression levels of subcerebral neuronal genes and restored the functional properties of corticothalamic neurons in *Tle4*$^{LacZ/LacZ}$ mice. These results support the conclusion that FEZF2 and TLE4 together repress the expression of FEZF2, BCL11B, and BHLHB5 in corticothalamic neurons. However, the reduced expression of corticothalamic neuronal genes, such as FOG2 and FOXP2 in *Tle4*$^{LacZ/LacZ}$ mice, was not rescued by the *Fezf2-EnR* allele. Furthermore, although corticothalamic axons to the dLGN were missing in *Fezf2*$^{-/-}$ mice, they were present in *Tle4*$^{LacZ/LacZ}$ mice. Thus, although FEZF2 and TLE4 together refine the molecular differentiation and function of corticothalamic neurons, each plays additional independent roles. The identity of possible co-repressor(s) for FEZF2 in subcerebral neurons remains unknown.

Recent progress and our current study show that the subtype identity of a cortical projection neuron is specified in the postmitotic stage. Multiple transcription factors, including *Tbr1* (Han et al., 2011; McKenna et al., 2011), *Sox5* (Kwan et al., 2008; Lai et al., 2008), *Fezf2* (B. Chen et al., 2005a; Chen et al., 2008a; J.-G. Chen et al., 2005; Molyneaux et al., 2005), and the chromatin remodeling protein *Satb2* (Alcamo et al., 2008; Britanova et al., 2008; Leone et al., 2015; McKenna et al., 2015), are essential for specifying cortical projection neuron subtype identities. A common phenotype of mice with mutations in these genes is that the

affected neuronal subtypes exhibit gene expression profiles and axonal projection patterns associated with alternate neuronal subtypes. This suggests that TBR1, SOX5, and SATB2 likely also function as selective repressors in their respective neuronal subtypes to inhibit expression of genes associated with alternate identities. In the future, it will be important to test whether these proteins act as transcriptional repressors, activators, or both in the context of cortical projection neuron subtype specification. Another common feature shared by the *Tbr1*, *Sox5*, and *Satb2* genes is that all are expressed in postmitotic neurons. Although *Fezf2* is expressed by both cortical RGCs and deep-layer neurons, our results indicate that it is required in postmitotic neurons for specifying cortical neuron subtype identities. These results suggest that projection neuron subtype-specific features are established through repressing genes associated with alternate subtype identities during postmitotic neuronal differentiation.

Although different subtypes of cortical projection neurons have distinct morphologies, axonal projection patterns, and molecular profiles, they share a common cortical regional identity and use glutamate as an excitatory neurotransmitter. A fundamental question in brain development is whether a single genetic program specifies both the pan-cortical excitatory neuron identity and the subtype-specific identity of a cortical projection neuron or these features are specified by distinct genetic programs. Projection neuron subtype identities are mis-specified

in *Fezf2*$^{-/-}$, *Tbr1*$^{-/-}$, *Sox5*$^{-/-}$, and *Satb2*$^{-/-}$ mice, but mutant cortical neurons maintain their glutamatergic identity and fail to acquire molecular features associated with GABAergic neurons. Thus, these subtype identity genes are not required for the adoption of a pan-cortical glutamatergic identity.

A different set of transcription factors, expressed in the RGCs and/or intermediate progenitors, including *Pax6, Tlx, Dmrt5, Dmrt3, Emx2, Ngn1, and Ngn2,* are essential for establishing the regional and glutamatergic identities of cortical projection neurons (Desmaris et al., 2018; Konno et al., 2019; Kroll and O'Leary, 2005; Schuurmans et al., 2004). Based on our results and previous studies, we propose that the common versus unique characteristics of cortical projection neuron subtypes are specified sequentially during development. At early stages of corticogenesis, transcription factors expressed in cortical RGCs and/or intermediate progenitors (including *Pax6*, *Tlx*, *Dmrt5*, *Dmrt3*, *Emx2*, *Ngn1*, and *Ngn2*) act in parallel pathways to ensure the generation of cortical glutamatergic projection neurons and prevent the production of ventral GABAergic neurons (Desmaris et al., 2018; Konno et al., 2019; Kroll and O'Leary, 2005; Schuurmans et al., 2004). As postmitotic cortical neurons begin to migrate and differentiate, genes such as *Fezf2*, *Tbr1*, *Sox5*, and *Satb2* repress the expression of genes associated with alternate neuronal subtype identities to establish specific subtype-specific identities. In the future, it will be necessary to rigorously test whether the proteins

encoded by these genes function as transcriptional repressors or activators during development and to determine how the expression of neuronal subtype identity genes is initially activated. Answers to these questions will be invaluable for designing novel and efficient strategies for using directed differentiation or trans-differentiation methods to repair damaged brain circuits in disease and injury.

Table 1: Key Resources Table

REAGENT or RESOURCE	SOURCE	IDENTIFIER
Antibodies		
Chicken anti-GFP polyclonal	Aves Labs	GFP-1020
Rat anti-BCL11B monoclonal	Abcam	ab18465
Rabbit anti-TBR1 polyclonal	Abcam	ab31940
Rabbit anti-SOX5 polyclonal	Abcam	ab94396
Rabbit anti-FEZF2 polyclonal	IBL	F441
Mouse anti-TLE4 monoclonal	Santa Cruz Biotechnology	sc-365406
Rabbit anti-FOXP2 polyclonal	Abcam	ab16046
Rabbit anti-ZFPM2 polyclonal	Santa Cruz Biotechnology	M-247
Chicken anti-B-GAL polyclonal	Abcam	ab9361
Rabbit anti-Activated Caspase 3 polyclonal	Cell Signaling Technology	#9661
Goat anti-BHLHB5 polyclonal	Santa Cruz Biotechnology	sc-6045
Rabbit anti-SATB2 polyclonal	Abcam	ab34735
Rabbit anti-Fosl2 polyclonal	Sigma	HPA004817
Mouse anti-GAPDH monoclonal	Covance	MMS-508S
Donkey anti-Chicken Alexa Fluor 488	Jackson ImmunoResearch Labs	703-545-155
Donkey anti-Mouse Alexa Fluor 488	Invitrogen	R37114
Donkey anti-Rabbit Alexa Fluor 488	Invitrogen	A-21206
Donkey anti-Goat Alexa Fluor 488	Invitrogen	A-11055
Donkey anti-Rat Alexa Fluor 488	Invitrogen	A-21208
Goat anti-Chicken Alexa Fluor 546	Invitrogen	A-11040
Donkey anti-Mouse Alexa Fluor 594	Jackson ImmunoResearch Labs	715-585-150

Donkey anti-Rabbit Alexa Fluor 546	Invitrogen	A-10040
Donkey anti-Goat Alexa Fluor 546	Invitrogen	A-11056
Donkey anti-Rat Alexa Fluor 555	Abcam	Ab150154
Donkey anti-Chicken Alexa Fluor 647	Jackson ImmunoResearch Labs	703-606-155
Donkey anti-Mouse Alexa Fluor 647	Invitrogen	A-31571
Donkey anti-Rabbit Alexa Fluor 647	Invitrogen	A-31573
Donkey anti-Goat Alexa Fluor 647	Invitrogen	A-21447
Donkey anti-Rat Alexa Fluor 647	Jackson ImmunoResearch Labs	712-605-153
Donkey anti-Mouse HRP	Invitrogen	A16011
Donkey anti-Rabbit HRP	Invitrogen	A16035
Rabbit anti GFP	Invitrogen	A1122
Goat anti MYC	Abcam	Ab9132
Donkey anti-Mouse IgG IRDye 800	Li-Cor	926-32212
Donkey anti-Goat IgG IRDye 800	Li-Cor	926-32214
Donkey anti-Rabbit IgG IRDye 680	Li-Cor	926-68073
Donkey anti-Mouse IgG IRDye 680	Li-Cor	926-68072
Anti FLAG-M2 Magnetic Beads	Sigma	M8823
Bacterial and Virus Strains		
AAV2-CMV-mCherry virus	Vector Biosystems Inc.	#7104
Biological Samples		
Mouse cortex	This paper	N/A
Chemicals, Peptides, and Recombinant Proteins		
EdU	Thermo Fisher	E10187
(+)-Sodium L-ascorbate	Sigma-Aldrich	A7631
Copper (II) Sulfate (CuSO4)	Sigma-Aldrich	451657
Rhodamine Azide	Invitrogen	A20012
Alexa Fluor 488 Azide	Invitrogen	A10266
Cholera Toxin Subunit B, Alexa Fluor 555 conjugate	Invitrogen	C22843
Saponin	Sigma-Aldrich	470366
Paraformaldehyde (PFA)	MP Biomedicals	150146
Citric Acid Monohydrate	Sigma-Aldrich	C0706
Horse Serum	Gibco	16050-114
T7 Polymerase	New England Biotechnology	M0251
SP6 Polymerase	Promega	P1085
DIG-Labeled Nucleotides	Sigma-Aldrich	11277073910

NBT/BCIP stock solution	Sigma-Aldrich	11681451001
SpeI Restriction Enzyme	New England Biotechnology	R3133
SalI Restriction Enzyme	New England Biotechnology	R0138
NcoI Restriction Enzyme	New England Biotechnology	R0193
NotI Restriction Enzyme	New England Biotechnology	R0189
XhoI Restriction Enzyme	New England Biotechnology	R0146
Trypan Blue Stain (0.4%)	Gibco	15250-061
Red Retrobeads	Lumafluor	R170
Avidin Alexa Fluor 488	Invitrogen	A21370
Critical Commercial Assays		
GenElute HP Plasmid Miniprep Kit	Sigma-Aldrich	NA0160
Qiaquick PCR Purification Kit	Qiagen	28106
RNeasy Plus Mini Kit	Qiagen	74134
TruSeq RNA Library Prep Kit	Illumina	RS-122-2001
Nuclear Complex Co-IP kit	Active Motif	54001
Deposited Data		
Fezf2$^{Plap/Plap}$, *Fezf2*$^{Plap/Plap}$; *Fezf2-EnR* and control RNA-seq data	This paper	GSE160202
Tle4$^{LacZ/LacZ}$ and control RNA-seq data	This paper	GSE142269
Experimental Models: Cell Lines		
Neuro-2a	ATCC	CCL-131
Experimental Models: Organisms/Strains		
Mouse: *Fezf2*^{Plap}	Chen et al., 2005	University of California, Santa Cruz
Mouse: *Fezf2*^{Flox}	Han et al., 2011	Yale University
Mouse: *Fezf2-EnR*	This Paper	N/A
Mouse: *Tle4*^{LacZ}	This Paper	N/A
Mouse: *Nex-Cre*	Goebbels et al., 2006	Max-Planck-Institute of Experimental Medicine
Oligonucleotides		
Primers for genotyping *Tle4* Wildtype allele	This Paper	N/A
For: gagatgtggctacagaagaggttcagagac	This Paper	N/A
Rev: atctgccccttgctattcctgcttgctctc	This Paper	N/A
Primers for genotyping *Tle4* mutant allele	This Paper	N/A
For: tgctctcccacaagctcgcttgtcgttcag	This Paper	N/A

Rev: aagagggctctgtcctccagtctcctcc ac	This Paper	N/A
Primers for genotyping *Fezf2* wildtype allele	This Paper	N/A
For: ttgaatgcaaatgggtgaccgggccg	This Paper	N/A
Rev: gttttagaagtggccggtgacgctcc	This Paper	N/A
Primers for genotyping *Fezf2^{Plap}* allele	This Paper	N/A
For: caccccggtgaacagctcctcgccctt gctcaccat	This Paper	N/A
Rev: ctgcatggctcggaacgcatctccttgg cggtgggggaaagag	This Paper	N/A
Primers for genotyping *Fezf2-EnR* allele	This Paper	N/A
For: caaaatcggttacggttgagtaata	This Paper	N/A
Rev: accatgccacttcccttctcag	This Paper	N/A
Primers for genotyping *Fezf2^{Flox}* allele	This Paper	N/A
For: tgccttgtacacctttctct	This Paper	N/A
Rev: gagacctaggcaagggacagt	This Paper	N/A
Primers for genotyping *Nex-Cre* allele	This Paper	N/A
For: gagtcctggaatcagtctttttc	This Paper	N/A
Rev: ccgcataaccagtgaaacag	This Paper	N/A
Primers for *Tcerg1l in situ* hybridization probe template	This Paper	N/A
For: ctctccccactgtggtattagc	This Paper	N/A
Rev: cagaactatttcccctcgtgac	This Paper	N/A
Primers for *Ldb2 in sit*u hybridization probe template	This Paper	N/A
For: cacctgattacgctgtccatag	This Paper	N/A
Rev: aagttcaacacacgagggagat	This Paper	N/A
Primers for *Ctgf in situ* hybridization probe template	This Paper	N/A
For: aaatcgccaagcctgtcaag	This Paper	N/A
Rev: ggcactgtgcgctaatgaac	This Paper	N/A
Primers for *Cryab in situ* hybridization probe template	This Paper	N/A
For: ctcagccctgcctgtgtt	This Paper	N/A
Rev: atctgggccagcccttag	This Paper	N/A
Primers for *Ephb1 in situ* hybridization probe template	Lodato *et al.,* 2014	N/A
For: cacatccatctccctttgct	Lodato *et al.,* 2014	N/A

Rev: tccagaaacccttttccctct	Lodato *et al.,* 2014	N/A
Primers for *Kif26a in situ* hybridization probe template	Lodato *et al.,* 2014	N/A
For: tcctcagctccagactccat	Lodato *et al.,* 2014	N/A
Rev: gcgacagtctttccatctcc	Lodato *et al.,* 2014	N/A
Primers for *Wnt7b in situ* hybridization probe template	Allen Brain Atlas	N/A
For: acgcaatggtggtctggt	Allen Brain Atlas	N/A
Rev: aagggcctgaggaaatgg	Allen Brain Atlas	N/A
Primers for VP16 domain	This Paper	N/A
For: gatcggatccgccgccaccatggccc ccccgaccgatgtcagcct		
Rev: gatcgatatccccaccgtactcgtcaat tccaa	This Paper	N/A
Recombinant DNA		
pGEM-T Easy Vector System	Promega	A1360
pCAG-Fezf2	Chen et al., 2005	University of California, Santa Cruz
pCAG-Fezf2-EnR	This Paper	N/A
pCAG-Fezf2-VP16	This Paper	N/A
pCAG-EGFP	Matsuda et al., 2004	Addgene #11150
pCMV-Tle4-Myc-DDK tag	This paper	Origene #MR231124
Software and Algorithms		
FIJI	Shindelin et al., 2012	https://imagej.net/Fiji
Adobe Illustrator	Adobe	https://adobe.com/products/illustrator.html
Adobe Photoshop	Adobe	https://adobe.com/products/photoshop.html
Imaris	Bitplane	https://imaris.oxinst.com/
Zen Imaging	Zeiss	https://www.zeiss.com/microscopy/us/products/microscope-software/zen.html
GraphPad prism v8	GraphPad	https://www.graphpad.com/scientific-software/prism/
RepeatMasker Library	Smit et al.,1996-2010	http://repeatmasker.org/libraries/
TopHat	Trapnell et al., 2009	https://encodeproject.org/software/tophat/
Bowtie	Langmead et al., 2009	http://bowtie-bio.sourceforge.net/index.shtml
SamTools	Li et al., 2009	http://samtools.sourceforge.net/

DESeq	Anders and Huber, 2010	https://bioconductor.org/packages/release/bioc/html/DESeq.html
Database for Annotation, Visualization and Integrated Discovery (DAVID)	Huang et al., 2008	https://david.ncifcrf.gov/
pClamp 10.6	Molecular Devices	http://go.moleculardevices.com/l/83942/2015-09-08/77t9w
ImageStudioLite	Li-Cor	https://www.licor.com/bio/image-studio-lite/download
Other		
7-mm Platinum Electrodes	BTX/Harvard Apparatus	45-0488
ECM 399 Electroporation System	BTX	45-0000
Zeiss 880 Confocal Microscope	Zeiss	LSM 880
Zeiss Axio Imager Z2 Widefield Microscope	Zeiss	Axio Imager 2
Zeiss LSM 710	Zeiss	LSM 710
MultiClamp 700B amplifier	Molecular Devices	1-CV-7B
Digidata 1440A	Molecular Devices	N/A

Resource availability

Materials availability

The *Tle4*^{LacZ} *and Fezf2-EnR* mouse lines will be deposited to the Jackson Laboratory. All unique/stable reagents generated in this study are available from the Lead Contact, but we may require a payment and/or a completed Materials Transfer Agreement if there is potential for commercial application.

Data and code availability

The RNA-seq data for the *Fezf2*$^{-/-}$, *Fezf2*$^{-/-}$*; Fezf2-EnR*, and littermate control *Fezf2*$^{+/+}$ cortices, and for the *Tle4*$^{LacZ/LacZ}$ and littermate

control *Tle4*$^{+/+}$ cortices can be accessed using GEO: GSE160202 and GEO: GSE142269, respectively.

Experimental model and subject details

Mice used in this study

Experiments were performed according to protocols approved by the Institutional Animal Care and Use Committee at University of California at Santa Cruz and at University of Arizona College of Medicine Phoenix, and were performed in accordance with institutional and federal guidelines. Experiments performed at Fudan University were in accordance with institutional guidelines.

We generated the *Tle4*^{LacZ} allele by inserting a *LacZ-ires-Plap* cassette in the intron after the exon 4 of the *Tle4* gene, using the targeted gene trap strategy (Friedel et al., 2005). Southern hybridization was performed to screen the E14a ES cell clones and identify the correct targeting.

The bacterial artificial chromosome (BAC) clone RP23-141E17 was modified by inserting the cDNA encoding the ENGRAILED transcriptional repressor domain (EnR) fused with the DNA binding domain of FEZF2, followed by the SV40 polyadenylate site (*Fezf2-EnR*), at the start codon of the mouse *Fezf2* gene. The BAC DNA was purified and sequenced and used for injection to generate the *Fezf2-EnR* transgenic mouse line.

The day of the vaginal plug detection was designated as E0.5. The day of birth was designated as P0. The genders of the embryonic and early postnatal mice were not determined.

The following mice were used in this study:

- *Fezf2*$^{+/+}$, *Fezf2*$^{+/-}$ and *Fezf2*$^{-/-}$ mice: P0, P7, and adult, both male and female mice were used.
- *Fezf2*$^{flox/+}$ and *Fezf2*$^{Flox/Flox}$ mice: adult, both male and female mice were used.
- *Nex-Cre* mice: adult, both male and female mice were used.
- *Nex-Cre; Fezf2*$^{+/-}$ and *Nex-Cre; Fezf2*$^{-/Flox}$ mice: P0 and P7, both male and female mice were used.
- *Fezf2-EnR* mice: adult, both male and female mice were used.
- *Fezf2*$^{-/-}$*; Fezf2-EnR* mice: P0, P7, and adult, both male and female mice were used.
- *Tle4*$^{+/+}$*, Tle4*$^{+/LacZ}$ and *Tle4*$^{LacZ/LacZ}$ mice: P0, P7, adult, both male and female mice were used.
- *Tle4*$^{LacZ/LacZ}$*; Fezf2-EnR* mice: P0, P7, adult, both male and female mice were used.

Cell lines used in this study

Neuro-2a (ATCC CCL-131) cells were used in this study for protein co-immunoprecipitation experiments. Cells were cultured at 37°C with 5% CO2 in 145 mm culture dishes (Greiner, #639960).

Method details

PLAP staining

Human placental alkaline phosphatase (PLAP) staining was performed as described previously (B. Chen et al., 2005a). P7 mice were anesthetized and 4% paraformaldehyde was delivered via trans-cardiac perfusion. Brains were post-fixed in 4% paraformaldehyde for 24 hours at 4°C and then immersed in 30% sucrose in PBS for 24 hours. Brains were then frozen and sectioned into 50 μm sections using a sliding microtome (Thermo Scientific, Microm HM 430). Sections were washed 3 times in PBS, immersed in a 1:50 solution of NBT/BCIP (Roche, 11681451001) in 0.1M Tris-HCl pH 9.5, 0.1M NaCl, and then incubated at 37°C for 4 hours. Sections were then washed in PBS with 0.3% Triton X-100 5 times over the course of 2 hours at 37°C to remove background. Sections were then mounted in Fluoromount-G.

Immunohistochemistry

4% paraformaldehyde was delivered to mice via trans-cardiac perfusion. Brains were post-fixed in 4% paraformaldehyde, 0.1% saponin, and PBS for 24 hours at 4°C, followed by cryoprotection in 30% sucrose in PBS. Immunohistochemistry was performed using standard protocols. Briefly, twenty-five-μm-thick brain sections were permeabilized with 0.03%

Triton X-100 in PBS for 30 min. Slides were then immersed in citrate buffer (10mM citric acid monohydrate, 0.05% Tween-20, pH 6.0), brought to a boil in a microwave and rested for 1 hour at RT. Slides were then incubated in a blocking buffer (5% donkey serum, 0.03% Triton X-100 in PBS) for 30 minutes. Blocking buffer was removed, and the sections were incubated with primary antibodies (diluted in the blocking buffer) for 24 hours at 4°C. The following primary antibodies were used in this study: GFP (Chicken, Aves Labs GFP-1020), BCL11B (Rat, Abcam ab18465), TBR1 (Rabbit, Abcam ab31940), SOX5 (Rabbit, Abcam ab94396), FEZF2 (Rabbit, IBL F441), TLE4 (Mouse, Santa Cruz Biotechnology sc-365406), FOXP2 (Rabbit, Abcam ab16046), ZFPM2 (Rabbit, Santa Cruz Biotechnology), B-GAL (Chicken, Abcam ab9361), activated caspase 3 (Rabbit, Cell Signaling Technology #9661), BHLHB5 (Goat, Santa Cruz Biotechnology sc-6045), SATB2 (Rabbit, Abcam ab34735), FOSL2 (Rabbit, Sigma HPA004817), and GAPDH (Covance, MMS-580S), The sections were washed in PBS, and incubated with secondary antibodies conjugated to Alexa 488, Alexa 546, or Alexa 647 for 2 hours at room temperature. Secondary antibodies were from Jackson ImmunoResearch and Invitrogen. Finally, the sections were counterstained with DAPI for 5min before being mounted in Fluoromount-G.

Protein co-immunoprecipitation

Neuro-2a (ATCC CCL-131) cells were cultured in 145 mm tissue culture treated dishes (Greiner, #639960) at 37°C with 5% CO2 and transfected with Lipofectamine 3000 reagent (Thermo, #L3000001) with the following plasmid combinations: Fezf2-his-myc + Tle4-flag-myc + GFP-his-myc, Fezf2-his-myc + GFP-his-myc, Tle4-flag-myc + GFP-his-myc, or GFP-his-myc alone. 24 hours later, cells were harvested, and nuclear extract was isolated using the Active Motif Nuclear Complex Co-IP kit (cat. #54001). The extracts were immunoprecipitated overnight at 4°C with either Flag-tagged beads (Sigma, #M8823) or GFP antibody (Rabbit, Invitrogen A11122) and eluted with 0.1M glycine, pH 2.5 at RT for 30 minutes with occasional agitation. The samples were denatured at 100°C for 5 minutes in 5x sample buffer, run on an 8% SDS-PAGE at 70V for 2 hours, transferred to PVDF (Sigma, IPVH85R) at 150mA for 90 minutes, and blocked for one hour in 1% non-fat dry milk-TBST. 2ug of Fezf2 (Rabbit, IBL F441), Tle4 (Mouse, Santa Cruz Biotechnology sc-365406), GFP (Chicken, Aves Labs GFP-1020), or Myc (Goat, Abcam ab9132) primary antibodies were added and incubated overnight at 4°C on an orbital shaker. The blot was developed with Li-Cor secondary antibodies (#926-32212, 926-32214, 926-68073, 926-68072) or Alexa 488 for one hour and images were processed using ImageStudioLite.

Western blotting

P7 cortices were dissected in ice cold 1X PBS supplemented with cOmplete Mini, EDTA-free protease inhibitor tablets (Roche, 04 693 159 001) and transferred to RIPA buffer for 20 minutes on ice. The tissue was homogenized by pushing through 25G and 27G needles sequentially, 3 times each. Cell homogenate was centrifuged at 14,000 g for 10 minutes at 4°C. The supernatant was removed, denatured at 100°C for 5 minutes in 5x sample buffer, run on an 8% SDS-PAGE at 70V for 2 hours, transferred to PVDF (Sigma, IPVH85R) at 150mA for 90 minutes, blocked for one hour in 1% non-fat dry milk-TBST, and immunoblotted overnight with 2ug of FEZF2 (Rabbit, IBL F441) primary antibody. The blot was developed with Li-Cor Donkey anti Rabbit secondary antibody (#926-68073) for one hour and images were processed using ImageStudioLite.

In situ hybridization

In situ hybridization was performed using a previously published protocol (Guo et al., 2013). In brief, digoxigenin-labeled probes used in this study were made from cDNAs amplified by PCR using the following primers:

Primers used for *In situ* hybridization probes

Gene	Forward Primer 5' → 3'	Reverse Primer 5' → 3'	Source
Tcerg1l	CTCTCCCCACTGTG GTATTAGC	CAGAACTATTTCCCC TCGTGAC	This paper
Ldb2	CACCTGATTACGCT GTCCATAG	AAGTTCAACACACGA GGGAGAT	This paper

Ctgf	AAATCGCCAAGCCTGTCAAG	GGCACTGTGCGCTAATGAAC	This paper
Cryab	CTCAGCCCTGCCTGTGTT	ATCTGGGCCAGCCCTTAG	This paper
Ephb1	CACATCCATCTCCCTTTGCT	TCCAGAAACCCTTTCCCTCT	(Lodato et al., 2014)
Kif26a	TCCTCAGCTCCAGACTCCAT	GCGACAGTCTTTCCATCTCC	(Lodato et al., 2014)
Wnt7b	ACGCAATGGTGGTCTGGT	AAGGGCCTGAGGAAATGG	Allen Brain Atlas

Amplified DNA fragments were ligated into pGEM-T Easy (Promega) plasmids, transformed into competent *E. coli* cells, and plated overnight on LB+Agar+Ampicillin plates. Colonies were picked, grown overnight in 3 mL LB+Ampicillin, and purified via miniprep kits (Sigma-Aldrich). Purified plasmids were sequenced to ensure sequence fidelity, and to determine insert orientation. Plasmids were then linearized with restriction enzymes from New England Biotech, and *in vitro* transcription reactions were performed with either T7 (NEB) or Sp6 (Promega) RNA polymerases, depending on insert orientation, in the presence of DIG-labeled nucleotides (Sigma-Aldrich). Tissue was prepared as previously described (Guo et al., 2013), and treated with DIG-labeled probes overnight at 65°C. Slides were developed with NBT/BCIP stock solution (Sigma-Aldrich).

EdU labeling

Timed pregnant *Tle4*$^{+/LacZ}$ mice were injected with a single dose of EdU (50mg/kg body weight; Thermo Fisher Scientific, E10187) at E12.5 or

E13.5. Brains were collected at P7. EdU was detected via a click-chemistry reaction containing the following reagents per 1 mL of reaction: 950ul 100mM Tris PH 7.4, 40ul 100 mM CuSO4, 10ul 200 mg/mL sodium ascorbate, and 1ul azide 488 or 555. *Tle4*$^{LacZ/LacZ}$ and littermate *Tle4*$^{+/+}$ control mice were analyzed.

Anterograde tracing using AAV

0.25 µl AAV2-CMV-mCherry virus (Vector Biosystems Inc.) were injected into the M1, S1 or V1 of *Tle4*$^{LacZ/LacZ}$ and littermate control *Tle4*$^{+/LacZ}$ or *Tle4*$^{+/+}$ mice at P21. The brains were collected at P35 and sectioned at 50-µm thickness.

Retrograde tracing

Retrograde tracing was performed using Alexa Fluor 555-conjugated cholera toxin subunit β (CTB) injections. 8 mg/ml CTB in PBS was used for all injections, and CTB solution was injected through a pulled glass pipet attached to a Picospritzer III (Parker). P4 mice were anesthetized, the pyramidal decussation was identified visually, and 1 µl CTB was injected. 0.2 to 0.5 µl CTB was injected into S1 in anesthetized P4 mice and injection sites were confirmed after brain collection at P7. Corticothalamic neurons were labeled by CTB injection (0.2 µl) into the

thalamus at P21 (coordinates: A/P −1.3 mm, M/L 3 mm, Z 3.15 mm) and injection sites were confirmed after brain collection at P28.

Cloning of the pCAG-Fezf2, pCAG-Fezf2-EnR, and the pCAG-Fezf2-VP16 expression plasmids

The cloning of *pCAG-Fezf2* plasmid was reported previously (B. Chen et al., 2005a). The EnR and VP16 plasmids were obtained from Dr. Thomas Jessell (Columbia University). The cDNA for DNA binding domains of FEZF2 was amplified using primers 5′-GATCGAATTCTCAGCTCTGAACTGTCCTGGCTAGGTC-3′ and 5′-GATCGGATCCGCCGCCGCCATGGAGCCCCGGCCTGCTGCGTTAGAGGC-3′. The cDNA for the EnR domain was amplified using primers 5′-GATCGATATCAAGCTTGGGCTGCATAGATCCCAG-3′ and 5′-GATCGGATCCGCCGCCACCATGGAGTTCCGCGATGCCCTGGAGGATCGC-3′. The cDNA for VP16 domain was amplified using primers 5′-GATCGGATCCGCCGCCACCATGGCCCCCCCCGACCGATGTCAGCCT-3′ and 5′-GATCGATATCCCCACCGTACTCGTCAATTCCAA-3′. The amplified DNA fragments were ligated into pCAG vector, using NotI and XhoI restriction sites. Sanger DNA sequencing was performed to ensure no mutation was generated during the cloning.

In utero electroporation

In utero electroporation experiment was performed according to a published protocol (B. Chen et al., 2005). In utero electroporation (IUE) of wild-type CD-1 embryos was performed at E15.5. Plasmids *pCAG-Fezf2*, *pCAG-Fezf2-EnR*, or *pCAG-Fezf2-VP16* were mixed with *pCAG-EGFP* (Addgene #11150) (final concentration of 1-2 μg/μl at a molecular ratio of 3:1, 0.5 μL each embryo) and 0.05% Fast Green (Sigma), and injected into the lateral ventricle of embryos using a beveled pulled glass micropipette. The control brains were electroporated with *pCAG-EGFP* plasmids alone. Five electrical pulses (duration: 50 ms) were applied at 35V across the uterine wall with a 950 ms interval between pulses. Electroporation was performed using a pair of 7-mm platinum electrodes (BTX, Tweezertrode 45-0488, Harvard Apparatus) connected to an electroporator (BTX, ECM830). The electroporated brains were collected at P5.

Image acquisition and analysis

Images for quantitative analyses were acquired with a Zeiss 880 confocal microscope. Laser power and gain were adjusted until < 1% of pixels were saturated. Cell counting was performed on single z-slices with FIJI. Z-slices were divided into 500 μm or 250 um wide regions and split into equally sized bins. Individual channels were adjusted with auto threshold

“Moments,” or a manual threshold was applied to discern BCL11B high versus low expressing cells. The dilate, erode, and watershed functions were sequentially used before particles were analyzed with a circularity of 0.3-1.0 and size exclusion of > 1μm. Brightfield images were acquired with a Zeiss AxioImager Z2 widefield microscope with a Zeiss AxioCam 506 (color) camera.

Statistical analysis was performed using GraphPad Prism 5.0, or R. Only single Z-slice confocal images were used in cell quantifications. For each brain, the number of marker^{+} cells in the cortex were quantified in a 500- or 250-μm-wide region from 3 sections each for S1, M1 and V1 areas. Care was taken to match the anterior-posterior, medial-lateral positions for the chosen areas between the mutant and control genotypes. For each genotype and each age, 3 different brains were analyzed. Data are shown as mean ± SEM and statistical significance for multiple comparisons was determined using the ordinary one-way ANOVA test followed by Tukey’s multiple comparisons test. Statistical significance for single comparisons was determined using the unpaired t test. Significance was set as * for $p < 0.05$, ** for $p < 0.01$, *** $p < 0.001$ for and $^{****}p < 0.0001$ all significance tests.

RNA-seq analysis of Tle4$^{LacZ/LacZ}$, Fezf2$^{-/-}$, and Fezf2$^{-/-}$; Fezf2-EnR cortices at P0

Cortices were dissected from P0 *Tle4$^{LacZ/LacZ}$* (n = 3 mice) and littermate control *Tle4$^{+/+}$* (n = 3) mice, P0 *Fezf2$^{-/-}$* (n = 4), *Fezf2$^{-/-}$; Fezf2-EnR* (n = 2), and littermate *Fezf2$^{+/+}$* mice (n = 4). Total RNA from each pair of cortical hemispheres was isolated using the RNAesay kit (QIAGEN) and used to prepare RNA-seq libraries (Illumina RNA Truseq Library Prep protocol). Libraries were paired-end (50 nucleotides per end) sequenced on the Illumina Hiseq2000 platform. The sequences were processed and analyzed for differential expression as previously described (Betancourt et al., 2014). The RNA-seq data for the *Fezf2$^{-/-}$*, *Fezf2$^{-/-}$; Fezf2-EnR*, and control *Fezf2$^{+/+}$* cortices, and for the *Tle4$^{LacZ/LacZ}$* and control *Tle4$^{+/+}$* cortices can be accessed using GSE160202 and GSE142269, respectively.

Electrophysiology and neuronal morphology

Whole cell recording was conducted in the primary somatosensory cortex (V1). To label layer 6 corticothalamic neurons, 50nl of retrobeads (Lumafluor) were injected into the POM nucleus unilaterally at least 24h prior to recording. 350-µm slices were made after a block cut of the posterior brain with a 45° angle to the mid-sagittal plane. Slices were cut in ice-cold ACSF (containing 126 mM NaCl, 2.5 mM KCl, 26 mM $NaHCO_3$,

2 mM $CaCl_2$, 1 mM $MgCl_2$, 1.25 mM NaH_2PO_4, and 10 mM glucose saturated with 95% O_2 and 5% CO_2). Slices were incubated at 32°C for 30 min before being transferred to the recording chamber.

Beads$^+$ neurons with soma in layer 6 were identified under a 60X objective (NA = 0.9). Only neurons with their soma at least 50 μm below the slice surface were targeted for whole cell recordings. The internal electrode solution contains: 130 mM K-gluconate, 10 mM HEPES, 4 mM KCl, 0.3 mM GTP-Na, 4 mM ATP-Mg, 2 mM NaCl,1 mM EGTA and 14 mM phosphocreatine (pH 7.2, 295-300 mOsm). 0.15% (W/V) biocytin was added when neuron morphology data were desired. Neuronal signals were amplified using a MultiClamp 700B amplifier (Molecular Devices, Forster City, CA), low-pass filtered at 1 kHz (current) or 10 kHz (voltage signals), and digitized at 20 kHz using a Digidata 1440A interface and pClamp 10.6 (Molecular Devices). mEPSCs were measured with D-AP5 (50 μM, Tocris) and tetrodotoxin (TTX, 1 μM, Tocris) included in the ACSF. To measure mIPSCs, TTX (1 μM) and CNQX (10 μM) were included and a symmetrical [Cl^-] electrode internal solution (containing: 125 mM KCl, 2.8 mM NaCl, 2 mM $MgCl_2$, 2 mM Mg^{2+}-ATP, 0.3 mM Na_3GTP, 10 mM HEPES, 1 mM EGTA and 10 mM phosphocreatine, pH 7.25, ~300 mOsm) was used. In experiments where neuronal excitability was measured, a series of current steps (−100

to 500pA in 50 pA increment) were injected, and numbers of AP firing were manually quantified.

To reconstruct neuronal morphologies, slices were fixed in 4% PFA overnight, followed by incubation with avidin-Alexa 488 (Invitrogen) for 24 h in PBS containing 0.2% Triton X-100. Slices were washed and mounted on slides with a 350-μm spacer to prevent crushing the tissue. Neuronal dendritic arbors were acquired by collecting Z stack images on a confocal microscope (Zeiss LSM 710). Maximal projection images were imported into FIJI/ImageJ, and neurite arborization and Sholl analysis (Sholl, 1953) were done using the Simple Neurite Tracer plugin. Due to the length of apical dendrites, dendrites were frequently cut off. Therefore, only basal dendrites were used for Sholl analysis. Morphometric features extracted included dendritic arbor, length, and number of intersections at various distances from soma. For dendritic spine analyses, Z stacks of spines from the basal dendrites (100-450 μm away from soma) were collected with a 63x objectives (Plan-Apochromat, NA 1.4). 512 × 512 pixels with 4 × digital zoom and 0.2 μm Z step size were used for Z stack acquisition. Imaris software (V8.02, Bitplane, South Windsor, CT) was used to measure spine head diameter, length, and density (Peng et al., 2016).

Quantification and statistical analysis

The statistical details of the experiments can be found in the figure legends and Method details section under the experiments. All n values and what n represents are listed in the figure legends, and all p values obtained are listed in the figure legends. GraphPad Prism version 8 was used to perform statistical tests in this study. The statistical tests used for each experiment are indicated in the figure legends.

Acknowledgements

This study was supported by grants to B.C. (NIH R01 MH094589 and R01 NS089777), N.S. (NIH U01 MH116488 and R01 NS095654), S.K.M. (NIH R01 EY08411), and S.Q. (University of Arizona startup funds). We thank Dr. Haihui Xue (Hackensack University Medical Center) for providing the mouse *Tle4* cDNA plasmid. We would like to acknowledge technical support and training from Benjamin Abrams in the UC Santa Cruz Life Sciences Microscopy Center. Use of the Zeiss 880 confocal microscope was made possible by the award of NIH S-10 Instrumentation grant 1S10OD23528-01. We would like to thank Dr. Hannah Maul-Newby and Dr. Melissa Jurica for technical assistance. We also thank our interns and volunteers that helped with the project, Cosmo Hahn, Hansen Lillemark, Emily Brumley, Litzy Rodriguez, Maanvi Thawani, and Sahiti Annadata. The graphical abstract was created with BioRender.com.

Chapter 3: Dose dependent regulation of cortical projection neuron development by Satb2

Summary

De novo mutations in Special AT-rich Binding Protein 2 (SATB2) result in SATB2-associated syndrome (SAS), a recently described disease characterized by developmental defects and intellectual deficiency. SATB2 expression in the brain is mostly restricted to the excitatory neurons in the cerebral cortex and the hippocampus, suggesting that the intellectual deficiency associated with SAS is likely due to defective cortical and hippocampal neurons. Extensive studies show that Satb2 regulates gene expression and plays a crucial role in specifying the identities of multiple cortical projection neuron subtypes. However, these studies were performed using Satb2 homozygous mutant mice. It remained unknown how SATB2 haploinsufficiency, as identified in the SAS patients, affects brain development. Utilizing Satb2 deficient mice, we show that Satb2 haploinsufficiency leads to gene mis-regulation, physiological changes, aberrant axonal projections, and cortical lamination defects. Chromatin immunoprecipitation and CUT&RUN experiments reveal that Satb2 binds to gene promoters and enhancers. We show that Satb2 both activates and represses gene expression, by recruiting distinct chromatin remodeling complexes. Our findings uncover fundamental

mechanisms underlying cortical projection neuron development and the etiology of SAS.

Introduction

The 6-layered neocortex is the seat of the most complex cognitive and perceptual functions in humans. Glutamatergic projection neurons occupy a central position in cortical neural circuits, serving as the principal input units and the sole output system. Although single-cell RNA-seq analysis has revealed many refined subtypes (Tasic et al., 2018; Zeng, 2022), cortical excitatory neurons can be broadly classified into three major subtypes based on hodology: corticothalamic (CT) neurons in layer 6 that project to the thalamus, subcerebral projection neurons (SCPNs) in layer 5b that projection to the midbrain, hindbrain, and spinal cord, and intra-telencephalic (IT) neurons that reside throughout layers 2-6 and project to ipsi- or contra-lateral cortical hemisphere (Greig et al., 2013; Leone et al., 2008).

During development, cortical excitatory neurons arise directly from radial glial cells (RGCs) or indirectly from intermediate progenitors (Kriegstein and Alvarez-Buylla, 2009; Malatesta et al., 2000; Miyata et al., 2001; Noctor et al., 2001). The earliest-born neurons form the preplate which is split into the marginal zone and subplate by incoming cortical plate neurons. The excitatory neurons within the cortical plate arise in a

temporal sequence where layer 6 neurons are produced first, followed by increasingly superficial layers up to layer 2 (Leone et al., 2008). Proper generation and differentiation of the cortical excitatory neurons is essential for proper cortical functions.

Extensive progress has been made toward delineating the molecular mechanisms underlying the production of distinct excitatory neuron subtypes. Development of distinct projection neuron subtypes depends on a network of transcription factors that mostly cross-inhibit the expression of one another (Greig et al., 2013). The zinc-finger transcription factor Fezf2 is expressed in deep-layer neurons where it promotes subcerebral neuronal identity while suppressing the expression of cell fate determining genes for corticothalamic (*Tbr1*) and callosal (*Satb2*) neurons (B. Chen et al., 2005b; Chen et al., 2008a; J.-G. Chen et al., 2005; Molyneaux et al., 2005; Tsyporin et al., 2021). *Tbr1* and *Sox5* promote corticothalamic neuronal fate and directly repress high levels of *Fezf2* and thus subcerebral identity in layer 6 neurons (Han et al., 2011; Kwan et al., 2008; Lai et al., 2008; McKenna et al., 2011). Satb2 was reported to be specifically expressed in callosal neurons and promote callosal neuron identity by repressing essential genes for subcerebral axon development (Alcamo et al., 2008; Britanova et al., 2008). Further studies revealed that Satb2 is also required for specifying layer 5 subcerebral neuron identity (McKenna et al., 2015).

SATB2 Associated Syndrome (SAS) is a newly identified neurodevelopmental disease that is characterized by developmental delay, severe intellectual deficiency with absent or limited speech, behavioral problems, and dysmorphic craniofacial features (Zarate et al., 2017). It is caused by *de novo* mutations of *SATB2*, a gene encoding SATB2, a DNA-binding protein involved in chromatin remodeling. In the brain, *SATB2* expression is mainly restricted to the projection neurons in the cerebral cortex and hippocampus, suggesting that the etiology of the intellectual deficiency of SAS is likely defective cortical and hippocampal projection neurons.

Studies in mice have shown that *Satb2* is required for specifying the subtype identities of both cortical callosal and SC neurons. In *Satb2* mutant mice, callosal neurons lose their molecular and axon projection identities, and express genes associated with layer 5 SC neurons, while the layer 5 SC neurons are missing and fail to extend axons to the brainstem and spinal cord (Alcamo et al., 2008; Britanova et al., 2008; Leone et al., 2015; McKenna et al., 2015). By recruiting the NuRD nucleosome remodeling complex, Satb2 represses the expression of *Bcl11b,* a gene essential for axonal projections of layer 5 SC neurons (Alcamo et al., 2008; Britanova et al., 2008). Despite these discoveries, the underlying molecular logic for how Satb2 broadly regulates gene expression programs is unknown. Furthermore, prior studies on Satb2

function in brain development were performed using homozygous mutant mice (Alcamo et al., 2008; Britanova et al., 2008; Leone et al., 2015; McKenna et al., 2015). It remains to be determined how haploinsufficiency of *SATB2*, as identified in SAS patients, affects brain development.

Here, using Satb2 deficient mice, we demonstrate that Satb2 regulates proper cortical laminar organization, intra-telencephalic axon development and gene expression in a gene-dosage-dependent manner. Our CUT&RUN analysis revealed that Satb2 directly regulates numerous genes implicated in cell fate specification as well as genes critical for cell adhesion, axon guidance, and neuronal physiology. We find that Satb2-mediated gene activation and repression is likely facilitated by the interaction of Satb2 with ATP-dependent chromatin remodeling complexes. Furthermore, we show that proper Satb2 dosage is required for cortical layer formation and that Satb2 haploinsufficiency affects IT neuron axon projections, gene expression programs, and neuronal physiology while sparing the SCPN and CT neuron projections, providing insights into the molecular underpinning of SAS etiology.

Results

Satb2 haploinsufficiency leads to defective cortical laminar organization

To examine how SATB2 haploinsufficiency affects brain development, we utilized *Satb2*$^{LacZ/+}$ mice, which carry a beta-galactosidase gene inserted at the start of the *Satb2* open reading frame (*Satb2*^{LacZ}) (Dobreva et al., 2006), effectively knocking out the *Satb2* gene (**Error! Reference source not found.**A). Western blot analysis revealed a 50% decrease of Satb2 protein in the *Satb2*$^{LacZ/+}$ cortices and absence of Satb2 protein in the *Satb2*$^{LacZ/LacZ}$ cortices (Figure Figure ***17: Layer size defects in* Satb2LacZ$^{/+}$ *cortices***)

We analyzed Satb2+/+ and Satb2LacZ/+ brains collected at postnatal day 1 (P1), P4, P7, and P28 (Figure 17B-Figure ***17***E). Immunostaining for markers of different cortical projection neuron subtypes and nuclear staining did not show any significant change in the *Satb2*$^{LacZ/+}$ cortices at P1 (Figure 17B and Figure ***17***D). Comparing cortices from *Satb2*$^{+/+}$ *and Satb2*$^{LacZ/+}$ mice at P4, P7, and P28 revealed changes in the thickness of cortical layers (Figure 17B-Figure ***17***E).

At P28 *Satb2*$^{LacZ/+}$ mice showed a 23.2% reduction for layer 6 (*Satb2*$^{+/+}$: 333.0 ± 22.5 μm (SEM) vs. *Satb2*$^{LacZ/+}$: 255.7 ± 15.6 μm), 38.6% reduction for layer 4 (*Satb2*$^{+/+}$: 133.1 ± 6.0 μm vs. *Satb2*$^{LacZ/+}$: 81.8 ± 2.9 μm), and 13.7% increase for layer 1 (*Satb2*$^{+/+}$: 107.8 ± 12.8 μm vs.

Satb2$^{LacZ/+}$: 123.6 ± 19.5 μm) in the S1 barrel field (BF) area, while the thickness for layer 5 and layers 2/3 was not significantly affected (***Figure 17***B-***Figure 17***E).

Layer 6 projection neurons include corticothalamic neurons (L6CT), intra-telencephalic neurons (IT), and a small population of deep-layer near-projecting neurons (DLNP) neurons, which can be distinguished by Tbr1 and Tle4 expression. L6 CTs and DLNPs express both Tbr1 and Tle4 (Tbr1^{+}Tle4^{+}), while L6 IT neurons express Tbr1 but not Tle4 (Tbr^{+}Tle4^{-}). The *Satb2*$^{LacZ/+}$ cortices showed a significant reduction of Tbr1^{+} neurons in layer 6 of at P4, P7, and P28. Among the Tbr1^{+} neurons, the numbers of Tbr1^{+}Tle4^{-} L6ITs were significantly reduced, while the numbers of Tbr1^{+}Tle4^{+} CTs and DLNPs were not significantly affected (Figure 17B and Figure ***17***E), suggesting that Satb2 haploinsufficiency results in a significant loss of L6ITs.

We examined layers 2-4 using antibodies for Rorb, Cux1 and Lhx2. We found that in the *Satb2*$^{LacZ/+}$ brains, the number of Rorb^{+} cells in layer 4 was significantly decreased in S1BF but increased in the more medial S1 Trunk (Tr) region (Figure 19A). A similar change for Cux1 expression was also observed (S2B), indicating a patterning defect of the S1Tr and S1BF regions. Immunostaining did not reveal neuronal subtype marker changes in layer 5 of the *Satb2*$^{LacZ/+}$ cortices (Figure 19D).

To investigate the cause of the thinner layer 6 and reduced Tbr1+ L6 ITs in the *Satb2*$^{LacZ/+}$ cortices (Figure 17B and Figure ***17***E), we examined the expression between Tbr1 and Satb2, and observed that Satb2 and Tbr1 were co-expressed as early as E13.5 and throughout embryogenesis. Thus, Satb2 is expressed in these neurons at or around the time of their birth (Figure 18C).

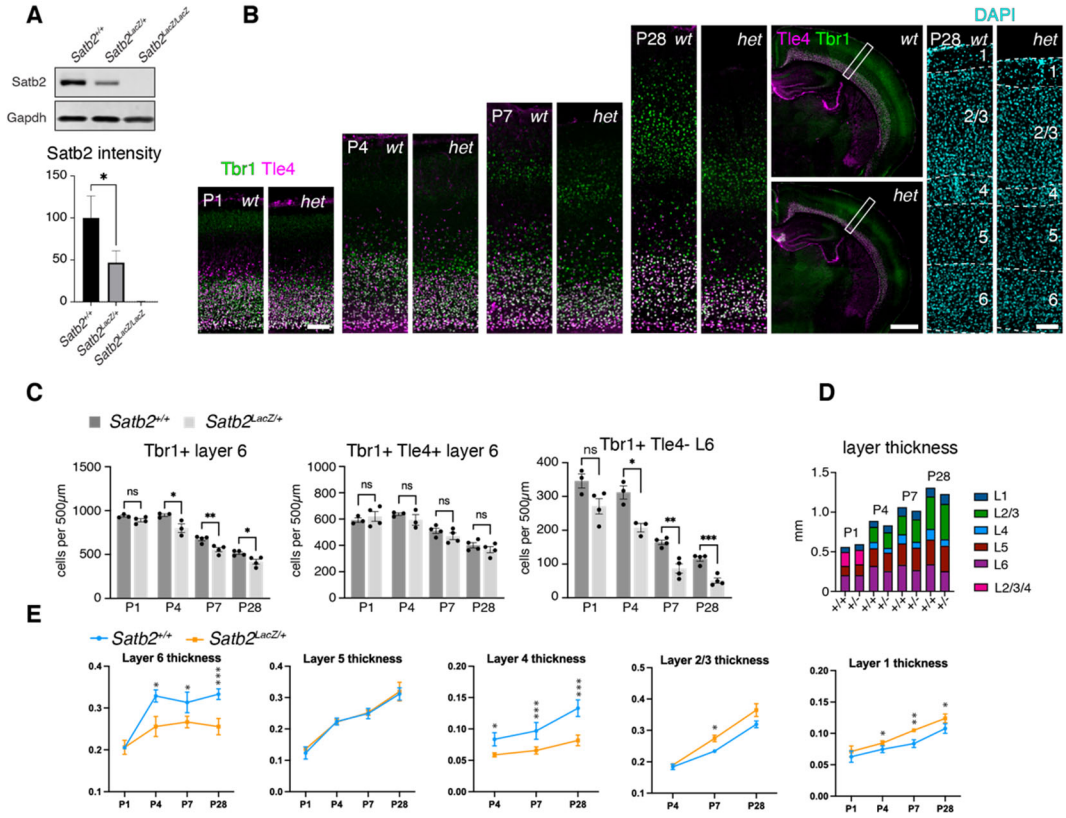

Figure 17: Layer size defects in *Satb2*$^{LacZ/+}$ cortices

(A) Western blot showing a reduction and absence in *Satb2*$^{LacZ/+}$ and *Satb2*$^{LacZ/LacZ}$ cortices. Satb2 signal was normalized to Gapdh signal in each lane. n = 3 brains per genotype. Statistical significance was determined using student's t-test (* $p < 0.05$)
(B) Immunostaining for Tbr1 and Tle4 on brain sections from P1, P4, P7, and P28 *Satb2*$^{+/+}$ and *Satb2*$^{LacZ/+}$ mice, and DAPI at P28.
(C) Quantifications of marker^{+} cells per 500µm wide section in layer 6. n = 3-4 brains per genotype, 3-4 sections per brain.
(D) Quantification of layer thickness in mm
(E) Quantification of layer thickness split up by individual layers.
In all graphs, n = 3-4 brains per genotype, 3-4 sections per brain. Error bars represent ± SEM. Statistical significance was determined using nested t-test (*$p < 0.05$, **$p < 0.01$, ***$p < 0.001$)

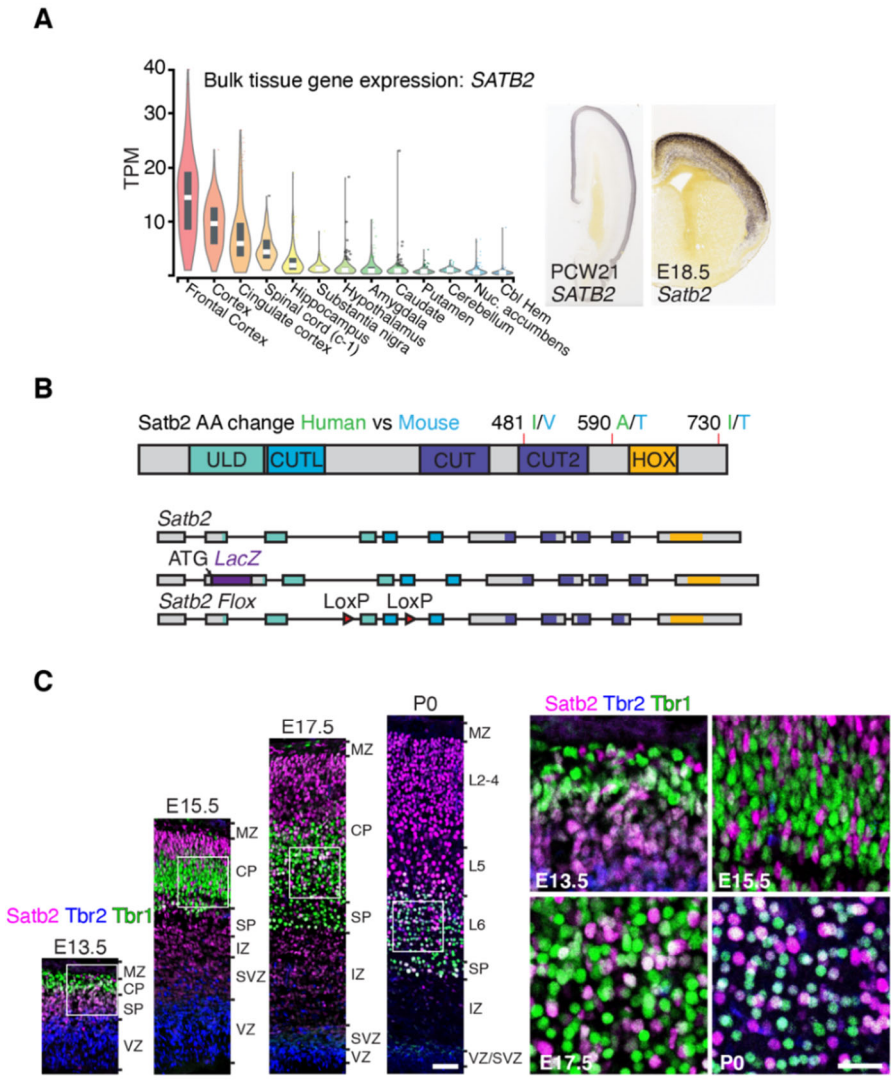

Figure 18: Satb2 is conserved between mouse and human and expressed across cortical layers

(A) Bulk tissue gene expression for *SATB2* and images from Allen Brain Atlas from PCW21 human embryo or E18.5 mouse embryo in-situ for *SATB2* or *Satb2* respectively.
(B) Diagram of Satb2 showing ammino acid changes between human and mouse. Blow is a diagram of the *Satb2* gene, $Satb2^{LacZ}$ allele, and $Satb2^{Flox}$ allele. ULD: ubiquitin-Like Domain, responsible for oligomerization. CUTL: CUT-like domain, similar to CUT domain, DNA binding motif. HOX: homeobox domain, DNA binding.
(C) Immunostaining for Satb2, Tbr2, and Tbr1 at E13.5, E15.5, E17.5, and P0. Satb2 expression is seen as early as E13.5 and co-expressed with Tbr1 but not Tbr2. Low mag scale bar 100μm, high mag scale bar 50μm.

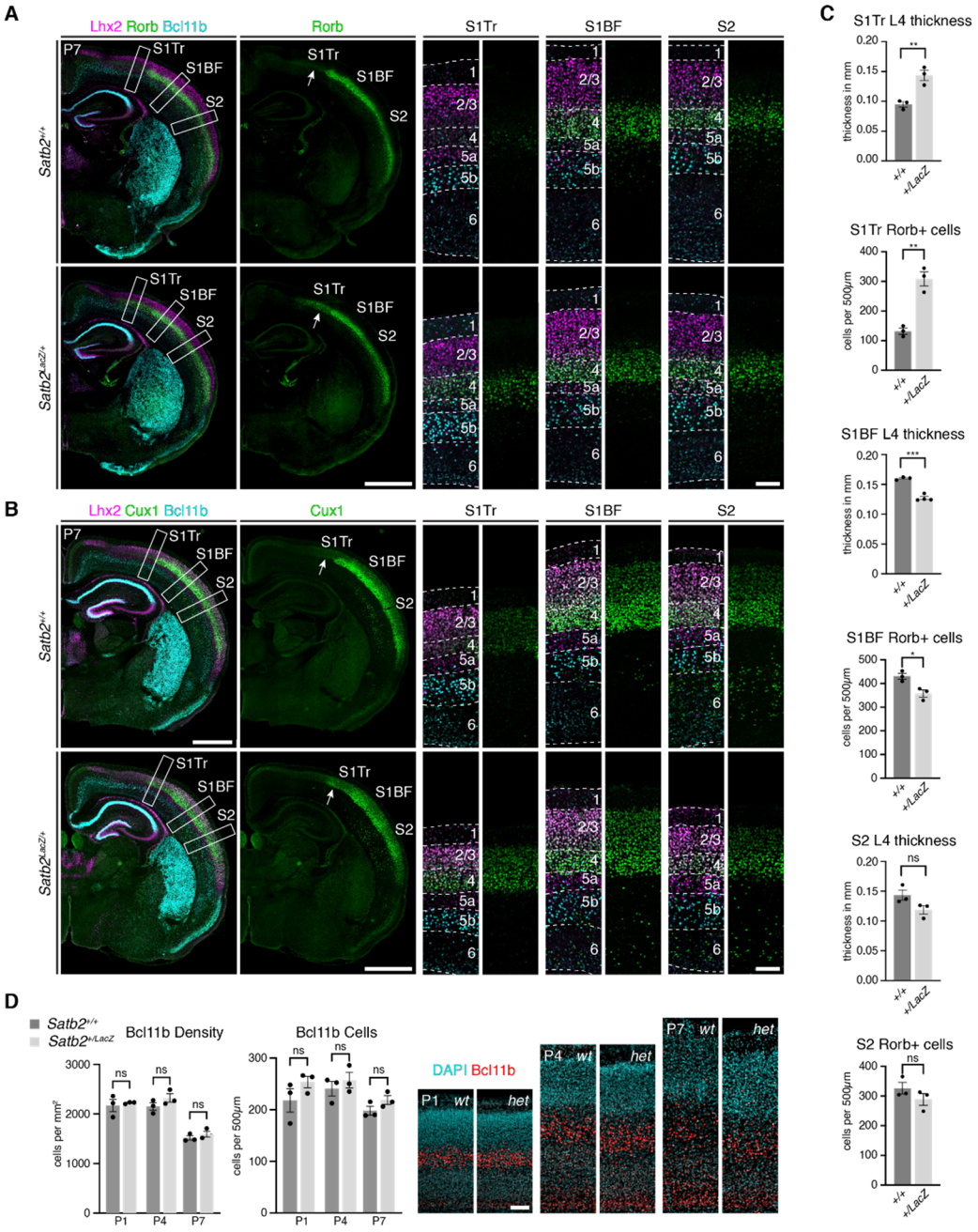
A
Lhx2 Rorb Bcl11b
Rorb
S1Tr
S1BF
S2
P7
Satb2+/+
Satb2lacZ/+
1
2/3
4
5a
5b
6
B
Lhx2 Cux1 Bcl11b
Cux1
C
S1Tr L4 thickness
thickness in mm
S1Tr Rorb+ cells
cells per 500μm
S1BF L4 thickness
S1BF Rorb+ cells
S2 L4 thickness
S2 Rorb+ cells
+/+
+/LacZ
D
Satb2+/+
Satb2+/LacZ
Bcl11b Density
cells per mm2
Bcl11b Cells
P1
P4
P7
ns
DAPI Bcl11b
wt
het

Figure 19: *Satb2*$^{LacZ/+}$ cortex exhibits thinner layer 4 in S1BF, and expansion of S1BF into S1Tr while layer 5 is unaffected

(A) Immunostaining for Lhx2, Rorb, and Bcl11b in P7 *Satb2*$^{+/+}$ and *Satb2*$^{LacZ/+}$ cortices. L2/3 and 5a marker Lhx2 and 5b marker Bcl1b are unaffected in *Satb2*$^{LacZ/+}$ cortices, while Rorb expression is decreased in L4 S1BF, expanded in S1Tr (white arrow), and unchanged in S2. Low magnification scale bar: 1000 μm, high magnification scale bar: 100 μm.
(B) Cux1 expression shows expansion into S1Tr (white arrow) in *Satb2*$^{LacZ/+}$ cortices. Low magnification scale bar: 1000 μm, high magnification scale bar: 100 μm.
(C) Quantifications of marker^{+} cells per 500 μm wide section. n = 3-4 brains per genotype, 3-4 sections per brain. Error bars represent ± SEM. Statistical significance was determined using nested t-test (*$p < 0.05$, **$p < 0.01$)

Satb2 haploinsufficiency results in defective callosal and thalamocortical projections

We examined whether Satb2 haploinsufficiency impacts axon development. Immunostaining with L1 antibody revealed that in *Satb2*$^{LacZ/+}$ mice, the corpus callosum length was significantly reduced along the anterior-posterior axis at P7 (Figure 20A). (*Satb2*$^{+/+}$: 2601 ± 126 μm; *Satb2*$^{LacZ/+}$: 2043 ± 67 μm; n = 10 mice per genotype, p = 0.0010, unpaired t-test). L1 and PKCγ staining did not reveal significant changes in corticothalamic and corticospinal axons. Ntng1 is highly expressed in the thalamic neurons and labels the thalamocortical axons (TCAs). In the *Satb2*$^{LacZ/+}$ cortices, Ntng1 staining in layer 4 in S1 was reduced, indicating less cortical TCA innervation (Figure 20B). We examined barrel fields, an easily discernable target of TCAs, using cytochrome oxidase (CO) staining. Barrel organization was easily discernable in the controls. However, in *Satb2*$^{LacZ/+}$ cortices, the barrel field was smaller overall, and the A1 row of barrels was consistently missing (Figure 20B).

To systematically examine the callosal, subcerebral, and corticothalamic projections, we injected Cholera toxin subunit B (CTB) into the corpus callosum (CC) close to the midline, cerebral peduncle (CP), and ventral posterior medial nucleus of the thalamus (VpM) at P28 and examined the brains at P33 (Figure 21). When CTB was injected into the CC, we observed both retrogradely labeled cells (and their axons) and

anterogradely labeled axons in the *Satb2*$^{+/+}$ and *Satb2*$^{LacZ/+}$ mice (Figure 21). We observed CTB-labeled cells and axons across layers 2/3, 5, and 6 in the ipsi and contralateral cortex in controls. However, in *Satb2*$^{LacZ/+}$ cortices, there was a near absence of cells and axons labeled in layers 2/3 and reduced labeling of cells and axons in layers 5 and 6 in the somatosensory regions (Figure 21A). In the more medial region, the labeling in the medial parietal association (MPtA) region of the cortex was similar to the *Satb2*$^{+/+}$ mice (Figure 21A). Injection into the CP revealed no discernable difference in labeling the layer 5 SCPNs between *Satb2*$^{+/+}$ and *Satb2*$^{LacZ/+}$ cortices (Figure 21B): CTB labeled cells were abundant in layer 5b, and all labeled cells expressed the layer 5b SCPN marker Bcl11b but not Tbr1 (Figure 21B). Brains injected with CTB into the VpM showed all CTB-labeled cells co-expressed CT markers Tbr1 and Tle4 (Figure 21C). No difference in the number of layer 6 CTs labeled between *Satb2*$^{+/+}$ and *Satb2*$^{LacZ/+}$ cortices (Figure 21C). However, in the *Satb2*$^{LacZ/+}$ mice, the CTB+ cells were more densely packed, consistent with the distribution of Tbr1^{+}Tle4^{+} neurons in these cortices (Figure 21C). These findings reveal that Satb2 haploinsufficiency leads to a severe reduction in callosal projection neurons located in somatosensory regions, while the number of callosal projection neurons more medially (MPtA region) were spared (Figure 21A)

Thus, Satb2 haploinsufficiency differentially affects the major cortical axon pathways. The subcerebral and corticothalamic axon projections (Figure 21B and Figure ***21***C) were mostly unaffected. However, there was almost complete absence of CTB^+ callosal neurons and axons in layer 2/3, and severely reduced labeling of CTB^+ callosal neurons and axons in layers 5/6 in S1 and S2 in the $Satb2^{LacZ/+}$ mice (Figure 21A). These results, combined with the results from the previous section, show that Satb2 haploinsufficiency leads to broad defects in cortical ITs.

The reduction of Ntng1 signal in layer 4 of the $Satb2^{LacZ/+}$ brain suggested that Satb2 expression in the cortex may play a role in TCA innervation and targeting. To determine the requirement of Satb2 for TCA innervation of the cortex, we utilized a conditional *Satb2* expression allele, $Satb2^{Flox}$, and $Emx1^{Cre}$ (Gorski et al., 2002) to generate $Satb2^{LacZ/flox}$; $Emx1^{Cre}$ (*Satb2 cko*) mice. We previously validated that Satb2 expression is entirely absent in the *Satb2 cko* cortex (McKenna et al., 2015). In the *Satb2 cko*, we observed a complete lack of barrel fields visualized by Ntng1 and CO staining in the cortex, but there was still diffuse Ntng1 staining within the cortex and subplate, indicating that TCAs can cross the pallial-subpallial boundary and enter the cortex in *Satb2 cko* brains, and that Satb2 is required for whisker barrel formation and may play a role in proper TCA targeting (Figure 20B)

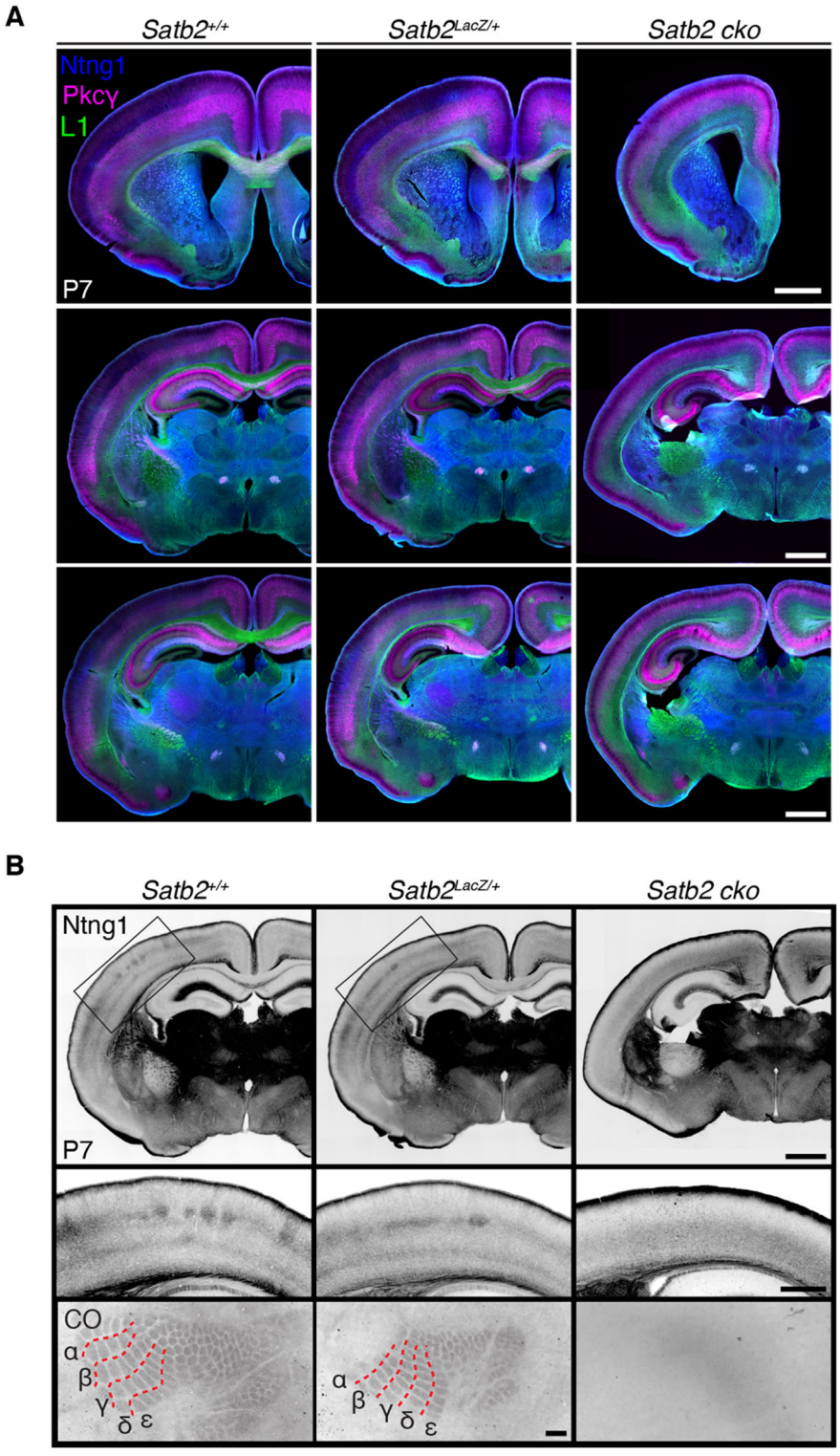
A
Satb2+/+
Satb2LacZ/+
Satb2 cko
Ntng1
Pkcγ
L1
P7
B
Satb2+/+
Satb2LacZ/+
Satb2 cko
Ntng1
P7
CO
α
β
γ
δ
ε

Figure 20: Corpus callosum and thalamocortical projection defects in *Satb2*$^{LacZ/+}$ and *Satb2 cko* cortices

(A) Immunostaining for Ntng1, Pkc γ and L1 in *Satb2*$^{+/+}$, *Satb2*$^{LacZ/+}$, and *Satb2*$^{LacZ/Flox}$; *Emx1*^{Cre} P7 cortices. Scale bars: 1000 μm
(B) Top two rows, Ntng1 staining. High magnification scale bar 1000 μm, low magnification scale bar 500 μm. Bottom row, CO stain on tangential sections at P7. Scale bar 100 μm.

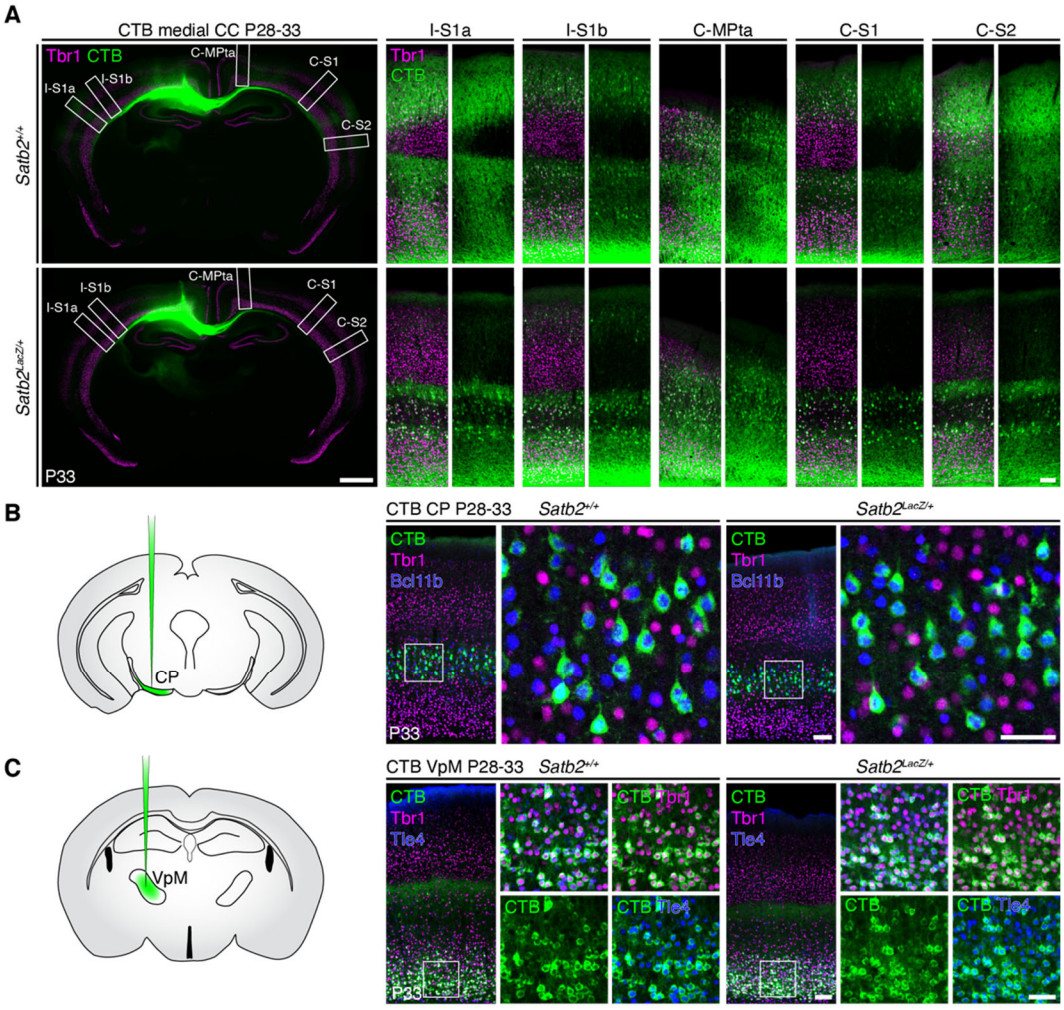

Figure 21: *Satb2*$^{LacZ/+}$ cortices exhibit callosal projection defects and normal subcerebral and corticothalamic axon projections

(A) CTB tracing from the corpus callosum (CC) and staining with Tbr1 to visualize layers. Low magnification scale bar: 1000 μm, high magnification scale bar 100 μm.
(B) Schematic showing injection of CTB into the CP in green. Brains were stained for Tbr1 and Bcl11b. Images taken of S1 regions in *Satb2*$^{+/+}$ and *Satb2*$^{LacZ/+}$ brains. Low magnification scale bar: 100 μm, high magnification scale bar 50 μm
(C) Schematic showing injection of CTB into the VpM. Brains were stained for Tbr1 and Tle4. Images taken of S1 regions in *Satb2*$^{+/+}$ and *Satb2*$^{LacZ/+}$ brains. Low magnification scale bar: 100 μm, high magnification scale bar 50 μm

CUT&RUN analysis reveals Satb2 targets

To identify targets of Satb2, we performed Cleavage Under Targets & Release Using Nuclease (CUT&RUN) (Skene and Henikoff, 2017) experiments using P0 wild-type cortices and antibodies for Satb2 and histone marks associated with active (H3K27Ac And H3K4Me3), and repressive (H3K27Me3) chromatin states (Bannister and Kouzarides, 2011). After mapping sequencing reads to the genome, binding peaks were called using SEACR (Meers et al., 2019), and we identified 8878 Satb2 binding peaks at both promoters (defined as less than 2kb upstream from the transcription start site, TSS), and potential enhancer regions (Figure 22A and Figure ***22***C). Satb2 binding peaks were enriched with all three histone marks analyzed, indicating that Satb2 interacts with active and repressive chromatin states.

Motif analysis revealed that Satb2 bound promoters are enriched in motifs for transcription activators, including Nfy, Sp2/5/1, and Klf1/5/14/3. Potential enhancer regions are enriched for binding motifs for CTCF and transcription factors (TF) including Neurog2, Neurod1, and Lhx2 (Figure 22A andFigure ***22***C). The enrichment of motifs for these TFs at Satb2-bound enhancers highlights its role in the development and differentiation of cortical projection neurons.

We identified 5589 Satb2 target genes after associating the Satb2 binding peaks to genes using ChIPseeker (Yu et al., 2015). We combined

this information with bulk RNA-seq of P0 *Satb2*$^{LacZ/LacZ}$ cortices (McKenna et al., 2015), and found 360 genes directly repressed and 628 genes directly activated by Satb2. Gene ontology analysis revealed that Satb2 activates genes coding for proteins involved in chromatin remodeling, transcription, and various neurodevelopmental processes, while the Satb2 represses genes encoding proteins related to glial cell development, myelination, and various other biological processes and functions unrelated to cortical development.

Satb2 specifies cell fate, in part, by regulating the expression of post-mitotic transcription factors that are essential for generating various projection neuron subtypes (Alcamo et al., 2008; Britanova et al., 2008; McKenna et al., 2015). Indeed, we identified numerous direct Satb2 targets included genes encoding cell fate and layer-specific transcription factors. Layer 5b specific genes that are directly repressed are *Bcl11b*, *Ldb2*, *Grm5*, *Sema5a*, and *Camd1* (Figure 22D). On the other hand, layer-specific genes that are directly activated include deep layer genes *Fezf2, Sox5, Tbr1, Tle4, Wnt7b,* and upper-layer genes *Cux1, Mdga1, Zbtb20,* and *Lhx2* (Figure 22D). These findings highlight the role of Satb2-mediated gene activation and repression for regulating the expression of layer-specific genes and genes involved in a multitude of developmental processes.

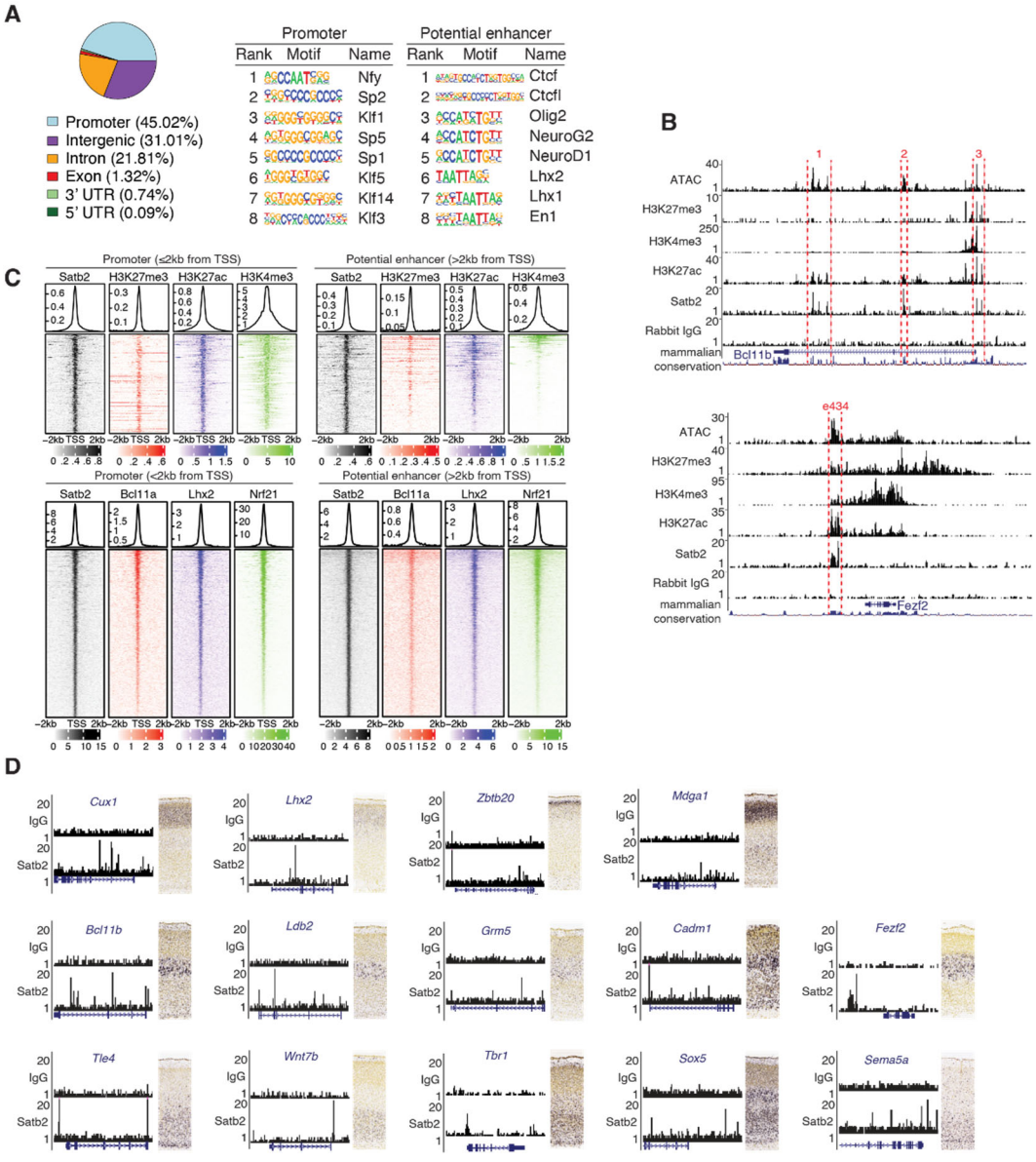
A
Promoter (45.02%)
Intergenic (31.01%)
Intron (21.81%)
Exon (1.32%)
3' UTR (0.74%)
5' UTR (0.09%)
Promoter
Rank Motif Name
1 Nfy
2 Sp2
3 Klf1
4 Sp5
5 Sp1
6 Klf5
7 Klf14
8 Klf3
Potential enhancer
Rank Motif Name
1 Ctcf
2 Ctcfl
3 Olig2
4 NeuroG2
5 NeuroD1
6 Lhx2
7 Lhx1
8 En1
B
ATAC
H3K27me3
H3K4me3
H3K27ac
Satb2
Rabbit IgG
mammalian conservation
Bcl11b
e434
Fezf2
C
Promoter (≤2kb from TSS)
Potential enhancer (>2kb from TSS)
Satb2
H3K27me3
H3K27ac
H3K4me3
Promoter (<2kb from TSS)
Potential enhancer (>2kb from TSS)
Satb2
Bcl11a
Lhx2
Nrf21
D
Cux1
Lhx2
Zbtb20
Mdga1
Bcl11b
Ldb2
Grm5
Cadm1
Fezf2
Tle4
Wnt7b
Tbr1
Sox5
Sema5a
IgG
Satb2

Figure 22: CUT&RUN reveals Satb2 binding sites

(A) Distribution of Satb2 binding sites and MEME motif analysis. Promoter regions are defined as ≤2kb from transcription start site. Potential enhancer regions are defined as >2kb from transcription start site.
(B) Example UCSC genome browser snapshots showing ATAC track as well as coverage tracks for H3K27me3, H3K27Ac, H3K4me3, Satb2, and Rabbit IgG. Satb2 binding sites are between red dashed lines.
(C) Satb2 binding sites are enriched for histone marks H3K27me3, H3K27Ac, and H3K4me3, and transcription factors Bcl11a, Lhx2, Nr2f1. Explain the scales?
(D) Example UCSC genome browser tracks showing IgG and Satb2 coverage tracks for layer-specific genes. P4 Allen brain atlas in-situ hybridization images are shown to the right of each genome browser graphic. Satb2 activates *Cux1, Mdga1, Zbtb20, Lhx2, Fezf2, Sox5, Tbr1, Tle4,* and *Wnt7b.* Satb2 represses *Bcl11b, Ldb2, Grm5, Sema5a,* and *Camd1*.

Misregulated gene expression due to Satb2 haploinsufficiency at P28

To understand the impact of Satb2 haploinsufficiency on gene expression in the cortex, we performed single nuclei RNA sequencing (snRNA-seq) on dissected S1 regions from P28 *Satb2*$^{+/+}$ and *Satb2*$^{LacZ/+}$ cortices. After filtering for quality control, 7865 *Satb2*$^{+/+}$ and 8389 *Satb2*$^{LacZ/+}$ cells were kept for analysis. We co-clustered the *Satb2*$^{+/+}$ and *Satb2*$^{LacZ/+}$ cells (Figure 23A) and performed differential expression analysis to assess the gene expression changes due to *Satb2* haploinsufficiency.

Clusters expressing *Satb2* included L2/3 IT, L6 CT, L6 IT, L4 IT, L4/5 IT, and L5 IT (clusters 0, 1, 2, 5, 7, and 11, respectively). Differential expression analysis within clusters between *Satb2*$^{+/+}$ and *Satb2*$^{LacZ/+}$ cells revealed that the *Satb2* expressing clusters exhibited many significant differentially expressed genes (DEGs, >150). Clusters corresponding to projection neuron subtypes that did not express *Satb2* included, L5NP, L5 PT, and L6b subplate cells (clusters 18, 13, and 20, respectively) had relatively few significant DEGs (<10), and non-neuronal subtypes such as endothelial cells (cluster 21) exhibited few if any significant DEGs (Figure 21B). This analysis revealed that *Satb2* haploinsufficiency leads to widespread gene misregulation in *Satb2* expressing cell types.

Among the top misregulated genes in *Satb2* expressing cells, were those related to axon guidance, cell adhesion, and ion channels. For

example, the following genes were misregulated in two or more *Satb2* expressing clusters and based on CUT&RUN analysis were identified as direct binding targets of Satb2: axon guidance genes *Epha3, Epha7, Gap43, Ppfia2, Slit2, Unc5c*, cell adhesion related genes *Alcam, Cdh10, Cntn3, Cntnap2, Ctnna3, Dock4, Lrfn5, Lsamp, Nectin3, Pcdh9, Sgcz,* and ion channel genes *Cacna1a, Cacna2dl, Kcnd3, Kcnh7, Kcnip3, Kcnip4, Kctd16*. This reveals the critical role of Satb2 in directly regulating genes essential for proper neuronal maturation and function.

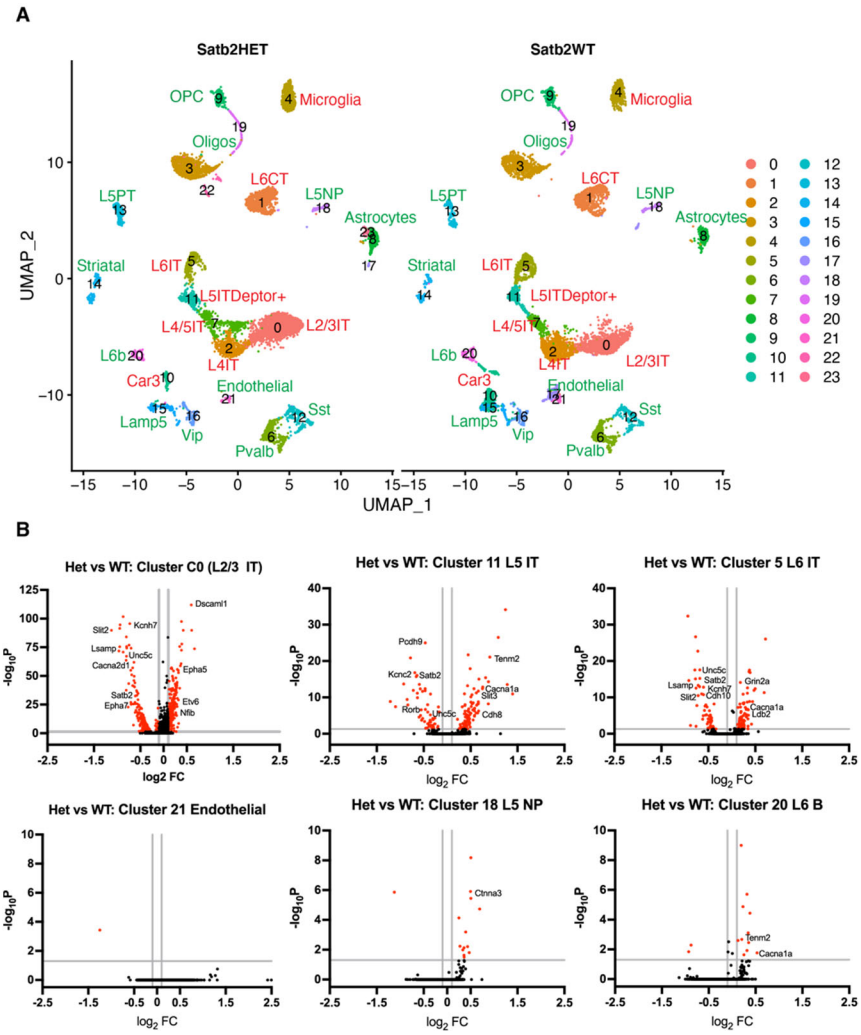

Figure 23: snRNA-seq with S1 P28 tissue reveals widespread misregulated gene expression in *Satb2*$^{LacZ/+}$ cortex

(A) UMAP generated from snRNA-seq from dissected S1 regions in P28 *Satb2*$^{+/+}$ and *Satb2*$^{LacZ/+}$ mice enabled identification of different projection neuron subtypes. Clusters labeled in green showed little to no gene expression changes between *Satb2*$^{+/+}$ and *Satb2*$^{LacZ/+}$ cell types while cells in red exhibited large gene expression changes.
(B) Plots of -log$_{10}$(p-adjusted value) vs log$_2$(fold change). Clusters 0, 11, and 6 are Satb2 expressing clusters exhibiting many significant DEGs while clusters 21, 18, and 20 do not express Satb2 and exhibited few significant DEGs. Verticle lines represent log$_2$(fold change) of ± 0.1 and horizontal lines represent -log$_{10}$(p-adjusted value = 0.05)

Satb2 haploinsufficiency results in altered electrophysiology of layer 5 neurons and local circuit defects

We performed whole-cell patch-clamp recordings on layer 5 neurons to investigate the impact of *Satb2* haploinsufficiency on the functional development of layer 5 neurons in S1 at P28 (Figure 24A-Figure ***24***D). We found that *Satb2*$^{LacZ/+}$ neurons exhibited increased rheobase current, wider action potential (AP) half width, and decreased AP firing in response to depolarizing current steps compared to control neurons (Figure 24A and Figure ***24***C). There was no change in AP threshold or membrane resistance (Figure 24A and Figure ***24***B). Our recording showed significantly decreased amplitude and frequency of mEPSCs for these neurons (Figure 24D). These data indicate that the S1 L5 projection neurons in *Satb2*$^{LacZ/+}$ mice are intrinsically less excitable.

To determine the impact of *Satb2* haploinsufficiency on local cortical circuitry at P28, we applied laser scanning photostimulation (LSPS), which allows for high throughput functional readout of local circuit connectivity with cellular resolution, and glutamate uncaging to map circuit connectivity (Figure 24F and Figure ***24***E) (Dantzker and Callaway, 2000; Qiu et al., 2011; Shepherd and Svoboda, 2005; Suter et al., 2010). We found that S1BF regions of *Satb2*$^{LacZ/+}$ brain slices exhibited disrupted topology of intracortical excitatory connectivity; inputs from layer 4 are reduced while inputs from layer 2/3 are increased, and inhibitory inputs

are unchanged (Figure 24F). These data indicate that *Satb2* haploinsufficiency leads to disrupted local excitatory circuit function in S1, potentially due to mis regulated ion channel genes.

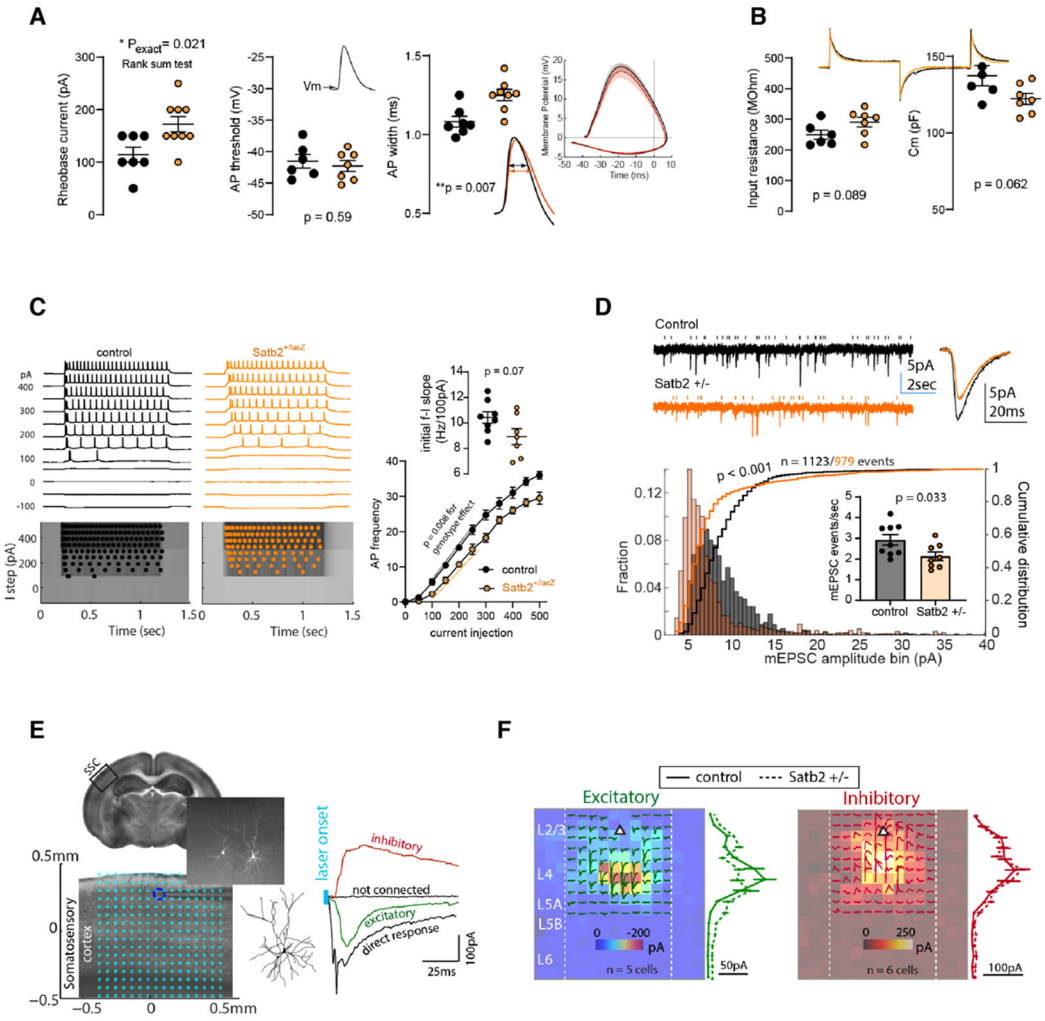
A
* P exact = 0.021
Rank sum test
Rheobase current (pA)
AP threshold (mV)
Vm
p = 0.59
AP width (ms)
**p = 0.007
Membrane Potential (mV)
Time (ms)
B
Input resistance (MOhm)
p = 0.089
Cm (pF)
p = 0.062
C
control
Satb2+/lacZ
pA
I step (pA)
Time (sec)
initial f-I slope (Hz/100pA)
p = 0.07
p = 0.008 for genotype effect
AP frequency
control
Satb2+/lacZ
current injection
D
Control
Satb2 +/-
5pA
2sec
5pA
20ms
p < 0.001
n = 1123/979 events
Fraction
Cumulative distribution
mEPSC amplitude bin (pA)
mEPSC events/sec
p = 0.033
control
Satb2 +/-
E
SSC
0.5mm
0
−0.5
Somatosensory cortex
laser onset
inhibitory
not connected
excitatory
direct response
100pA
25ms
F
control
Satb2 +/-
Excitatory
Inhibitory
L2/3
L4
L5A
L5B
L6
0
-200
pA
n = 5 cells
50pA
0
250
pA
n = 6 cells
100pA

Figure 24: Altered physiology and local circuit connectivity in *Satb2*$^{LacZ/+}$ brain slices

(A) Increased Rheobase current indicating significantly higher current is needed to elicit *Satb2*$^{LacZ/+}$ layer 5 axon potential. No change in action potential threshold. Increased AP width and altered waveforms.
(B) Input resistance and membrane capacitance not significantly changed.
(C) Sample responses of membrane voltages to increasing depolarizing current injections in Satb2+/+ and Satb2LacZ/+ neurons. AP density plots are presented below. Satb2LacZ/+ neurons show significantly lower AP firing in response to current injection indicating reduced excitability.
(D) Sample mEPSC responses from control and Satb2LacZ/+ neurons. Vertical ticks indicate detected mEPSCs. Below is the amplitude distribution and cumulative distribution of mEPSCs. Satb2 LacZ/+ neurons exhibit smaller mEPSC amplitude and reduced frequency.
(E) Illustration of recording L2/3 pyramidal neuron location, and LSPS mapping glutamate uncaging locations. Representative L2/3 neuron morphology shown. Graph showing laser onset and different responses based on uncaging locations.
(F) Pooled responses of EPSC/IPSC maps. Averaged responses from 5-6 neurons. Average synaptic responses (mean ± SD) binned by laminar location to the right of the color maps showing different distribution patterns for excitatory maps but not inhibitory. (n = 4 *Satb2*$^{+/+}$, n = 3 *Satb2*$^{LacZ/+}$ mice)

Satb2 regulates gene expression in part by recruiting the BAF complex

Although the mechanism of Satb2 mediated gene repression is known (Britanova et al., 2008), it is unclear how Satb2 activates gene expression. We performed protein co-immunoprecipitation (co-IP) using a Satb2 antibody and protein extracts from *Satb2*$^{+/+}$ P0 cortices and confirmed that Satb2 interacts with NuRD components HDAC1 and MTA1/2 (data not shown). We investigated the possibility that Satb2 interacts with the BAF complex, an ATP-dependent chromatin remodeling complex generally associated with gene activation. We found Brg1, the core ATPase in the BAF complex, was co-IPed with a Satb2 antibody from *Satb2*$^{+/+}$, but not *Satb2*$^{LacZ/LacZ}$ cortices Figure 25A). We also performed the reverse co-IPs, and found a Brg1 antibody, but not a control IgG, was able to co-IP Satb2 from control cortices. Supporting this finding, a co-IP experiment followed by mass spectrometry using a Brg1 antibody with extracts from a primary cortical neuron culture, identified Satb2 as one of the top enriched proteins (data not shown). Immunostaining confirmed their co-expression in the cortical plate (Figure 23B). This interaction highlights the dynamic mechanisms by which Satb2 mediates gene regulation.

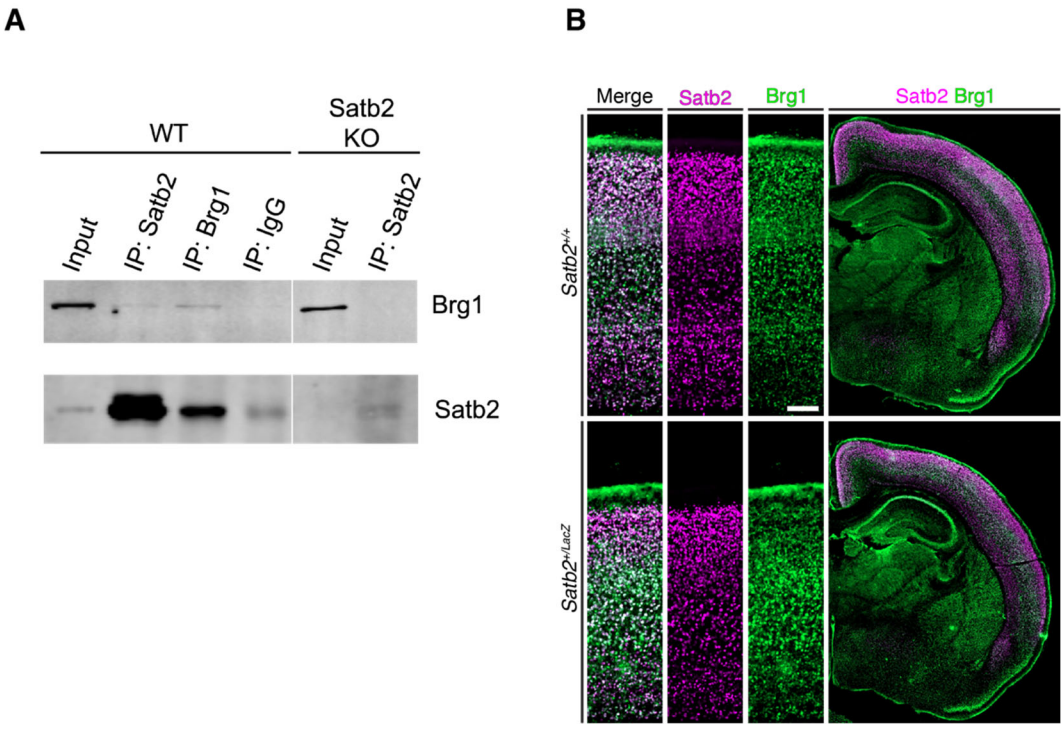

Figure 25: Satb2 and Brg1 can bind to each other and are co-expressed in the cortical plate

(A) Co-immunoprecipitation experiment showed that Satb2 and Brg1 can bind to each other. Satb2 and Brg1 are co-IPed from P0 *Satb2*$^{+/+}$ cortices using either a Brg1 or Satb2 antibody, but not from *Satb2*$^{LacZ/LacZ}$ cortices. Note that there was a non-specific band that co-IPed with control IgG that ran the size of Satb2, and the non-specific band was also co-IPed in *Satb2*$^{LacZ/LacZ}$ cortices.
(B) Satb2 and Brg1 staining revealed that they are co-expressed in cortical neurons in the cortical plate at P7.

Discussion

Understanding the genetic and molecular origin of neurodevelopmental disorders entails deciphering the detailed molecular mechanisms underlying brain development. The molecular and genetic interplay underpinning the generation of cortical projection neurons is beginning to be unraveled, but a comprehensive understanding of these processes is needed. These data shed light on the necessity of proper Satb2 expression for the generation and development of cortical projection neurons. We show that in the *Satb2*$^{LacZ/+}$ animals, there is a 50% reduction of Satb2 protein which leads to widespread gene misregulation, particularly of cell adhesion, axon guidance, and ion channel genes, providing potential a mechanism underlying the axon projection and electrophysiology defects observed. The reduction of Satb2 essentially permitted the specification of cortical projection neuron classes, yet the insufficient protein levels resulted in severe callosal projection neuron defects. This finding is analogous to the corpus callosum agenesis seen in human SAS patients and provides a molecular mechanism for this pathology.

Previous studies using complete or conditional *Satb2* knockouts, precluded the ability to examine the role of Satb2 in neuronal subtypes that are completely missing in these models. The *Satb2*^{LacZ} allele allowed us to study the role of Satb2 in neuronal maturation, a process distinct

from the initial cell fate specification. We confirmed that Satb2 is expressed in CT neurons (McKenna et al., 2015) and found that there are no apparent CT targeting defects in the *Satb2*$^{LacZ/+}$ cortices. However, the layer 6 CT neurons exhibited significant gene expression changes by P28 indicating defective development of these cell types. Interestingly the layer 5 pyramidal tract (PT) neurons showed no apparent gene expression or projection defects in the *Satb2*$^{LacZ/+}$ brain, despite Satb2 being necessary for their birth and specification (Leone et al., 2015; McKenna et al., 2015). Satb2 expression in the layer 5 PT neurons is transient, and high levels of Fezf2 extinguish Satb2 expression in this neuronal subtype (Chen et al., 2008b; McKenna et al., 2015). Therefore, the reduced Satb2 was sufficient to specify the proper number of these neurons which were ultimately unaffected by Satb2 haploinsufficiency. Satb2 is also required for the specification of callosal neurons, and its expression is maintained in this cell population after the neurons are born. Although markers of upper-layer projection neurons appeared normal in our immunohistochemistry analysis, gene expression defects were prevalent in our snRNA-seq experiment and callosal projection defects were severe. These findings implicate Satb2 dosage to be a critical factor in facilitating neuronal maturation. The subtypes of neurons most affected by Satb2 haploinsufficiency are those that express Satb2 long term, suggesting that

IT and CT neuronal subtypes are particularly vulnerable to deficient levels of Satb2. This highlights the vulnerable cell types in SAS.

Satb2 regulates the generation of multiple neuronal subtypes. The question then arises of how Satb2 functions in distinct but essential ways in different projection neuron subtypes. Our findings suggest that the combinatorial action of Satb2 with ATP-dependent chromatin remodeling complexes is one mechanism by which Satb2 regulates gene expression in a cell-context dependent manner. We confirmed previous findings that Satb2 interacts with the NuRD nucleosome remodeling complex which inhibits gene expression through its deacetylase activity (Hoffmann and Spengler, 2019). We found that Satb2 also interacts with the BAF complex which utilizes ATP to mobilize nucleosomes resulting in increased chromatin accessibility (Sokpor et al., 2017), providing a mechanism by which Satb2 activates gene expression. Our CUT&RUN analysis revealed that Satb2 binding sites are enriched for transcription factor binding sites including Bcl11a, Lhx2, and Nr2f1. These findings suggest that the combinatorial action of Satb2 with other chromatin remodeling complexes and transcription factors facilitates its cell-context dependent functions.

Mutations in a single copy of *SATB2* resulting in a nonfunctional SATB2 protein cause Satb2-Associated Syndrome (Zarate and Fish, 2017). Satb2 function is also implicated in autism, schizophrenia, and intellectual deficiency (Blumenthal et al., 2014; Ripke et al., 2014; Whitton

et al., 2018). Our findings highlight how projection neuron development is sensitive to Satb2 dosage, particularly in neurons that express Satb2 after their birth and specification. In the *Satb2*$^{LacZ/+}$ brain it appears that the major detrimental effects are due to improper maturation. This opens the possibility for therapies aimed at SAS that do not have to be implemented during early neonatal development. Finally, this work illuminates the function of Satb2 in heathy brains and sheds light on the etiology of SAS in particular cell types.

Mice used in this study

Experiments were performed according to protocols approved by the Institutional Animal Care and Use Committee at University of California at Santa Cruz and at University of Arizona College of Medicine Phoenix, and were performed in accordance with institutional and federal guidelines. The *Satb2*$^{lacZ/+}$, and *Emx1*^{Cre}, reporter mice were described previously (Dobreva et al., 2003; Gorski et al., 2002). The *Satb2tm1a(KOMP)Wtsi/+* mice were obtained from the Knockout Mouse Project (KOMP) repository and bred with *Rosa26Sortm2(FLP*)Sor* mice from the Jackson Laboratory (JAX number 007844) to generate the *Satb2flox(KOMP)/+* mice (referred as *Satb2flox* mice in this study).

The day of the vaginal plug detection was designated as E0.5. The day of birth was designated as P0. The genders of the embryonic and early postnatal mice were not determined.

The following mice were used in this study:

Satb2$^{+/+}$, *Satb2*$^{LacZ/+}$ and *Satb2*$^{LacZ/LacZ}$ mice: E13.5, E15.5, E17.5, P0, P1, P4, P7, P28, and adult, both male and female mice were used.

Satb2$^{flox/LacZ}$*;Emx1*$^{cre/+}$ mice: P7 and adult, both male and female mice were used.

Method Details

Immunohistochemistry

To prepare tissue for staining, mice were first anesthetized and prepared for trans-cardiac perfusion. 1XPBS was delivered to the body into the left ventricle. When the fluid exiting the right atrium ran clear, 4% paraformaldehyde was pumped until the body stiffened. Brains were then dissected and post-fixed in 4% paraformaldehyde, 0.1% saponin, 1XPBS for 24 hours at 4°C and then cryoprotected by submerging in 30% sucrose 1XPBS for 24 hours. The brains were sectioned using a sliding microtome into 50μm sections. Sections were permeabilized with 0.06% Triton X-100 in PBS for 30 minutes before incubated in blocking buffer (5% horse serum, 0.03% Triton X-100, 1XPBS) for 1 hour. Blocking buffer was removed, and the sections were incubated with primary antibodies diluted in blocking buffer for 24 hours at 4°C. The following antibodies were used for immunohistochemistry in this study: Bcl11b, 1:1000 (rat, Abcam, ab18465) Brg1, 1:500 (mouse, Santa Cruz Biotechnology, sc-17796),

Cux1, 1:500 (rabbit, Santa Cruz Biotechnology, sc-6327), Lhx2, 1:500 (goat, Santa Cruz Biotechnology, sc-19344), L1, 1:500 (rat, MilliporeSigma, MAB5272), Ntng1 1:100 (goat, R&D Systems, AF1166), Pkcg, 1:500 (rabbit, Santa Cruz Biotechnology, sc-211), Rorb (rabbit, Proteintech 17635-1-AP), Satb2, 1:1000 (rabbit, Abcam, ab34735), Tbr1 (rabbit, Abcam, ab31940), Tbr2, 1:500 (rat, Abcam, ab23345), Tle4, 1:100 (mouse, Santa Cruz Biotechnology, sc-365406). The sections were washed three times with 1XPBS 0.03% triton X-100 for 5 minutes each, and then incubated with secondary antibodies conjugated to Alexa 488, 555, or 647 fluorophores, all diluted in blocking buffer at a ratio of 1:1000. Secondary antibodies were incubated for 2 hours at room temperature. Nuclear staining was performed by incubating with 4',6-Diamidino-2-Phenylindole, Dihydrochloride (DAPI) 1:10,000 (Invitrogen, D1306) in 1XPBS for 10 minutes. Sections were then manually arranged on microscope slides before being mounted in Fluoromount-G. Embryonic tissue was sectioned at 20μm using a Leica Cryostat, and staining was performed as described above but on microscope slides.

Cytochrome oxidase staining

Brains used for cytochrome oxidase staining were dissected from perfused mice as described in the “Immunohistochemistry” methods section. We cut the brains in half along the midline and removed all subcortical structures with standard dissecting tools to obtain cortices. We

then flattened the cortices between two glass slides with a 1mm spacer in-between and placed in 4%PFA 1XPBS at 4°C overnight. The following day, we removed the glass slides and placed the flattened cortex in 30% sucrose 1XPBS. The flattened cortices were then sectioned on a sliding microtome at 50µm. Sections were washed with 1X PBS and then incubated at 37°C in CO staining buffer containing: 5% sucrose, 0.03% cytochrome C, 0.02% catalase, 0.05% 3,3′-Diaminobenzidine, and 0.1M phosphate buffer for 2-3 hours. Sections were then washed with 1X PBS and mounted in Permount.

EdU labeling

Timed pregnant mice were injected with a single dose of EdU (25mg/kg body weight; Thermo Fisher Scientific, E10187) at E12.5, or E13.5. Brains were collected at P7 as described in “immunohistochemistry.” Primary and secondary antibody staining was performed as usual, and at the end of the protocol, sections were immersed in the following solution 1 mL of reaction: 950ul 100mM Tris PH 7.4, 40µL 100 mM $CuSO_4$, 10µL 200 mg/mL sodium ascorbate, and 1µL azide 488 or 555 at room temperature for 30 minutes. Sections were then washed and cover slipped. *Satb2*$^{LacZ/+}$ and littermate *Satb2*$^{+/+}$ control mice were analyzed for each timepoint.

CUT&RUN

P0 brains were quickly dissected and dropped into ice cold 1X PBS with protease inhibitor (Roche 11873580001). Cortices were then dissected under a dissection microscope. The pial surface was carefully removed and the cortices were cut into small pieces. The tissue was then washed with 400µL ice cold Accumax solution (Sigma-Aldrich A7089). Ice cold Accumax was removed and 400µL prewarmed 37°C Accumax was added. The tissue incubated at 37°C for 5 minutes before being manually dissociated with a P1000 pipet tip. Dissociated cells were spun down at 600g for 3 minutes and resuspended in 1mL ice cold wash buffer (20mM HEPES pH 7.5, 150mM NaCl, 0.5mM Spermidine, 1X EDTA-free protease inhibitor). The cells were washed three times. Cells were then quantified and bound to Concanavalin-A beads (Bangs Laboratories, PB531). All CUT&RUN samples were generated with 500,000 cells. Cells were then bound to beads at a ratio of 500,000 cells per 10µL beads. Cells bound to beads were then placed on a magnetic stand and the wash buffer was removed. Each sample was resuspended in 150µL antibody buffer (wash buffer with 2mM EDTA, 0.03% Digitonin, MilliporeSigma, 300410). All antibodies were used at a dilution of 1:100, except the IgG which was added to a final concentration of 1µg/µL. The following antibodies were used in CUT&RUN experiments: Satb2 (rabbit, Abcam, ab34735), Cux1 (rabbit, Santa Cruz Biotechnology, sc-6327), Lhx2 (goat, Santa Cruz

Biotechnology, sc-19344), H3K27me3 (Cell Signaling, 9733S), H3K27Ac (Abcam, Ab4729), H3K4me3 (Cell Signaling, 97515), Rabbit IgG (Invitrogen 02-6102). Samples were incubated at 4°C overnight with shaking a 400rpm at a 30° angle (the tubes were never inverted). The following day, beads were washed twice with 1mL DIG-wash buffer (Wash Buffer with 0.03% Digitonin), and incubated with protein A/G-MNase (EpiCypher, 15-1016), 2.5µL per 50µL DIG-wash buffer per sample, for 1 hour at 4°C shaking. Beads were washed twice with DIG-wash buffer and resuspended in 100µL DIG-wash buffer and Ca^{2+} was added to a final concentration of 1mM and the samples incubated for 1 hour at 0°C in a heat block immersed in an ice water slurry. The reaction was inhibited by adding 100µL 2X STOP buffer (170mM NaCl, 20mM EGTA, 0.05%, 50µg/mL RNAse A, 20µg/mL Glycogen, 250pg *E. coli* Spike-in DNA, EpiCypher 18-1401). Samples were then incubated at 37°C for 30 minutes, and supernatant was transferred to fresh tubes. Phenol chloroform isoamyl alcohol extraction was performed to purify CUT&RUN DNA which was resuspended in 30µL 1mM Tris-HCl pH 8.0, 0.1mM EDTA.

CUT&RUN Library Prep and Sequencing and Analysis

We used the NEBNext Ultra II DNA Library Prep Kit (E7645L) with some modifications to the protocol. For the adapter ligation step, the NEBNext

Adaptor for Illumina was diluted 1:50, to 0.3μM. The adaptor ligated DNA was then cleaned up with 2.1X AMPure XP beads (Beckman A63881) before proceeding. PCR was performed with NEBNext Multiplex Oligos for Illumina (E7600S) with the following thermocycler conditions: Initial denaturation 98°C, 30s, denaturation 98°C, 10s, annealing and extension 65°C, 12s, repeat denaturing and annealing and extension 14 times, final extension 65°C, 5 minutes in a Bio-Rad T100 Thermal Cycler. After amplification, 0.5X AMPure beads were added to the reaction, mixed, incubated for 10 minutes, and samples were placed on a magnet stand. Supernatant was transferred to fresh tubes and then cleaned up with 2X AMPure beads. DNA concentrations were determined using Bioanalyzer High Sensitivity DNA kit (5067-4626). DNA between 146 and 600bp was quantified for the analysis. The primer-dimer peak was removed with Pippin size selection. Samples were pooled such that equimolar amounts of each sample were present in the pool, and sequenced on the NextSeq platform (high output, 75 cycles). The sequencing was demultiplexed, and sequencing reads were mapped to the genome. Binding peaks were called using SEACR, and peaks were assigned to genes using ChIPseeker. MEME motif analysis was used to determine Satb2 binding motifs.

snRNAseq

P28 mice were anesthetized and brains were quickly dissected and placed into ice cold PBS. The brains were then sectioned at 300 μm using a vibratome. S1 regions were then manually excised from the brain sections and flash frozen in liquid nitrogen. Nuclei were then isolated and libraries made using the 10X genomics single cell gene expression workflow. Libraries were sequenced on the NovaSeq platform. Quality control analysis was performed using the Seurat workflow. Harmony (Korsunsky et al., 2019) to co-cluster the datasets and perform differential expression analysis.

CTB labeling

Injections for tracing experiments were performed using Alexa Fluor 555-conjugated cholera toxin subunit-B (CTB) at a concentration of 4 mg/mL in 1XPBS injected through a pulled glass pipet attached to a Picospritzer III (Parker). Stereotaxic surgery was performed on P28 mice by anesthetizing them and placing on a stereotaxic frame (Kopf). The skull was exposed, and coordinates were measured by using the bregma as the zero point. A craniotomy was performed, and the pulled glass pipet with CTB was placed on the brain surface. The needle was then lowered to the desired Z position, and 0.25μL was injected. After 5 minutes, the needle was retracted, and the skin was glued back together. Brains were

analyzed 5-days later. Injections were performed using the following coordinates: VpM injection, AP -1 mm, ML 2.85 mm, Z -3.35 mm, CP injection AP -3.28 mm, ML 1.3 mm, Z -4.8 mm, CC injection AP -1.7 mm, ML 0.8 mm, Z -1.3 mm.

Image acquisition and analysis

Images for quantitative analysis were acquired with a Zeiss 880 confocal microscope. Laser power and gain were adjusted until < 1% of pixels were saturated. Cell counting was performed on single z-slices. Images were divided into 500 μm wide regions and split into equally sized bins or cortical layers. A gaussian blur was applied to the image with a rolling ball radius of 1μm and then an appropriate threshold was set for each channel. Particles were analyzed with a circularity of 0.3-1.0 and size exclusion of > 1μm. The same threshold was used across all images between genotypes. Brightfield images were acquired with a Zeiss AxioImager Z2 widefield microscope with a Zeiss AxioCam 506 (color) camera. Statistical analysis was performed using GraphPad Prism 9.0. For each brain, the number of marker+ cells in the cortex were quantified in a 500 μm wide region from at least 3-4 matching sections. Care was taken to match the anterior-posterior, medial-lateral positions for the chosen areas between the mutant and control genotypes. For each genotype and each age, at least 3 different brains were analyzed. Data are shown as mean ± SEM. Statistical significance for single comparisons was determined using

a nested t-test. Significance was set as $*$ for $p < 0.05$, $**$ for $p < 0.01$, and $***$ $p < 0.001$ for all significance tests.

Western blot analysis

P0 cortices were dissected in ice cold 1X PBS with protease inhibitor. The tissue was homogenized in RIPA buffer by manually triturating with a P1000 pipet tip before incubating on ice for 20 minutes. The cell homogenate was centrifuged at 14,000 g for 10 minutes at 4°C. The supernatant was removed, and proteins were denatured at 100°C for 5 minutes in laemmli buffer. The sample was then run on an 8% SDS-PAGE at 70V for 2 hours, transferred to a PVDF membrane (Sigma, IPVH85R) at 150 mA for 90 minutes. The blot was blocked for one hour in 1% non-fat milk in 1X Tris-Buffered Saline, 0.1% Tween 20 (TBST). After blocking in 10mL solution, 2µg Satb2 antibody (rabbit, Abcam, ab34735) was added and incubated at 4°C overnight. The blot was then washed with TBST and incubated in Li-Cor Donkey anti Rabbit secondary antibody (#926-68073) at a 1:17,000 dilution for one hour and images were processed using ImageStudioLite.

Chapter 4: Conclusions and Future Directions

In the previous chapters, I presented work examining how Fezf2, Tle4, and Satb2 function to specify projection neuron subtypes and the effect of Satb2 haploinsufficiency on brain development. These findings support a model of projection neuron fate specification in which radial glial stem cells initially specify a pan glutamatergic identity. Next, the combinatorial expression of post-mitotic transcription factors regulates subtype-specific molecular expression programs that ultimately specify subtype identity.

Role of Fezf2 in progenitors

Despite being expressed in radial glial cells (RGCs), Fezf2 does not appear to play a role in specifying cell fate at the level of the progenitor in the developing cerebral cortex. Our use of conditional mouse genetics spared Fezf2 expression in RGCs while knocking it out in newly born neurons, yielding a phenotype almost identical to that of the complete knockout. That begs the question, what is the role of Fezf2 in progenitors?

There is evidence from zebrafish and flies that *Fezf2* plays essential roles in neurogenesis. *Fezf2* regulates *neurogenin1* expression to promote the generation of dopaminergic neurons in zebrafish forebrain (Jeong et al., 2006). It also promotes Wnt/B-Catenin signaling in zebrafish by physically interacting with Tle4 to repress the Wnt pathway inhibitors

Lhx2 and *Lhx9*. In this way, Fezf2 controls the timing and location of the onset of neurogenesis through genetic repression (Zhang et al., 2014). This also demonstrates that one of the principal mechanisms by which Fezf2 represses gene expression is conserved between zebrafish and mice. In flies*, Fezf2* (*Drosophila, erm*) prevents intermediate progenitors from dedifferentiating back into the neuroblast state by inhibiting Notch signaling (Weng et al., 2010).

In mice, however, our understanding is quite limited regarding the role of Fezf2 in progenitors during and after cortical neurogenesis. It was shown that Fezf1 and Fezf2 promote neurogenesis by inhibiting notch activity by repressing *Hes5,* a repressor of the proneural gene *neurogenin2* in early telencephalon patterning (Shimizu et al., 2010). These defects are not evident in the *Fezf2* knockout. Perhaps in the full *Fezf2* knockout, *Fezf1* can compensate for the loss of *Fezf2* in early telencephalon patterning. However, at the onset of cortical neurogenesis, *Fezf1* and *Fezf2* are not co-expressed in the dorsal ventricular zone, yet in the complete *Fezf2* knockout, neuron birth and migration are unaffected (B. Chen et al., 2005c; Molyneaux et al., 2005). We recently showed that knocking out *Fezf2* in RGCs from E13.5 onwards resulted in reduced RGC differentiation based on s-phase EdU incorporation, cell cycle marker staining, and reduced numbers of $Tbr2^{+}$ intermediate progenitors by P0 (Huebner, 2020), but the consequences of this remain unanswered. *Fezf2*

expression continues in post-natal neural stem cells in the ventricular-subventricular and subgranular zones into adulthood (data not shown), implicating *Fezf2* in regulating adult neurogenesis of olfactory bulb interneurons and granule neurons in the dentate gyrus.

Tle4 in corticothalamic neuron development

Before we published the *Tle4* knockout phenotype, Tle4 was known to be a marker of CT neurons, but its function was unknown. *Tbr1* is the cell fate specification gene for CT neurons (Fazel Darbandi et al., 2018; Han et al., 2011; Hevner et al., 2001; McKenna et al., 2011). When *Tle4* is knocked out, the CT neurons were still born and projected to proper thalamic targets. However, we observed increased layer 5 gene expression in layer 6 in the *Tle4* knockout and altered electrophysiology, indicating that *Tle4* is important for the proper molecular and physiological identity of these neurons.

Defective CT neurons have been associated with autism (Kwan, 2013) and are implicated in epilepsy (Avoli, 2012). This highlights the importance of understanding the precise molecular mechanisms underlying the formation and development of this class of neurons. Furthermore, we observed that the $Tle4^{LacZ/+}$ brains exhibited subtle but increased layer 5 gene expression in layer 6, indicating that CT neurons are sensitive to *Tle4* dosage (data not shown).

Context-dependent functions of sequence-specific transcription factors.

It's remarkable that single transcription factors have dramatically different functions depending on cell contexts. For instance, Fezf2 inhibits the expression of layer 5 genes when it complexes with Tle4 in layer 6, yet in layer 5, high levels of Fezf2 inhibit the expression of layer 6 genes. I proposed that Fezf2 regulates different sets of genes by its combinatorial action with other co-repressors. Similarly, I proposed that Satb2 executes cell-context dependent functions by partnering with different chromatin remodeling complexes. Interestingly, Tle4 does not have a DNA binding domain of its own, and therefore the sequence specificity of the Fezf2-Tle4 complex, in theory, is dictated exclusively by the Fezf2 DNA binding domain. How Fezf2 binds to different targets is unknown.

To gain insights into the mechanism by which Fezf2 functions, I performed CUT&RUN in a Fezf2 overexpression model and identified Fezf2 binding sites (data not shown). As expected, Fezf2 peaks were associated with layer-specific genes including upper layer genes such as *Cux1*, *Cux2*, and *Lhx2*, as well as layer 6 genes such as *Tbr1*, and *Fosl2*, and layer 5 genes *Bcl11b* and *Fezf2* itself which is expressed at high levels in layer 5. These findings support our model in that the genes we expect Fezf2 inhibits are bound by Fezf2. It would be useful to test the

validity of our claims that Fezf2 binds different targets in different cell-types. This could be accomplished by performing CUT&RUN on purified populations of different projection neuron subtypes.

Perhaps the chromatin architecture plays a permissive role in dictating Fezf2 binding. Based on my immunohistochemical observations, Fezf2 is not present in the subventricular zone or intermediate zone. Rather, Fezf2 appears to turn on in the neurons once they have entered the cortical plate. It is likely that the chromatin architecture is different in newborn layer 5 and layer 6 neurons. The chromatin organization may dictate which Fezf2 targets are available in the different cell types. Integrating Fezf2 binding site data generated by CUT&RUN with combined single cell multiome ATAC and gene expression datasets generated from neocortex during the peak time of layer 6 and 5 neurogenesis will help to answer this question.

It's also feasible that the expression level of Fezf2 itself can influence the function of Fezf2. Fezf2 expression is titrated in different cell types. It is expressed at exceedingly low levels in RGCs, slightly higher levels in layer 6, and highest levels in layer 5b. I've also observed that Fezf2 is expressed in layer 5a callosal projection neurons at a notably lower level than in the layer 5b neurons (data not shown). The concentration of Fezf2 protein may affect its ability to bind specific DNA regions. For instance, in the case of very high concentrations of Fezf2, it

may be able to access more inaccessible targets in the genome by forcing the equilibrium between bound and unbound towards binding. On the other hand, when Fezf2 is expressed at lower levels, such as in layer 6, it may only bind to more readily accessible regions, but in complex with Tle4, it can function as a strong repressor for those genes.

We did not uncover additional Fezf2 binding partners in our study. Co-IP followed by mass spectrometry using a Fezf2 antibody and rabbit IgG control antibody in both wild-type and Fezf2 mutant brains will accomplish this. Fezf2 likely complexes with other Tle proteins, and may interact with chromatin remodeling complexes such as the Nucleosome Remodeling and Deacetylase (NuRD) or Polychrome Repressive Complexes, which are mostly associated with repression. If this is the case, it would implicate Fezf2 as a regulator of chromatin architecture in addition to directly repressing gene expression.

Satb2 mediated gene expression is highly associated with chromatin remodeling complexes as discussed in Chapter 3. Therefore, Satb2 actively regulates chromatin architecture, but does so uniquely in different contexts. Its combinatorial action with different chromatin remodelers may be a primary mechanism by which it executes its context-dependent regulatory functions.

How is the combinatorial network of transcription factors and chromatin remodeling complexes initially set up? Recent single cell

analysis of radial glial cells and their progeny, carefully followed over time, found that the radial glial cells express and bestow transcriptional programs to their progeny reflective of their final cell identities (Telley et al., 2019). This result provides evidence that although newborn glutamatergic projection neurons have not acquired their subtype identity, different combinations of transcription factors and chromatin remodeling complexes become expressed based on inherited transcriptional programs, providing a mechanism by which different combinations of these proteins are initially established.

It will be productive to combine single cell gene expression and chromatin accessibility (multiomic) data sets with transcription factor binding sites generated from CUT&RUN for a multitude of sequence-specific transcription factors implicated in cell fate specification. Associating binding peaks to accessible genomic regions in different cell types across developmental time and in different genetic backgrounds (i.e. Satb2, Fezf2, or Tbr1 knockout animals) will elucidate the mechanisms by which the combinatorial actions of sequence specific transcription factors function through enhancer regulation. Proximity ligation-assisted ChIP-Seq (PLAC-seq) is a method that quantifies chromatin contacts at genomic regions, and is a powerful tool to determine physical enhancer promoter contacts (Yu et al., 2021). When high quality PLAC-seq datasets generated from different populations of sorted human cells become

publicly available, integrating the binding sites identified by CUT&RUN to the 3D enhancer/promoter data will illuminate the function of Fezf2, Satb2, and any additional sequence specific transcription factors with high quality CUT&RUN or ChIP-seq data in human brain development, revealing the precise binding sites and gene promoters they interact with.

Finally, to validate the predictions made by the combination of sequence-specific transcription factor CUT&RUN, multiome, and PLAC-seq, an exhaustive catalogue of enhancer knockout mice must be generated to validate the predictions.

Relevance to human health

By studying brain development, we can better understand the mechanisms underlying debilitating neurodevelopmental diseases such as autism, schizophrenia, and intellectual disability. The work presented here has uncovered fundamental molecular mechanisms by which Fezf2, Tle4, and Satb2 function.

Neurodegenerative diseases and brain injuries are devastating occurrences and insults, and few treatments are available. *Fezf2* is a master regulator of corticospinal motor neuron generation, the principal cell type that degenerates in ALS. The mechanisms uncovered here may guide the development for regenerative therapies and provide an intellectual framework for considering how reprogramming strategies using

Fezf2 would work at the molecular level. Recently, there has been major success in the transplantation of reprogrammed dopaminergic neurons into patients with Parkinson's. A previously untreatable disease which shows great potential in finding a cure.

In addition to brain development, Fezf2, Satb2, and Tle4 are critical for the proper development and function of other bodily systems. Fezf2 plays a central role in regulating autoimmunity, and indeed, mice lacking *Fezf2* displayed severe autoimmune symptoms (Takaba et al., 2015). It has also been identified as a tumor suppressor gene in nasopharyngeal carcinoma (Shu et al., 2013). Satb2 plays a major role in bone health and development (Huang et al., 2022; Zhao et al., 2014), maintenance of adult colonic stem cells (Gu et al., 2022), and is involved in many cancers originating outside the central nervous system (Berg and Schaeffer, 2017; Inzani et al., 2022; Roy et al., 2020; Warmke et al., 2022; Wu et al., 2016; Xu et al., 2019). Tle4 functions in muscle stem cell biology (Agarwal et al., 2022), bone development (Shin et al., 2021), cancer progression (Wang et al., 2016), and the inflammatory response (Zhang et al., 2019) among many others. Therefore, in addition to the central role these proteins play in cortical development, understanding the precise molecular mechanisms underlying Fezf2, Satb2, and Tle4 function has wide ranging implications for understanding diseases and functions of the body.

References

Agarwal, M., Bharadwaj, A., Mathew, S.J., 2022. TLE4 regulates muscle stem cell quiescence and skeletal muscle differentiation. J. Cell Sci. 135, jcs256008. https://doi.org/10.1242/jcs.256008

Agarwal, M., Kumar, P., Mathew, S.J., 2015. The Groucho/Transducin-like enhancer of split protein family in animal development. IUBMB Life 67, 472–481. https://doi.org/10.1002/iub.1395

Alcamo, E.A., Chirivella, L., Dautzenberg, M., Dobreva, G., Fariñas, I., Grosschedl, R., McConnell, S.K., 2008. Satb2 regulates callosal projection neuron identity in the developing cerebral cortex. Neuron 57, 364–377. https://doi.org/10.1016/j.neuron.2007.12.012

Andrews, M.G., Kriegstein, A.R., 2022. Challenges of Organoid Research. Annu. Rev. Neurosci. 45, 23–39. https://doi.org/10.1146/annurev-neuro-111020-090812

Arlotta, P., Molyneaux, B.J., Chen, J., Inoue, J., Kominami, R., Macklis, J.D., 2005. Neuronal subtype-specific genes that control corticospinal motor neuron development in vivo. Neuron 45, 207–221. https://doi.org/10.1016/j.neuron.2004.12.036

Autism Spectrum Disorder Working Group of the Psychiatric Genomics Consortium, BUPGEN, Major Depressive Disorder Working Group of the Psychiatric Genomics Consortium, 23andMe Research Team, Grove, J., Ripke, S., Als, T.D., Mattheisen, M., Walters, R.K., Won, H., Pallesen, J., Agerbo, E., Andreassen, O.A., Anney, R., Awashti, S., Belliveau, R., Bettella, F., Buxbaum, J.D., Bybjerg-Grauholm, J., Bækvad-Hansen, M., Cerrato, F., Chambert, K., Christensen, J.H., Churchhouse, C., Dellenvall, K., Demontis, D., De Rubeis, S., Devlin, B., Djurovic, S., Dumont, A.L., Goldstein, J.I., Hansen, C.S., Hauberg, M.E., Hollegaard, M.V., Hope, S., Howrigan, D.P., Huang, H., Hultman, C.M., Klei, L., Maller, J., Martin, J., Martin, A.R., Moran, J.L., Nyegaard, M., Nærland, T., Palmer, D.S., Palotie, A., Pedersen, C.B., Pedersen, M.G., dPoterba, T., Poulsen, J.B., Pourcain, B.S., Qvist, P., Rehnström, K., Reichenberg, A., Reichert, J., Robinson, E.B., Roeder, K., Roussos, P., Saemundsen, E., Sandin, S., Satterstrom, F.K., Davey Smith, G., Stefansson, H., Steinberg, S., Stevens, C.R., Sullivan, P.F., Turley, P., Walters, G.B., Xu, X., Stefansson, K., Geschwind, D.H., Nordentoft, M., Hougaard, D.M., Werge, T., Mors, O., Mortensen, P.B., Neale, B.M., Daly, M.J., Børglum, A.D., 2019. Identification of common genetic risk variants for autism spectrum disorder. Nat. Genet. 51, 431–444. https://doi.org/10.1038/s41588-019-0344-8

Avoli, M., 2012. A brief history on the oscillating roles of thalamus and cortex in absence seizures. Epilepsia 53, 779–789. https://doi.org/10.1111/j.1528-1167.2012.03421.x

Azevedo, F.A.C., Carvalho, L.R.B., Grinberg, L.T., Farfel, J.M., Ferretti, R.E.L., Leite, R.E.P., Filho, W.J., Lent, R., Herculano-Houzel, S., 2009. Equal numbers of neuronal and nonneuronal cells make the human brain an isometrically scaled-up primate brain. J. Comp. Neurol. 513, 532–541. https://doi.org/10.1002/cne.21974

Berg, K.B., Schaeffer, D.F., 2017. SATB2 as an Immunohistochemical Marker for Colorectal Adenocarcinoma: A Concise Review of Benefits and Pitfalls. Arch. Pathol. Lab. Med. 141, 1428–1433. https://doi.org/10.5858/arpa.2016-0243-RS

Betancourt, J., Katzman, S., Chen, B., 2014. Nuclear factor one B regulates neural stem cell differentiation and axonal projection of corticofugal neurons. J. Comp. Neurol. 522, 6–35. https://doi.org/10.1002/cne.23373

Blumenthal, I., Ragavendran, A., Erdin, S., Klei, L., Sugathan, A., Guide, J.R., Manavalan, P., Zhou, J.Q., Wheeler, V.C., Levin, J.Z., Ernst, C., Roeder, K., Devlin, B., Gusella, J.F., Talkowski, M.E., 2014. Transcriptional consequences of 16p11.2 deletion and duplication in mouse cortex and multiplex autism families. Am. J. Hum. Genet. 94, 870–883. https://doi.org/10.1016/j.ajhg.2014.05.004

Briscoe, J., Pierani, A., Jessell, T.M., Ericson, J., 2000. A Homeodomain Protein Code Specifies Progenitor Cell Identity and Neuronal Fate in the Ventral Neural Tube. Cell 101, 435–445. https://doi.org/10.1016/S0092-8674(00)80853-3

Britanova, O., de Juan Romero, C., Cheung, A., Kwan, K.Y., Schwark, M., Gyorgy, A., Vogel, T., Akopov, S., Mitkovski, M., Agoston, D., Sestan, N., Molnár, Z., Tarabykin, V., 2008. Satb2 is a postmitotic determinant for upper-layer neuron specification in the neocortex. Neuron 57, 378–392. https://doi.org/10.1016/j.neuron.2007.12.028

Calegari, F., Huttner, W.B., 2003. An inhibition of cyclin-dependent kinases that lengthens, but does not arrest, neuroepithelial cell cycle induces premature neurogenesis. J. Cell Sci. 116, 4947–4955. https://doi.org/10.1242/jcs.00825

Chen, B., Schaevitz, L.R., McConnell, S.K., 2005a. Fezl regulates the differentiation and axon targeting of layer 5 subcortical projection neurons in cerebral cortex. Proc. Natl. Acad. Sci. 102, 17184–17189. https://doi.org/10.1073/pnas.0508732102

Chen, B., Wang, S.S., Hattox, A.M., Rayburn, H., Nelson, S.B., McConnell, S.K., 2008a. The Fezf2-Ctip2 genetic pathway regulates the fate choice of subcortical projection neurons in the developing cerebral cortex. Proc. Natl. Acad. Sci. U. S. A. 105, 11382–11387. https://doi.org/10.1073/pnas.0804918105

Chen, C., Meng, Q., Xia, Y., Ding, C., Wang, L., Dai, R., Cheng, L., Gunaratne, P., Gibbs, R.A., Min, S., Coarfa, C., Reid, J.G., Zhang, C., Jiao, C., Jiang, Y., Giase, G., Thomas, A., Fitzgerald, D., Brunetti, T., Shieh, A., Xia, C., Wang, Yongjun, Wang, Yunpeng, Badner, J.A., Gershon, E.S., White, K.P., Liu, C., 2018. The transcription factor POU3F2 regulates a gene coexpression network in brain tissue from patients with psychiatric disorders. Sci. Transl. Med. 10, eaat8178. https://doi.org/10.1126/scitranslmed.aat8178

Chen, J.-G., Rašin, M.-R., Kwan, K.Y., Šestan, N., 2005. Zfp312 is required for subcortical axonal projections and dendritic morphology of deep-layer pyramidal neurons of the cerebral cortex. Proc. Natl. Acad. Sci. 102, 17792–17797. https://doi.org/10.1073/pnas.0509032102

Chenn, A., Walsh, C.A., 2002. Regulation of Cerebral Cortical Size by Control of Cell Cycle Exit in Neural Precursors. Science 297, 365–369. https://doi.org/10.1126/science.1074192

Clare, A.J., Wicky, H.E., Empson, R.M., Hughes, S.M., 2017. RNA-Sequencing Analysis Reveals a Regulatory Role for Transcription Factor Fezf2 in the Mature Motor Cortex. Front. Mol. Neurosci. 10, 283. https://doi.org/10.3389/fnmol.2017.00283

De la Rossa, A., Bellone, C., Golding, B., Vitali, I., Moss, J., Toni, N., Lüscher, C., Jabaudon, D., 2013. In vivo reprogramming of circuit connectivity in postmitotic neocortical neurons. Nat. Neurosci. 16, 193–200. https://doi.org/10.1038/nn.3299

Desai, A.R., McConnell, S.K., 2000. Progressive restriction in fate potential by neural progenitors during cerebral cortical development. Development 127, 2863–2872. https://doi.org/10.1242/dev.127.13.2863

Desmaris, E., Keruzore, M., Saulnier, A., Ratié, L., Assimacopoulos, S., De Clercq, S., Nan, X., Roychoudhury, K., Qin, S., Kricha, S., Chevalier, C., Lingner, T., Henningfeld, K.A., Zarkower, D., Mallamaci, A., Theil, T., Campbell, K., Pieler, T., Li, M., Grove, E.A., Bellefroid, E.J., 2018. DMRT5, DMRT3, and EMX2 Cooperatively Repress Gsx2 at the Pallium-Subpallium Boundary to Maintain Cortical Identity in Dorsal Telencephalic Progenitors. J. Neurosci. Off. J. Soc. Neurosci. 38, 9105–9121. https://doi.org/10.1523/JNEUROSCI.0375-18.2018

Di Bella, D.J., Habibi, E., Stickels, R.R., Scalia, G., Brown, J., Yadollahpour, P., Yang, S.M., Abbate, C., Biancalani, T., Macosko, E.Z., Chen, F., Regev, A., Arlotta, P., 2021. Molecular logic of cellular diversification in the mouse cerebral cortex. Nature 595, 554–559. https://doi.org/10.1038/s41586-021-03670-5

Diao, Y., Cui, L., Chen, Y., Burbridge, T.J., Han, W., Wirth, B., Sestan, N., Crair, M.C., Zhang, J., 2018. Reciprocal Connections Between Cortex and Thalamus Contribute to Retinal Axon Targeting to Dorsal Lateral Geniculate Nucleus. Cereb. Cortex N. Y. N 1991 28, 1168–1182. https://doi.org/10.1093/cercor/bhx028

Dobreva, G., Chahrour, M., Dautzenberg, M., Chirivella, L., Kanzler, B., Fariñas, I., Karsenty, G., Grosschedl, R., 2006. SATB2 is a multifunctional determinant of craniofacial patterning and osteoblast differentiation. Cell 125, 971–986. https://doi.org/10.1016/j.cell.2006.05.012

Dobreva, G., Dambacher, J., Grosschedl, R., 2003. SUMO modification of a novel MAR-binding protein, SATB2, modulates immunoglobulin μ gene expression. Genes Dev. 17, 3048–3061. https://doi.org/10.1101/gad.1153003

Doe, C.Q., 2017. Temporal Patterning in the Drosophila CNS. Annu. Rev. Cell Dev. Biol. 33, 219–240. https://doi.org/10.1146/annurev-cellbio-111315-125210

Eckler, M.J., Nguyen, T.D., McKenna, W.L., Fastow, B.L., Guo, C., Rubenstein, J.L.R., Chen, B., 2015. Cux2-Positive Radial Glial Cells Generate Diverse Subtypes of Neocortical Projection Neurons and Macroglia. Neuron 86, 1100–1108. https://doi.org/10.1016/j.neuron.2015.04.020

Ericson, J., Morton, S., Kawakami, A., Roelink, H., Jessell, T.M., 1996. Two critical periods of Sonic Hedgehog signaling required for the specification of motor neuron identity. Cell 87, 661–673. https://doi.org/10.1016/s0092-8674(00)81386-0

Fazel Darbandi, S., Robinson Schwartz, S.E., Qi, Q., Catta-Preta, R., Pai, E.L.-L., Mandell, J.D., Everitt, A., Rubin, A., Krasnoff, R.A., Katzman, S., Tastad, D., Nord, A.S., Willsey, A.J., Chen, B., State, M.W., Sohal, V.S., Rubenstein, J.L.R., 2018. Neonatal Tbr1 Dosage Controls Cortical Layer 6 Connectivity. Neuron 100, 831-845.e7. https://doi.org/10.1016/j.neuron.2018.09.027

Franco, S.J., Gil-Sanz, C., Martinez-Garay, I., Espinosa, A., Harkins-Perry, S.R., Ramos, C., Müller, U., 2012. Fate-Restricted Neural Progenitors in the Mammalian Cerebral Cortex. Science 337, 746–749. https://doi.org/10.1126/science.1223616

Frantz, G.D., McConnell, S.K., 1996. Restriction of late cerebral cortical progenitors to an upper-layer fate. Neuron 17, 55–61. https://doi.org/10.1016/s0896-6273(00)80280-9

Friedel, R.H., Plump, A., Lu, X., Spilker, K., Jolicoeur, C., Wong, K., Venkatesh, T.R., Yaron, A., Hynes, M., Chen, B., Okada, A., McConnell, S.K., Rayburn, H., Tessier-Lavigne, M., 2005. Gene targeting using a promoterless gene trap vector ("targeted trapping") is an efficient method to mutate a large fraction of genes. Proc. Natl. Acad. Sci. 102, 13188–13193. https://doi.org/10.1073/pnas.0505474102

Galazo, M.J., Sweetser, D., Macklis, J.D., 2022. Tle4 controls both developmental acquisition and postnatal maintenance of corticothalamic projection neuron identity. https://doi.org/10.1101/2022.05.09.491192

Gandal, M.J., Zhang, P., Hadjimichael, E., Walker, R.L., Chen, C., Liu, S., Won, H., van Bakel, H., Varghese, M., Wang, Y., Shieh, A.W., Haney, J., Parhami, S., Belmont, J., Kim, M., Moran Losada, P., Khan, Z., Mleczko, J., Xia, Y., Dai, R., Wang, D., Yang, Y.T., Xu, M., Fish, K., Hof, P.R., Warrell, J., Fitzgerald, D., White, K., Jaffe, A.E., PsychENCODE Consortium, Peters, M.A., Gerstein, M., Liu, C., Iakoucheva, L.M., Pinto, D., Geschwind, D.H., Ashley-Koch, A.E., Crawford, G.E., Garrett, M.E., Song, L., Safi, A., Johnson, G.D., Wray, G.A., Reddy, T.E., Goes, F.S., Zandi, P., Bryois, J., Jaffe, A.E., Price, A.J., Ivanov, N.A., Collado-Torres, L., Hyde, T.M., Burke, E.E., Kleiman, J.E., Tao, R., Shin, J.H., Akbarian, S., Girdhar, K., Jiang, Yan, Kundakovic, M., Brown, L., Kassim, B.S., Park, R.B., Wiseman, J.R., Zharovsky, E., Jacobov, R., Devillers, O., Flatow, E., Hoffman, G.E., Lipska, B.K., Lewis, D.A., Haroutunian, V., Hahn, C.-G., Charney, A.W., Dracheva, S., Kozlenkov, A., Belmont, J., DelValle, D., Francoeur, N., Hadjimichael, E., Pinto, D., van Bakel, H., Roussos, P., Fullard, J.F., Bendl, J., Hauberg, M.E., Mangravite, L.M., Peters, M.A., Chae, Y., Peng, J., Niu, M., Wang, X., Webster, M.J., Beach, T.G., Chen, C., Jiang, Yi, Dai, R., Shieh, A.W., Liu, C., Grennan, K.S., Xia, Y., Vadukapuram, R., Wang, Y., Fitzgerald, D., Cheng, L., Brown, Miguel, Brown, Mimi, Brunetti, T., Goodman, T., Alsayed, M., Gandal, M.J., Geschwind, D.H., Won, H., Polioudakis, D., Wamsley, B., Yin, J., Hadzic, T., De La Torre Ubieta, L., Swarup, V., Sanders, S.J., State, M.W., Werling, D.M., An, J.-Y., Sheppard, B., Willsey, A.J., White, K.P., Ray, M., Giase, G., Kefi, A., Mattei, E., Purcaro, M., Weng, Z., Moore, J., Pratt, H., Huey, J., Borrman, T., Sullivan, P.F., Giusti-Rodriguez, P., Kim, Y., Sullivan, P., Szatkiewicz, J., Rhie, S.K., Armoskus, C., Camarena, A., Farnham, P.J., Spitsyna, V.N., Witt, H., Schreiner, S., Evgrafov, O.V., Knowles, J.A., Gerstein, M., Liu, S., Wang, D., Navarro, F.C.P., Warrell, J., Clarke, D., Emani, P.S., Gu, M., Shi, X., Xu, M., Yang, Y.T., Kitchen, R.R., Gürsoy, G., Zhang, J., Carlyle, B.C., Nairn, A.C., Li, M., Pochareddy, S., Sestan, N., Skarica, M., Li, Z., Sousa, A.M.M., Santpere, G., Choi, J., Zhu, Y., Gao, T., Miller, D.J., Cherskov,

A., Yang, M., Amiri, A., Coppola, G., Mariani, J., Scuderi, S., Szekely, A., Vaccarino, F.M., Wu, F., Weissman, S., Roychowdhury, T., Abyzov, A., 2018. Transcriptome-wide isoform-level dysregulation in ASD, schizophrenia, and bipolar disorder. Science 362, eaat8127. https://doi.org/10.1126/science.aat8127

Gao, P., Postiglione, M.P., Krieger, T.G., Hernandez, L., Wang, C., Han, Z., Streicher, C., Papusheva, E., Insolera, R., Chugh, K., Kodish, O., Huang, K., Simons, B.D., Luo, L., Hippenmeyer, S., Shi, S.-H., 2014. Deterministic Progenitor Behavior and Unitary Production of Neurons in the Neocortex. Cell 159, 775–788. https://doi.org/10.1016/j.cell.2014.10.027

Gil-Sanz, C., Espinosa, A., Fregoso, S.P., Bluske, K.K., Cunningham, C.L., Martinez-Garay, I., Zeng, H., Franco, S.J., Müller, U., 2015. Lineage Tracing Using Cux2-Cre and Cux2-CreERT2 Mice. Neuron 86, 1091–1099. https://doi.org/10.1016/j.neuron.2015.04.019

Goebbels, S., Bormuth, I., Bode, U., Hermanson, O., Schwab, M.H., Nave, K.-A., 2006. Genetic targeting of principal neurons in neocortex and hippocampus of NEX-Cre mice. Genes. N. Y. N 2000 44, 611–621. https://doi.org/10.1002/dvg.20256

Gorski, J.A., Talley, T., Qiu, M., Puelles, L., Rubenstein, J.L.R., Jones, K.R., 2002. Cortical Excitatory Neurons and Glia, But Not GABAergic Neurons, Are Produced in the Emx1-Expressing Lineage. J. Neurosci. 22, 6309–6314. https://doi.org/10.1523/JNEUROSCI.22-15-06309.2002

Greig, L.C., Woodworth, M.B., Galazo, M.J., Padmanabhan, H., Macklis, J.D., 2013a. Molecular logic of neocortical projection neuron specification, development and diversity. Nat. Rev. Neurosci. 14, 755–769. https://doi.org/10.1038/nrn3586

Greig, L.C., Woodworth, M.B., Galazo, M.J., Padmanabhan, H., Macklis, J.D., 2013b. Molecular logic of neocortical projection neuron specification, development and diversity. Nat. Rev. Neurosci. 14, 755–769. https://doi.org/10.1038/nrn3586

Gu, W., Wang, H., Huang, X., Kraiczy, J., Singh, P.N.P., Ng, C., Dagdeviren, S., Houghton, S., Pellon-Cardenas, O., Lan, Y., Nie, Y., Zhang, J., Banerjee, K.K., Onufer, E.J., Warner, B.W., Spence, J., Scherl, E., Rafii, S., Lee, R.T., Verzi, M.P., Redmond, D., Longman, R., Helin, K., Shivdasani, R.A., Zhou, Q., 2022. SATB2 preserves colon stem cell identity and mediates ileum-colon conversion via enhancer remodeling. Cell Stem Cell 29, 101-115.e10. https://doi.org/10.1016/j.stem.2021.09.004

Guo, C., Eckler, M.J., McKenna, W.L., McKinsey, G.L., Rubenstein, J.L.R., Chen, B., 2013. Fezf2 Expression Identifies a Multipotent Progenitor for

Neocortical Projection Neurons, Astrocytes, and Oligodendrocytes. Neuron 80, 1167–1174. https://doi.org/10.1016/j.neuron.2013.09.037

Han, W., Kwan, K.Y., Shim, S., Lam, M.M.S., Shin, Y., Xu, X., Zhu, Y., Li, M., Sestan, N., 2011. TBR1 directly represses Fezf2 to control the laminar origin and development of the corticospinal tract. Proc. Natl. Acad. Sci. U. S. A. 108, 3041–3046. https://doi.org/10.1073/pnas.1016723108

Hashimoto, H., Yabe, T., Hirata, T., Shimizu, T., Bae, Y., Yamanaka, Y., Hirano, T., Hibi, M., 2000. Expression of the zinc finger gene fez-like in zebrafish forebrain. Mech. Dev. 97, 191–195. https://doi.org/10.1016/S0925-4773(00)00418-4

Haubensak, W., Attardo, A., Denk, W., Huttner, W.B., 2004. Neurons arise in the basal neuroepithelium of the early mammalian telencephalon: a major site of neurogenesis. Proc. Natl. Acad. Sci. U. S. A. 101, 3196–3201. https://doi.org/10.1073/pnas.0308600100

Hébert, J.M., Fishell, G., 2008. The genetics of early telencephalon patterning: some assembly required. Nat. Rev. Neurosci. 9, 678–685. https://doi.org/10.1038/nrn2463

Hevner, R.F., Hodge, R.D., Daza, R.A.M., Englund, C., 2006. Transcription factors in glutamatergic neurogenesis: conserved programs in neocortex, cerebellum, and adult hippocampus. Neurosci. Res. 55, 223–233. https://doi.org/10.1016/j.neures.2006.03.004

Hevner, R.F., Shi, L., Justice, N., Hsueh, Y.-P., Sheng, M., Smiga, S., Bulfone, A., Goffinet, A.M., Campagnoni, A.T., Rubenstein, J.L.R., 2001. Tbr1 Regulates Differentiation of the Preplate and Layer 6. Neuron 29, 353–366. https://doi.org/10.1016/S0896-6273(01)00211-2

Hill, R.S., Walsh, C.A., 2005. Molecular insights into human brain evolution. Nature 437, 64–67. https://doi.org/10.1038/nature04103

Hobert, O., Kratsios, P., 2019. Neuronal identity control by terminal selectors in worms, flies, and chordates. Curr. Opin. Neurobiol. 56, 97–105. https://doi.org/10.1016/j.conb.2018.12.006

Hoffmann, A., Spengler, D., 2019. Chromatin Remodeling Complex NuRD in Neurodevelopment and Neurodevelopmental Disorders. Front. Genet. 10.

Huang, X., Chen, Q., Luo, W., Pakvasa, M., Zhang, Y., Zheng, L., Li, S., Yang, Z., Zeng, H., Liang, F., Zhang, F., Hu, D.A., Qin, K.H., Wang, E.J., Qin, D.S., Reid, R.R., He, T.-C., Athiviraham, A., El Dafrawy, M., Zhang, H., 2022. SATB2: A versatile transcriptional regulator of craniofacial and skeleton development, neurogenesis and tumorigenesis, and its

applications in regenerative medicine. Genes Dis. 9, 95–107. https://doi.org/10.1016/j.gendis.2020.10.003

Huebner, L., 2020. FEZF2's Role in Differentiation and Proliferation in Radial Glial Cells During Cortical Development. UC Santa Cruz.

Iacopetti, P., Michelini, M., Stuckmann, I., Oback, B., Aaku-Saraste, E., Huttner, W.B., 1999. Expression of the antiproliferative gene TIS21 at the onset of neurogenesis identifies single neuroepithelial cells that switch from proliferative to neuron-generating division. Proc. Natl. Acad. Sci. U. S. A. 96, 4639–4644. https://doi.org/10.1073/pnas.96.8.4639

Inzani, F., Angelico, G., Santoro, A., Travaglino, A., Insabato, L., Raffone, A., Arciuolo, D., Scaglione, G., D'Alessandris, N., Valente, M., Carlino, A., Rindi, G., Zannoni, G.F., 2022. SATB2 is expressed in neuroendocrine carcinoma of the uterine cervix. Virchows Arch. Int. J. Pathol. 480, 873–877. https://doi.org/10.1007/s00428-021-03255-7

Jain, D., Baldi, S., Zabel, A., Straub, T., Becker, P.B., 2015. Active promoters give rise to false positive "Phantom Peaks" in ChIP-seq experiments. Nucleic Acids Res. 43, 6959–6968. https://doi.org/10.1093/nar/gkv637

Jennings, B.H., Ish-Horowicz, D., 2008. The Groucho/TLE/Grg family of transcriptional co-repressors. Genome Biol. 9, 205. https://doi.org/10.1186/gb-2008-9-1-205

Jeong, J.-Y., Einhorn, Z., Mercurio, S., Lee, S., Lau, B., Mione, M., Wilson, S.W., Guo, S., 2006. Neurogenin1 is a determinant of zebrafish basal forebrain dopaminergic neurons and is regulated by the conserved zinc finger protein Tof/Fezl. Proc. Natl. Acad. Sci. 103, 5143–5148. https://doi.org/10.1073/pnas.0600337103

Jessell, T.M., 2000. Neuronal specification in the spinal cord: inductive signals and transcriptional codes. Nat. Rev. Genet. 1, 20–29. https://doi.org/10.1038/35049541

Juric-Sekhar, G., Hevner, R.F., 2019. Malformations of Cerebral Cortex Development: Molecules and Mechanisms. Annu. Rev. Pathol. Mech. Dis. 14, 293–318. https://doi.org/10.1146/annurev-pathmechdis-012418-012927

Keller, D., Erö, C., Markram, H., 2018. Cell Densities in the Mouse Brain: A Systematic Review. Front. Neuroanat. 12.

Kepecs, A., Fishell, G., 2014. Interneuron cell types are fit to function. Nature 505, 318–326. https://doi.org/10.1038/nature12983

Kessaris, N., Fogarty, M., Iannarelli, P., Grist, M., Wegner, M., Richardson, W.D., 2006. Competing waves of oligodendrocytes in the forebrain and postnatal elimination of an embryonic lineage. Nat. Neurosci. 9, 173–179. https://doi.org/10.1038/nn1620

Kohwi, M., Petryniak, M.A., Long, J.E., Ekker, M., Obata, K., Yanagawa, Y., Rubenstein, J.L.R., Alvarez-Buylla, A., 2007. A subpopulation of olfactory bulb GABAergic interneurons is derived from Emx1- and Dlx5/6-expressing progenitors. J. Neurosci. Off. J. Soc. Neurosci. 27, 6878–6891. https://doi.org/10.1523/JNEUROSCI.0254-07.2007

Komuta, Y., Hibi, M., Arai, T., Nakamura, S., Kawano, H., 2007. Defects in reciprocal projections between the thalamus and cerebral cortex in the early development of Fezl-deficient mice. J. Comp. Neurol. 503, 454–465. https://doi.org/10.1002/cne.21401

Konno, D., Kishida, C., Maehara, K., Ohkawa, Y., Kiyonari, H., Okada, S., Matsuzaki, F., 2019. Dmrt factors determine the positional information of cerebral cortical progenitors via differential suppression of homeobox genes. Dev. Camb. Engl. 146, dev174243. https://doi.org/10.1242/dev.174243

Konstantinides, N., Holguera, I., Rossi, A.M., Escobar, A., Dudragne, L., Chen, Y.-C., Tran, T.N., Martínez Jaimes, A.M., Özel, M.N., Simon, F., Shao, Z., Tsankova, N.M., Fullard, J.F., Walldorf, U., Roussos, P., Desplan, C., 2022. A complete temporal transcription factor series in the fly visual system. Nature 604, 316–322. https://doi.org/10.1038/s41586-022-04564-w

Korsunsky, I., Millard, N., Fan, J., Slowikowski, K., Zhang, F., Wei, K., Baglaenko, Y., Brenner, M., Loh, P., Raychaudhuri, S., 2019. Fast, sensitive and accurate integration of single-cell data with Harmony. Nat. Methods 16, 1289–1296. https://doi.org/10.1038/s41592-019-0619-0

Kriegstein, A., Alvarez-Buylla, A., 2009. The Glial Nature of Embryonic and Adult Neural Stem Cells. Annu. Rev. Neurosci. 32, 149–184. https://doi.org/10.1146/annurev.neuro.051508.135600

Kroll, T.T., O'Leary, D.D.M., 2005. Ventralized dorsal telencephalic progenitors in Pax6 mutant mice generate GABA interneurons of a lateral ganglionic eminence fate. Proc. Natl. Acad. Sci. U. S. A. 102, 7374–7379. https://doi.org/10.1073/pnas.0500819102

Kwan, K.Y., 2013. Transcriptional dysregulation of neocortical circuit assembly in ASD. Int. Rev. Neurobiol. 113, 167–205. https://doi.org/10.1016/B978-0-12-418700-9.00006-X

Kwan, K.Y., Lam, M.M.S., Krsnik, Ž., Kawasawa, Y.I., Lefebvre, V., Šestan, N., 2008. SOX5 postmitotically regulates migration, postmigratory differentiation, and projections of subplate and deep-layer neocortical neurons. Proc. Natl. Acad. Sci. 105, 16021–16026. https://doi.org/10.1073/pnas.0806791105

Kwan, K.Y., Sestan, N., Anton, E.S., 2012. Transcriptional co-regulation of neuronal migration and laminar identity in the neocortex. Dev. Camb. Engl. 139, 1535–1546. https://doi.org/10.1242/dev.069963

Lai, T., Jabaudon, D., Molyneaux, B.J., Azim, E., Arlotta, P., Menezes, J.R.L., Macklis, J.D., 2008. SOX5 controls the sequential generation of distinct corticofugal neuron subtypes. Neuron 57, 232–247. https://doi.org/10.1016/j.neuron.2007.12.023

Landisman, C.E., Connors, B.W., 2007. VPM and PoM nuclei of the rat somatosensory thalamus: intrinsic neuronal properties and corticothalamic feedback. Cereb. Cortex N. Y. N 1991 17, 2853–2865. https://doi.org/10.1093/cercor/bhm025

Lange, C., Huttner, W.B., Calegari, F., 2009. Cdk4/CyclinD1 Overexpression in Neural Stem Cells Shortens G1, Delays Neurogenesis, and Promotes the Generation and Expansion of Basal Progenitors. Cell Stem Cell 5, 320–331. https://doi.org/10.1016/j.stem.2009.05.026

Leone, D.P., Heavner, W.E., Ferenczi, E.A., Dobreva, G., Huguenard, J.R., Grosschedl, R., McConnell, S.K., 2015. Satb2 Regulates the Differentiation of Both Callosal and Subcerebral Projection Neurons in the Developing Cerebral Cortex. Cereb. Cortex N. Y. N 1991 25, 3406–3419. https://doi.org/10.1093/cercor/bhu156

Leone, D.P., Srinivasan, K., Chen, B., Alcamo, E., McConnell, S.K., 2008. The determination of projection neuron identity in the developing cerebral cortex. Curr. Opin. Neurobiol. 18, 28–35. https://doi.org/10.1016/j.conb.2008.05.006

Li, M., Santpere, G., Imamura Kawasawa, Y., Evgrafov, O.V., Gulden, F.O., Pochareddy, S., Sunkin, S.M., Li, Zhen, Shin, Y., Zhu, Y., Sousa, A.M.M., Werling, D.M., Kitchen, R.R., Kang, H.J., Pletikos, M., Choi, J., Muchnik, S., Xu, X., Wang, D., Lorente-Galdos, B., Liu, S., Giusti-Rodríguez, P., Won, H., de Leeuw, C.A., Pardiñas, A.F., BrainSpan Consortium, PsychENCODE Consortium, PsychENCODE Developmental Subgroup, Hu, M., Jin, F., Li, Y., Owen, M.J., O'Donovan, M.C., Walters, J.T.R., Posthuma, D., Reimers, M.A., Levitt, P., Weinberger, D.R., Hyde, Thomas M., Kleinman, J.E., Geschwind, D.H., Hawrylycz, M.J., State, M.W., Sanders, S.J., Sullivan, P.F., Gerstein, M.B., Lein, E.S., Knowles, J.A., Sestan, N., Willsey, A.J., Oldre, A., Szafer, A., Camarena, A.,

Cherskov, A., Charney, A.W., Abyzov, A., Kozlenkov, A., Safi, A., Jones, A.R., Ashley-Koch, A.E., Ebbert, A., Price, A.J., Sekijima, A., Kefi, A., Bernard, A., Amiri, A., Sboner, A., Clark, A., Jaffe, A.E., Tebbenkamp, A.T.N., Sodt, A.J., Guillozet-Bongaarts, A.L., Nairn, A.C., Carey, A., Huttner, A., Chervenak, A., Szekely, A., Shieh, A.W., Harmanci, A., Lipska, B.K., Carlyle, B.C., Gregor, B.W., Kassim, B.S., Sheppard, B., Bichsel, C., Hahn, C.-G., Lee, C.-K., Chen, C., Kuan, C.L., Dang, C., Lau, C., Cuhaciyan, C., Armoskus, C., Mason, C.E., Liu, C., Slaughterbeck, C.R., Bennet, C., Pinto, D., Polioudakis, D., Franjic, D., Miller, D.J., Bertagnolli, D., Lewis, D.A., Feng, D., Sandman, D., Clarke, D., Williams, D., DelValle, D., Fitzgerald, D., Shen, E.H., Flatow, E., Zharovsky, E., Burke, E.E., Olson, E., Fulfs, E., Mattei, E., Hadjimichael, E., Deelman, E., Navarro, F.C.P., Wu, F., Lee, F., Cheng, F., Goes, F.S., Vaccarino, F.M., Liu, F., Hoffman, G.E., Gürsoy, G., Gee, G., Mehta, G., Coppola, G., Giase, G., Sedmak, G., Johnson, G.D., Wray, G.A., Crawford, G.E., Gu, G., van Bakel, H., Witt, H., Yoon, H.J., Pratt, H., Zhao, H., Glass, I.A., Huey, J., Arnold, J., Noonan, J.P., Bendl, J., Jochim, J.M., Goldy, J., Herstein, J., Wiseman, J.R., Miller, J.A., Mariani, J., Stoll, J., Moore, J., Szatkiewicz, J., Leng, J., Zhang, J., Parente, J., Rozowsky, J., Fullard, J.F., Hohmann, J.G., Morris, J., Phillips, J.W., Warrell, J., Shin, J.H., An, J.-Y., Belmont, J., Nyhus, J., Pendergraft, J., Bryois, J., Roll, K., Grennan, K.S., Aiona, K., White, K.P., Aldinger, K.A., Smith, K.A., Girdhar, K., Brouner, K., Mangravite, L.M., Brown, L., Collado-Torres, L., Cheng, L., Gourley, L., Song, L., Ubieta, L.D.L.T., Habegger, L., Ng, L., Hauberg, M.E., Onorati, M., Webster, M.J., Kundakovic, M., Skarica, M., Reimers, M., Johnson, M.B., Chen, M.M., Garrett, M.E., Sarreal, M., Reding, M., Gu, M., Peters, M.A., Fisher, M., Gandal, M.J., Purcaro, M., Smith, M., Brown, Miguel, Shibata, M., Brown, Mimi, Xu, M., Yang, M., Ray, M., Shapovalova, N.V., Francoeur, N., Sjoquist, N., Mastan, N., Kaur, N., Parikshak, N., Mosqueda, N.F., Ngo, N.-K., Dee, N., Ivanov, N.A., Devillers, O., Roussos, P., Parker, P.D., Manser, P., Wohnoutka, P., Farnham, P.J., Zandi, P., Emani, P.S., Dalley, R.A., Mayani, R., Tao, R., Gittin, R., Straub, R.E., Lifton, R.P., Jacobov, R., Howard, R.E., Park, R.B., Dai, R., Abramowicz, S., Akbarian, S., Schreiner, S., Ma, S., Parry, S.E., Shapouri, S., Weissman, S., Caldejon, S., Mane, S., Ding, S.-L., Scuderi, S., Dracheva, S., Butler, S., Lisgo, S.N., Rhie, S.K., Lindsay, S., Datta, S., Souaiaia, T., Roychowdhury, T., Gomez, T., Naluai-Cecchini, T., Beach, T.G., Goodman, T., Gao, T., Dolbeare, T.A., Fliss, T., Reddy, T.E., Chen, T., Hyde, Tom M., Brunetti, T., Lemon, T.A., Desta, T., Borrman, T., Haroutunian, V., Spitsyna, V.N., Swarup, V., Shi, X., Jiang, Yan, Xia, Y., Chen, Y.-H., Jiang, Yi, Wang, Y., Chae, Y., Yang, Y.T., Kim, Y., Riley, Z.L., Krsnik, Z., Deng, Z., Weng, Z., Lin, Z., Li, Zhuo, 2018. Integrative functional genomic analysis of human brain development and neuropsychiatric risks. Science 362, eaat7615. https://doi.org/10.1126/science.aat7615

Li, X., Liu, G., Yang, L., Li, Z., Zhang, Z., Xu, Z., Cai, Y., Du, H., Su, Z., Wang, Z., Duan, Y., Chen, H., Shang, Z., You, Y., Zhang, Q., He, M., Chen, B.,

Yang, Z., 2021. Decoding Cortical Glial Cell Development. Neurosci. Bull. 37, 440–460. https://doi.org/10.1007/s12264-021-00640-9

Llorca, A., Ciceri, G., Beattie, R., Wong, F.K., Diana, G., Serafeimidou-Pouliou, E., Fernández-Otero, M., Streicher, C., Arnold, S.J., Meyer, M., Hippenmeyer, S., Maravall, M., Marin, O., 2019. A stochastic framework of neurogenesis underlies the assembly of neocortical cytoarchitecture. eLife 8, e51381. https://doi.org/10.7554/eLife.51381

Lodato, S., Molyneaux, B.J., Zuccaro, E., Goff, L.A., Chen, H.-H., Yuan, W., Meleski, A., Takahashi, E., Mahony, S., Rinn, J.L., Gifford, D.K., Arlotta, P., 2014. Gene co-regulation by Fezf2 selects neurotransmitter identity and connectivity of corticospinal neurons. Nat. Neurosci. 17, 1046–1054. https://doi.org/10.1038/nn.3757

Machon, O., Backman, M., Machonova, O., Kozmik, Z., Vacik, T., Andersen, L., Krauss, S., 2007. A dynamic gradient of Wnt signaling controls initiation of neurogenesis in the mammalian cortex and cellular specification in the hippocampus. Dev. Biol. 311, 223–237. https://doi.org/10.1016/j.ydbio.2007.08.038

Malatesta, P., Hartfuss, E., Gotz, M., 2000. Isolation of radial glial cells by fluorescent-activated cell sorting reveals a neuronal lineage. Development 127, 5253–5263. https://doi.org/10.1242/dev.127.24.5253

Martí, E., Takada, R., Bumcrot, D.A., Sasaki, H., McMahon, A.P., 1995. Distribution of Sonic hedgehog peptides in the developing chick and mouse embryo. Dev. Camb. Engl. 121, 2537–2547. https://doi.org/10.1242/dev.121.8.2537

Matho, K.S., Huilgol, D., Galbavy, W., He, M., Kim, G., An, X., Lu, J., Wu, P., Di Bella, D.J., Shetty, A.S., Palaniswamy, R., Hatfield, J., Raudales, R., Narasimhan, A., Gamache, E., Levine, J.M., Tucciarone, J., Szelenyi, E., Harris, J.A., Mitra, P.P., Osten, P., Arlotta, P., Huang, Z.J., 2021. Genetic dissection of the glutamatergic neuron system in cerebral cortex. Nature 598, 182–187. https://doi.org/10.1038/s41586-021-03955-9

McConnell, S., 1988. Fates of visual cortical neurons in the ferret after isochronic and heterochronic transplantation. J. Neurosci. 8, 945–974. https://doi.org/10.1523/JNEUROSCI.08-03-00945.1988

McConnell, S.K., 1995. Constructing the cerebral cortex: Neurogenesis and fate determination. Neuron 15, 761–768. https://doi.org/10.1016/0896-6273(95)90168-X

McConnell, S.K., Kaznowski, C.E., 1991. Cell cycle dependence of laminar determination in developing neocortex. Science 254, 282–285. https://doi.org/10.1126/science.254.5029.282

McKenna, W.L., Betancourt, J., Larkin, K.A., Abrams, B., Guo, C., Rubenstein, J.L.R., Chen, B., 2011. Tbr1 and Fezf2 regulate alternate corticofugal neuronal identities during neocortical development. J. Neurosci. Off. J. Soc. Neurosci. 31, 549–564. https://doi.org/10.1523/JNEUROSCI.4131-10.2011

McKenna, W.L., Ortiz-Londono, C.F., Mathew, T.K., Hoang, K., Katzman, S., Chen, B., 2015. Mutual regulation between Satb2 and Fezf2 promotes subcerebral projection neuron identity in the developing cerebral cortex. Proc. Natl. Acad. Sci. U. S. A. 112, 11702–11707. https://doi.org/10.1073/pnas.1504144112

Meng, Q., Wang, K., Brunetti, T., Xia, Y., Jiao, C., Dai, R., Fitzgerald, D., Thomas, A., Jay, L., Eckart, H., Grennan, K., Imamura-Kawasawa, Y., Li, M., Sestan, N., White, K.P., Chen, C., Liu, C., 2018. The *DGCR5* long noncoding RNA may regulate expression of several schizophrenia-related genes. Sci. Transl. Med. 10, eaat6912. https://doi.org/10.1126/scitranslmed.aat6912

Miyata, T., Kawaguchi, A., Okano, H., Ogawa, M., 2001. Asymmetric Inheritance of Radial Glial Fibers by Cortical Neurons. Neuron 31, 727–741. https://doi.org/10.1016/S0896-6273(01)00420-2

Molnár, Z., Pollen, A., 2014. How unique is the human neocortex? Development 141, 11–16. https://doi.org/10.1242/dev.101279

Molyneaux, B.J., Arlotta, P., Hirata, T., Hibi, M., Macklis, J.D., 2005. Fezl Is Required for the Birth and Specification of Corticospinal Motor Neurons. Neuron 47, 817–831. https://doi.org/10.1016/j.neuron.2005.08.030

Molyneaux, B.J., Arlotta, P., Menezes, J.R.L., Macklis, J.D., 2007. Neuronal subtype specification in the cerebral cortex. Nat. Rev. Neurosci. 8, 427–437. https://doi.org/10.1038/nrn2151

Molyneaux, B.J., Goff, L.A., Brettler, A.C., Chen, H.-H., Hrvatin, S., Rinn, J.L., Arlotta, P., 2015. DeCoN: genome-wide analysis of in vivo transcriptional dynamics during pyramidal neuron fate selection in neocortex. Neuron 85, 275–288. https://doi.org/10.1016/j.neuron.2014.12.024

Muhr, J., Andersson, E., Persson, M., Jessell, T.M., Ericson, J., 2001. Groucho-mediated transcriptional repression establishes progenitor cell pattern and neuronal fate in the ventral neural tube. Cell 104, 861–873. https://doi.org/10.1016/s0092-8674(01)00283-5

Mutch, C.A., Funatsu, N., Monuki, E.S., Chenn, A., 2009. β-Catenin Signaling Levels in Progenitors Influence the Laminar Cell Fates of Projection Neurons. J. Neurosci. 29, 13710–13719. https://doi.org/10.1523/JNEUROSCI.3022-09.2009

Mutch, C.A., Schulte, J.D., Olson, E., Chenn, A., 2010. Beta-catenin signaling negatively regulates intermediate progenitor population numbers in the developing cortex. PloS One 5, e12376. https://doi.org/10.1371/journal.pone.0012376

Nieuwenhuys, R., 1994. The neocortex: An overview of its evolutionary development, structural organization and synaptology. Anat. Embryol. (Berl.) 190. https://doi.org/10.1007/BF00187291

Noctor, S.C., Flint, A.C., Weissman, T.A., Dammerman, R.S., Kriegstein, A.R., 2001. Neurons derived from radial glial cells establish radial units in neocortex. Nature 409, 714–720. https://doi.org/10.1038/35055553

O'Leary, D.D., Koester, S.E., 1993. Development of projection neuron types, axon pathways, and patterned connections of the mammalian cortex. Neuron 10, 991–1006. https://doi.org/10.1016/0896-6273(93)90049-w

Ozkan, A., MacDonald, J.L., Fame, R.M., Itoh, Y., Peter, M., Durak, O., Macklis, J.D., 2020. Chapter 19 - Specification of cortical projection neurons: transcriptional mechanisms, in: Rubenstein, J., Rakic, P., Chen, B., Kwan, K.Y. (Eds.), Patterning and Cell Type Specification in the Developing CNS and PNS (Second Edition). Academic Press, pp. 427–459. https://doi.org/10.1016/B978-0-12-814405-3.00019-9

Pearson, B.J., Doe, C.Q., 2004. Specification of temporal identity in the developing nervous system. Annu. Rev. Cell Dev. Biol. 20, 619–647. https://doi.org/10.1146/annurev.cellbio.19.111301.115142

Peng, Y., Lu, Z., Li, G., Piechowicz, M., Anderson, M., Uddin, Y., Wu, J., Qiu, S., 2016. The autism-associated MET receptor tyrosine kinase engages early neuronal growth mechanism and controls glutamatergic circuits development in the forebrain. Mol. Psychiatry 21, 925–935. https://doi.org/10.1038/mp.2015.182

Pierani, A., Moran-Rivard, L., Sunshine, M.J., Littman, D.R., Goulding, M., Jessell, T.M., 2001. Control of Interneuron Fate in the Developing Spinal Cord by the Progenitor Homeodomain Protein Dbx1. Neuron 29, 367–384. https://doi.org/10.1016/S0896-6273(01)00212-4

Pilaz, L.-J., Patti, D., Marcy, G., Ollier, E., Pfister, S., Douglas, R.J., Betizeau, M., Gautier, E., Cortay, V., Doerflinger, N., Kennedy, H., Dehay, C., 2009.

Forced G1-phase reduction alters mode of division, neuron number, and laminar phenotype in the cerebral cortex. Proc. Natl. Acad. Sci. 106, 21924–21929. https://doi.org/10.1073/pnas.0909894106

Pollen, A.A., Bhaduri, A., Andrews, M.G., Nowakowski, T.J., Meyerson, O.S., Mostajo-Radji, M.A., Di Lullo, E., Alvarado, B., Bedolli, M., Dougherty, M.L., Fiddes, I.T., Kronenberg, Z.N., Shuga, J., Leyrat, A.A., West, J.A., Bershteyn, M., Lowe, C.B., Pavlovic, B.J., Salama, S.R., Haussler, D., Eichler, E.E., Kriegstein, A.R., 2019. Establishing Cerebral Organoids as Models of Human-Specific Brain Evolution. Cell 176, 743-756.e17. https://doi.org/10.1016/j.cell.2019.01.017

Rakic, P., 1988. Specification of cerebral cortical areas. Science 241, 170–176. https://doi.org/10.1126/science.3291116

Ripke, S., Neale, B.M., Corvin, A., Walters, J.T., Farh, K.-H., Holmans, P.A., Lee, P., Bulik-Sullivan, B., Collier, D.A., Huang, H., Pers, T.H., Agartz, I., Agerbo, E., Albus, M., Alexander, M., Amin, F., Bacanu, S.A., Begemann, M., Belliveau, R.A., Bene, J., Bergen, S.E., Bevilacqua, E., Bigdeli, T.B., Black, D.W., Bruggeman, R., Buccola, N.G., Buckner, R.L., Byerley, W., Cahn, W., Cai, G., Campion, D., Cantor, R.M., Carr, V.J., Carrera, N., Catts, S.V., Chambert, K.D., Chan, R.C., Chan, R.Y., Chen, E.Y., Cheng, W., Cheung, E.F., Chong, S.A., Cloninger, C.R., Cohen, D., Cohen, N., Cormican, P., Craddock, N., Crowley, J.J., Curtis, D., Davidson, M., Davis, K.L., Degenhardt, F., Del Favero, J., Demontis, D., Dikeos, D., Dinan, T., Djurovic, S., Donohoe, G., Drapeau, E., Duan, J., Dudbridge, F., Durmishi, N., Eichhammer, P., Eriksson, J., Escott-Price, V., Essioux, L., Fanous, A.H., Farrell, M.S., Frank, J., Franke, L., Freedman, R., Freimer, N.B., Friedl, M., Friedman, J.I., Fromer, M., Genovese, G., Georgieva, L., Giegling, I., Giusti-Rodríguez, P., Godard, S., Goldstein, J.I., Golimbet, V., Gopal, S., Gratten, J., de Haan, L., Hammer, C., Hamshere, M.L., Hansen, M., Hansen, T., Haroutunian, V., Hartmann, A.M., Henskens, F.A., Herms, S., Hirschhorn, J.N., Hoffmann, P., Hofman, A., Hollegaard, M.V., Hougaard, D.M., Ikeda, M., Joa, I., Julià, A., Kahn, R.S., Kalaydjieva, L., Karachanak-Yankova, S., Karjalainen, J., Kavanagh, D., Keller, M.C., Kennedy, J.L., Khrunin, A., Kim, Y., Klovins, J., Knowles, J.A., Konte, B., Kucinskas, V., Kucinskiene, Z.A., Kuzelova-Ptackova, H., Kähler, A.K., Laurent, C., Lee, J., Lee, S.H., Legge, S.E., Lerer, B., Li, M., Li, T., Liang, K.-Y., Lieberman, J., Limborska, S., Loughland, C.M., Lubinski, J., Lönnqvist, J., Macek, M., Magnusson, P.K., Maher, B.S., Maier, W., Mallet, J., Marsal, S., Mattheisen, M., Mattingsdal, M., McCarley, R.W., McDonald, C., McIntosh, A.M., Meier, S., Meijer, C.J., Melegh, B., Melle, I., Mesholam-Gately, R.I., Metspalu, A., Michie, P.T., Milani, L., Milanova, V., Mokrab, Y., Morris, D.W., Mors, O., Murphy, K.C., Murray, R.M., Myin-Germeys, I., Müller-Myhsok, B., Nelis, M., Nenadic, I., Nertney, D.A., Nestadt, G., Nicodemus, K.K., Nikitina-Zake, L., Nisenbaum, L., Nordin, A., O'Callaghan, E., O'Dushlaine, C., O'Neill, F.A., Oh, S.-Y., Olincy, A., Olsen, L., Van Os, J.,

Pantelis, C., Papadimitriou, G.N., Papiol, S., Parkhomenko, E., Pato, M.T., Paunio, T., Pejovic-Milovancevic, M., Perkins, D.O., Pietiläinen, O., Pimm, J., Pocklington, A.J., Powell, J., Price, A., Pulver, A.E., Purcell, S.M., Quested, D., Rasmussen, H.B., Reichenberg, A., Reimers, M.A., Richards, A.L., Roffman, J.L., Roussos, P., Ruderfer, D.M., Salomaa, V., Sanders, A.R., Schall, U., Schubert, C.R., Schulze, T.G., Schwab, S.G., Scolnick, E.M., Scott, R.J., Seidman, L.J., Shi, J., Sigurdsson, E., Silagadze, T., Silverman, J.M., Sim, K., Slominsky, P., Smoller, J.W., So, H.-C., Spencer, C.C.A., Stahl, E.A., Stefansson, H., Steinberg, S., Stogmann, E., Straub, R.E., Strengman, E., Strohmaier, J., Stroup, T.S., Subramaniam, M., Suvisaari, J., Svrakic, D.M., Szatkiewicz, J.P., Söderman, E., Thirumalai, S., Toncheva, D., Tosato, S., Veijola, J., Waddington, J., Walsh, D., Wang, D., Wang, Q., Webb, B.T., Weiser, M., Wildenauer, D.B., Williams, N.M., Williams, S., Witt, S.H., Wolen, A.R., Wong, E.H., Wormley, B.K., Xi, H.S., Zai, C.C., Zheng, X., Zimprich, F., Wray, N.R., Stefansson, K., Visscher, P.M., Adolfsson, R., Andreassen, O.A., Blackwood, D.H., Bramon, E., Buxbaum, J.D., Børglum, A.D., Cichon, S., Darvasi, A., Domenici, E., Ehrenreich, H., Esko, T., Gejman, P.V., Gill, M., Gurling, H., Hultman, C.M., Iwata, N., Jablensky, A.V., Jönsson, E.G., Kendler, K.S., Kirov, G., Knight, J., Lencz, T., Levinson, D.F., Li, Q.S., Liu, J., Malhotra, A.K., McCarroll, S.A., McQuillin, A., Moran, J.L., Mortensen, P.B., Mowry, B.J., Nöthen, M.M., Ophoff, R.A., Owen, M.J., Palotie, A., Pato, C.N., Petryshen, T.L., Posthuma, D., Rietschel, M., Riley, B.P., Rujescu, D., Sham, P.C., Sklar, P., St Clair, D., Weinberger, D.R., Wendland, J.R., Werge, T., Daly, M.J., Sullivan, P.F., O'Donovan, M.C., 2014. Biological Insights From 108 Schizophrenia-Associated Genetic Loci. Nature 511, 421–427. https://doi.org/10.1038/nature13595

Roelink, H., Porter, J.A., Chiang, C., Tanabe, Y., Chang, D.T., Beachy, P.A., Jessell, T.M., 1995. Floor plate and motor neuron induction by different concentrations of the amino-terminal cleavage product of sonic hedgehog autoproteolysis. Cell 81, 445–455. https://doi.org/10.1016/0092-8674(95)90397-6

Rouaux, C., Arlotta, P., 2013. Direct lineage reprogramming of post-mitotic callosal neurons into corticofugal neurons in vivo. Nat. Cell Biol. 15, 214–221. https://doi.org/10.1038/ncb2660

Rouaux, C., Arlotta, P., 2010. Fezf2 directs the differentiation of corticofugal neurons from striatal progenitors in vivo. Nat. Neurosci. 13, 1345–1347. https://doi.org/10.1038/nn.2658

Roy, S.K., Shrivastava, A., Srivastav, S., Shankar, S., Srivastava, R.K., 2020. SATB2 is a novel biomarker and therapeutic target for cancer. J. Cell. Mol. Med. 24, 11064–11069. https://doi.org/10.1111/jcmm.15755

Schuurmans, C., Armant, O., Nieto, M., Stenman, J.M., Britz, O., Klenin, N., Brown, C., Langevin, L.-M., Seibt, J., Tang, H., Cunningham, J.M., Dyck, R., Walsh, C., Campbell, K., Polleux, F., Guillemot, F., 2004. Sequential phases of cortical specification involve Neurogenin-dependent and -independent pathways. EMBO J. 23, 2892–2902. https://doi.org/10.1038/sj.emboj.7600278

Shim, S., Kwan, K.Y., Li, M., Lefebvre, V., Sestan, N., 2012. Cis-regulatory control of corticospinal system development and evolution. Nature 486, 74–79. https://doi.org/10.1038/nature11094

Shimizu, Takeshi, Nakazawa, M., Kani, S., Bae, Y.-K., Shimizu, Takashi, Kageyama, R., Hibi, M., 2010. Zinc finger genes Fezf1 and Fezf2 control neuronal differentiation by repressing Hes5 expression in the forebrain. Development 137, 1875–1885. https://doi.org/10.1242/dev.047167

Shin, T.H., Theodorou, E., Holland, C., Yamin, R., Raggio, C.L., Giampietro, P.F., Sweetser, D.A., 2021. TLE4 Is a Critical Mediator of Osteoblast and Runx2-Dependent Bone Development. Front. Cell Dev. Biol. 9, 671029. https://doi.org/10.3389/fcell.2021.671029

Sholl, D.A., 1953. Dendritic organization in the neurons of the visual and motor cortices of the cat. J. Anat. 87, 387-406.1.

Shu, X.-S., Li, L., Ji, M., Cheng, Y., Ying, J., Fan, Y., Zhong, L., Liu, X., Tsao, S.W., Chan, A.T.C., Tao, Q., 2013. FEZF2, a novel 3p14 tumor suppressor gene, represses oncogene EZH2 and MDM2 expression and is frequently methylated in nasopharyngeal carcinoma. Carcinogenesis 34, 1984–1993. https://doi.org/10.1093/carcin/bgt165

Shue, Y.T., Drainas, A.P., Li, N.Y., Pearsall, S.M., Morgan, D., Sinnott-Armstrong, N., Hipkins, S.Q., Coles, G.L., Lim, J.S., Oro, A.E., Simpson, K.L., Dive, C., Sage, J., 2022. A conserved YAP/Notch/REST network controls the neuroendocrine cell fate in the lungs. Nat. Commun. 13, 2690. https://doi.org/10.1038/s41467-022-30416-2

Silbereis, J.C., Pochareddy, S., Zhu, Y., Li, M., Sestan, N., 2016. The Cellular and Molecular Landscapes of the Developing Human Central Nervous System. Neuron 89, 248–268. https://doi.org/10.1016/j.neuron.2015.12.008

Sokpor, G., Xie, Y., Rosenbusch, J., Tuoc, T., 2017. Chromatin Remodeling BAF (SWI/SNF) Complexes in Neural Development and Disorders. Front. Mol. Neurosci. 10.

Soufi, A., Dalton, S., 2016. Cycling through developmental decisions: how cell cycle dynamics control pluripotency, differentiation and reprogramming. Development 143, 4301–4311. https://doi.org/10.1242/dev.142075

Takaba, H., Morishita, Y., Tomofuji, Y., Danks, L., Nitta, T., Komatsu, N., Kodama, T., Takayanagi, H., 2015. Fezf2 Orchestrates a Thymic Program of Self-Antigen Expression for Immune Tolerance. Cell 163, 975–987. https://doi.org/10.1016/j.cell.2015.10.013

Takahashi, T., Nowakowski, R.S., Caviness, V.S., 1995. The cell cycle of the pseudostratified ventricular epithelium of the embryonic murine cerebral wall. J. Neurosci. 15, 6046–6057. https://doi.org/10.1523/JNEUROSCI.15-09-06046.1995

Tantirigama, M.L.S., Oswald, M.J., Clare, A.J., Wicky, H.E., Day, R.C., Hughes, S.M., Empson, R.M., 2016. Fezf2 expression in layer 5 projection neurons of mature mouse motor cortex. J. Comp. Neurol. 524, 829–845. https://doi.org/10.1002/cne.23875

Tasic, B., Yao, Z., Graybuck, L.T., Smith, K.A., Nguyen, T.N., Bertagnolli, D., Goldy, J., Garren, E., Economo, M.N., Viswanathan, S., Penn, O., Bakken, T., Menon, V., Miller, J., Fong, O., Hirokawa, K.E., Lathia, K., Rimorin, C., Tieu, M., Larsen, R., Casper, T., Barkan, E., Kroll, M., Parry, S., Shapovalova, N.V., Hirschstein, D., Pendergraft, J., Sullivan, H.A., Kim, T.K., Szafer, A., Dee, N., Groblewski, P., Wickersham, I., Cetin, A., Harris, J.A., Levi, B.P., Sunkin, S.M., Madisen, L., Daigle, T.L., Looger, L., Bernard, A., Phillips, J., Lein, E., Hawrylycz, M., Svoboda, K., Jones, A.R., Koch, C., Zeng, H., 2018. Shared and distinct transcriptomic cell types across neocortical areas. Nature 563, 72–78. https://doi.org/10.1038/s41586-018-0654-5

Taverna, E., Götz, M., Huttner, W.B., 2014. The cell biology of neurogenesis: toward an understanding of the development and evolution of the neocortex. Annu. Rev. Cell Dev. Biol. 30, 465–502. https://doi.org/10.1146/annurev-cellbio-101011-155801

Telley, L., Agirman, G., Prados, J., Amberg, N., Fièvre, S., Oberst, P., Bartolini, G., Vitali, I., Cadilhac, C., Hippenmeyer, S., Nguyen, L., Dayer, A., Jabaudon, D., 2019. Temporal patterning of apical progenitors and their daughter neurons in the developing neocortex. Science 364, eaav2522. https://doi.org/10.1126/science.aav2522

Teytelman, L., Thurtle, D.M., Rine, J., van Oudenaarden, A., 2013. Highly expressed loci are vulnerable to misleading ChIP localization of multiple unrelated proteins. Proc. Natl. Acad. Sci. U. S. A. 110, 18602–18607. https://doi.org/10.1073/pnas.1316064110

Tirone, F., 2001. The gene PC3(TIS21/BTG2), prototype member of the PC3/BTG/TOB family: regulator in control of cell growth, differentiation, and DNA repair? J. Cell. Physiol. 187, 155–165. https://doi.org/10.1002/jcp.1062

Tsyporin, J., Tastad, D., Ma, X., Nehme, A., Finn, T., Huebner, L., Liu, G., Gallardo, D., Makhamreh, A., Roberts, J.M., Katzman, S., Sestan, N., McConnell, S.K., Yang, Z., Qiu, S., Chen, B., 2021. Transcriptional repression by FEZF2 restricts alternative identities of cortical projection neurons. Cell Rep. 35, 109269. https://doi.org/10.1016/j.celrep.2021.109269

Turki-Judeh, W., Courey, A.J., 2012. Groucho: a corepressor with instructive roles in development. Curr. Top. Dev. Biol. 98, 65–96. https://doi.org/10.1016/B978-0-12-386499-4.00003-3

Uylings, H.B.M., van Eden, C.G., 1991. Chapter 3 Qualitative and quantitative comparison of the prefrontal cortex in rat and in primates, including humans, in: Progress in Brain Research. Elsevier, pp. 31–62. https://doi.org/10.1016/S0079-6123(08)62675-8

Ventura, R.E., Goldman, J.E., 2007. Dorsal Radial Glia Generate Olfactory Bulb Interneurons in the Postnatal Murine Brain. J. Neurosci. 27, 4297–4302. https://doi.org/10.1523/JNEUROSCI.0399-07.2007

Wang, S.-Y., Gao, K., Deng, D.-L., Cai, J.-J., Xiao, Z.-Y., He, L.-Q., Jiao, H.-L., Ye, Y.-P., Yang, R.-W., Li, T.-T., Liang, L., Liao, W.-T., Ding, Y.-Q., 2016. TLE4 promotes colorectal cancer progression through activation of JNK/c-Jun signaling pathway. Oncotarget 7, 2878–2888. https://doi.org/10.18632/oncotarget.6694

Warmke, L.M., Maloney, N., Leung, C.H., Lin, H., Lazar, A.J., Wang, W.-L., 2022. SATB2 Expression in Undifferentiated Pleomorphic Sarcomas of Bone. Am. J. Clin. Pathol. 158, 235–241. https://doi.org/10.1093/ajcp/aqac033

Weng, M., Golden, K.L., Lee, C.-Y., 2010. dFezf/Earmuff maintains the restricted developmental potential of intermediate neural progenitors in Drosophila. Dev. Cell 18, 126–135. https://doi.org/10.1016/j.devcel.2009.12.007

Whitton, L., Apostolova, G., Rieder, D., Dechant, G., Rea, S., Donohoe, G., Morris, D.W., 2018. Genes regulated by SATB2 during neurodevelopment contribute to schizophrenia and educational attainment. PLoS Genet. 14, e1007515. https://doi.org/10.1371/journal.pgen.1007515

Wrobel, C.N., Mutch, C.A., Swaminathan, S., Taketo, M.M., Chenn, A., 2007. Persistent expression of stabilized beta-catenin delays maturation of

radial glial cells into intermediate progenitors. Dev. Biol. 309, 285–297. https://doi.org/10.1016/j.ydbio.2007.07.013

Wu, L., Chen, J., Qin, Y., Mo, X., Huang, M., Ru, H., Yang, Y., Liu, J., Lin, Y., 2016. SATB2 suppresses gastric cancer cell proliferation and migration. Tumour Biol. J. Int. Soc. Oncodevelopmental Biol. Med. 37, 4597–4602. https://doi.org/10.1007/s13277-015-4282-5

Xing, S., Shao, P., Li, F., Zhao, X., Seo, W., Wheat, J.C., Ramasamy, S., Wang, J., Li, X., Peng, W., Yu, S., Liu, C., Taniuchi, I., Sweetser, D.A., Xue, H.-H., 2018. Tle corepressors are differentially partitioned to instruct CD8+ T cell lineage choice and identity. J. Exp. Med. 215, 2211–2226. https://doi.org/10.1084/jem.20171514

Xu, M., Xu, X., Pan, B., Chen, X., Lin, K., Zeng, K., Liu, X., Xu, T., Sun, L., Qin, J., He, B., Pan, Y., Sun, H., Wang, S., 2019. LncRNA SATB2-AS1 inhibits tumor metastasis and affects the tumor immune cell microenvironment in colorectal cancer by regulating SATB2. Mol. Cancer 18, 135. https://doi.org/10.1186/s12943-019-1063-6

Yang, D., Qu, F., Cai, H., Chuang, C.-H., Lim, J.S., Jahchan, N., Grüner, B.M., S Kuo, C., Kong, C., Oudin, M.J., Winslow, M.M., Sage, J., 2019. Axon-like protrusions promote small cell lung cancer migration and metastasis. eLife 8, e50616. https://doi.org/10.7554/eLife.50616

Young, K.M., Fogarty, M., Kessaris, N., Richardson, W.D., 2007. Subventricular zone stem cells are heterogeneous with respect to their embryonic origins and neurogenic fates in the adult olfactory bulb. J. Neurosci. Off. J. Soc. Neurosci. 27, 8286–8296. https://doi.org/10.1523/JNEUROSCI.0476-07.2007

Yu, M., Juric, I., Abnousi, A., Hu, M., Ren, B., 2021. Proximity Ligation-Assisted ChIP-Seq (PLAC-Seq), in: Borggrefe, T., Giaimo, B.D. (Eds.), Enhancers and Promoters: Methods and Protocols, Methods in Molecular Biology. Springer US, New York, NY, pp. 181–199. https://doi.org/10.1007/978-1-0716-1597-3_10

Zarate, Y.A., Fish, J.L., 2017. SATB2-associated syndrome: Mechanisms, phenotype, and practical recommendations. Am. J. Med. Genet. A. 173, 327–337. https://doi.org/10.1002/ajmg.a.38022

Zarate, Y.A., Kalsner, L., Basinger, A., Jones, J.R., Li, C., Szybowska, M., Xu, Z.L., Vergano, S., Caffrey, A.R., Gonzalez, C.V., Dubbs, H., Zackai, E., Millan, F., Telegrafi, A., Baskin, B., Person, R., Fish, J.L., Everman, D.B., 2017. Genotype and phenotype in 12 additional individuals with SATB2-associated syndrome. Clin. Genet. 92, 423–429. https://doi.org/10.1111/cge.12982

Zeng, H., 2022. What is a cell type and how to define it? Cell 185, 2739–2755. https://doi.org/10.1016/j.cell.2022.06.031

Zhang, S., Li, J., Lea, R., Vleminckx, K., Amaya, E., 2014. Fezf2 promotes neuronal differentiation through localised activation of Wnt/β-catenin signalling during forebrain development. Dev. Camb. Engl. 141, 4794–4805. https://doi.org/10.1242/dev.115691

Zhang, X., Li, X., Ning, F., Shang, Y., Hu, X., 2019. TLE4 acts as a corepressor of Hes1 to inhibit inflammatory responses in macrophages. Protein Cell 10, 300–305. https://doi.org/10.1007/s13238-018-0554-3

Zhang, Y., Liu, G., Guo, T., Liang, X.G., Du, H., Yang, L., Bhaduri, A., Li, X., Xu, Z., Zhang, Z., Li, Z., He, M., Tsyporin, J., Kriegstein, A.R., Rubenstein, J.L., Yang, Z., Chen, B., 2020a. Cortical Neural Stem Cell Lineage Progression Is Regulated by Extrinsic Signaling Molecule Sonic Hedgehog. Cell Rep. 30, 4490-4504.e4. https://doi.org/10.1016/j.celrep.2020.03.027

Zhang, Y., Liu, G., Guo, T., Liang, X.G., Du, H., Yang, L., Bhaduri, A., Li, X., Xu, Z., Zhang, Z., Li, Z., He, M., Tsyporin, J., Kriegstein, A.R., Rubenstein, J.L., Yang, Z., Chen, B., 2020b. Cortical Neural Stem Cell Lineage Progression Is Regulated by Extrinsic Signaling Molecule Sonic Hedgehog. Cell Rep. 30, 4490-4504.e4. https://doi.org/10.1016/j.celrep.2020.03.027

Zhao, X., Qu, Z., Tickner, J., Xu, J., Dai, K., Zhang, X., 2014. The role of SATB2 in skeletogenesis and human disease. Cytokine Growth Factor Rev. 25, 35–44. https://doi.org/10.1016/j.cytogfr.2013.12.010